

Review of the Lower Triassic play in the Roer Valley Graben, SE onshore Netherlands

Emphasis on oil charge from the Lower Jurassic Posidonia Shale.

R.F.M. van der Kroef

Faculty of Geosciences, Departement of Earth Sciences, Utrecht University, The Netherlands

Supervision:

Dr. J.H.P. de Bresser (UU) & Michiel Harings (EBN)

Summary

In the last decades extensive E&P efforts have led to a great variety of proven hydrocarbon plays and traps in the sedimentary succession of the Netherlands, both on- and offshore. The majority of the fields encountered have gas, only several small fields contain oil. The distribution of the TOC rich Posidonia shale formation of lower Jurassic (Toarcian) age clearly controlled the location of the oil fields. It has been an active source and kitchen in the West Netherlands basin, resulting in an abundance of oil fields in the Rijswijk License. The Roer Valley Graben is in fact the SE extension of this basin, although with a different burial history. It was only mildly inverted during the Sub-Hercynian tectonic pulse and has strong ongoing subsidence with tectonic activity. Currently, it is believed that the Posidonia Shale is near or at maturity level. This gives reason to believe that there may lie oil potential in the Lower Triassic play in the Roer Valley Graben. The scope of this study is to re-evaluate the available 3D and 2D seismic, well data and literature on the Roer Valley Graben to review its prospectivity, particularly focusing on oil from the Posidonia Shale and trapping style of the Main Buntsandstein Subgroup. The approach for the prospectivity review was the creation of a high resolution structural framework for the Roer Valley Graben using the structural framework module in Petrel which allows models to be built on the fly in a 'Modeling while interpreting' workflow. The results were a detailed 3D structural fault framework and four new detailed structural maps in elevation time of the top Posidonia Shale, base Altona Group and near top and base Main Buntsandstein Subgroup. The following step was to convert this interpretation to depth. For this purpose a hybrid velocity model was constructed which includes input from the Velmod-2 model of TNO and input calculated in Petrel from the available checkshot data. This process resulted in two detailed structural maps in depth for top and base Main Buntsandstein Subgroup. These surfaces were used in the identification of potential leads. A total of 25 leads were identified of which 7 possible oil leads, the other were identified as having gas potential. For each lead a rough estimate has been calculated for the STOIP and GIIP. In the end a risk qualification was made based on the trap type, configuration and its location with respect to already drilled sites as well as the probability of maturity. From this classification the most promising leads were identified. These are located in fault-dip closures in the northwestern sector (lead 1, 9, 10 and 11), in a fault-dip closure south of the Waalwijk South field (lead 22) and in a down-thrown fault-dip closure in the southern sector (lead 5). From the re-evaluation it can be concluded that the juxtaposition for the Posidonia Shale below the Main Buntsandstein Subgroup is not ideal and oil charge into this reservoir from this source is deemed very unlikely. However, stratigraphically higher formations, such as the Brabant Limestones might prove successful as well as gas charge from Carboniferous Coal measures into the leads that have been identified.

A secondary objective to this study was to assess the quality of 2D lines which are reconverted from paper copies back to digital SEG Y files. The conclusion of this process is that it greatly enhances the quality and usefulness of old 2D seismic data. After digitization the regenerated accurate digital seismic signal from a seismic image can be used in the interpretation on a workstation.

CONTENTS

SUMMARY	2
1. INTRODUCTION.....	5
2. GEOLOGICAL FRAMEWORK OF THE ROER VALLEY GRABEN.....	7
2.1 STRUCTURAL EVOLUTION OF THE ROER VALLEY GRABEN	8
2.2 STRATIGRAPHY.....	11
2.2.1 <i>Foreland basin mega-sequence</i>	11
2.2.2 <i>Pre-rift mega-sequence</i>	11
2.2.3 <i>Syn-rift mega-sequence</i>	11
2.2.4 <i>Post-rift mega-sequence</i>	12
3. WORKFLOW	13
3.1 DATA HANDLING.....	13
3.1.1 <i>Mis-tie corrections & Phase shifts</i>	13
3.1.2 <i>Hydrocarbon shows & pseudo show logs</i>	15
3.1.4 <i>Digitization 2D seismic lines</i>	16
3.2 SEISMIC INTERPRETATION.....	17
3.3 STRUCTURAL FRAMEWORK MODELING (PETREL)	18
3.3.1 <i>Fault framework modeling</i>	19
3.3.2 <i>Horizon modeling</i>	19
3.3.3 <i>Depth Structural Framework</i>	19
3.4 VELOCITY MODEL AND TIME-DEPTH CONVERSION.....	20
3.5 LEAD IDENTIFICATION	21
4. THE HYDROCARBON SYSTEM OF THE ROER VALLEY GRABEN.....	22
4.1 RESERVOIR	24
4.2 SOURCE	25
4.2.1 <i>Posidonia Shale Formation</i>	25
4.3 SEAL	28
4.4 TRAPPING MECHANISMS	28
4.4.1 <i>Brakel, Andel & Kerkwijk</i>	28
4.4.2 <i>Waalwijk Area</i>	30
4.4.3 <i>Hilvarenbeek & Broekzijde</i>	30
4.4.4 <i>Oisterwijk & Veldhoven</i>	30
4.4.5 <i>Varik & Gewande</i>	31
4.4.6 <i>Sint-Michelsgestel & Heeswijk</i>	35
4.4.7 <i>Keldonk</i>	35
4.5 DRY HOLE ANALYSIS	37
4.6 TIMING.....	38
5. RESULTS	39
5.1 STRUCTURAL FRAMEWORK MODELING & TIME-DEPTH CONVERSION.....	39
5.2 OIL LEADS.....	40
5.3 GAS LEADS.....	45

6. DISCUSSION	50
6.1 UNCERTAINTIES.....	50
6.2 STRUCTURAL FRAMEWORK MODELING WORKFLOW.....	50
6.2.1 <i>Isochore maps TNO</i>	52
6.2 OIL LEADS.....	52
6.3 GAS LEADS.....	55
6.4 RISK QUALIFICATION.....	57
7. CONCLUSIONS.....	60
8. RECOMMENDATIONS.....	61
9. ACKNOWLEDGEMENTS	61
10. REFERENCES	62
APPENDIX A: HYDROCARBON SHOWS	65
APPENDIX B: CROSS-SECTION STRUCTURAL FRAMEWORK MODEL.....	69
APPENDIX C: STRUCTURAL FRAMEWORK ELEVATION TIME MAPS	72
APPENDIX D: STRUCTURAL FRAMEWORK ELEVATION DEPTH MAPS.....	76
APPENDIX E: DERIVATION EXPANSION FACTOR.....	78

1. Introduction

In the last decades extensive E&P efforts have led to a great variety of proven hydrocarbon plays and traps in the sedimentary succession of the Netherlands, both on- and offshore. The majority of the fields encountered have gas, only several small fields contain oil of which the largest is Schoonebeek (figure 1.1). The distribution of the lower Jurassic organic rich Posidonia Shale Formation clearly controlled the location of the oil fields. However, the large Schoonebeek Field was not sourced by the Posidonia, but by lowermost Cretaceous source rocks (*de Jager & Geluk, 2007*).

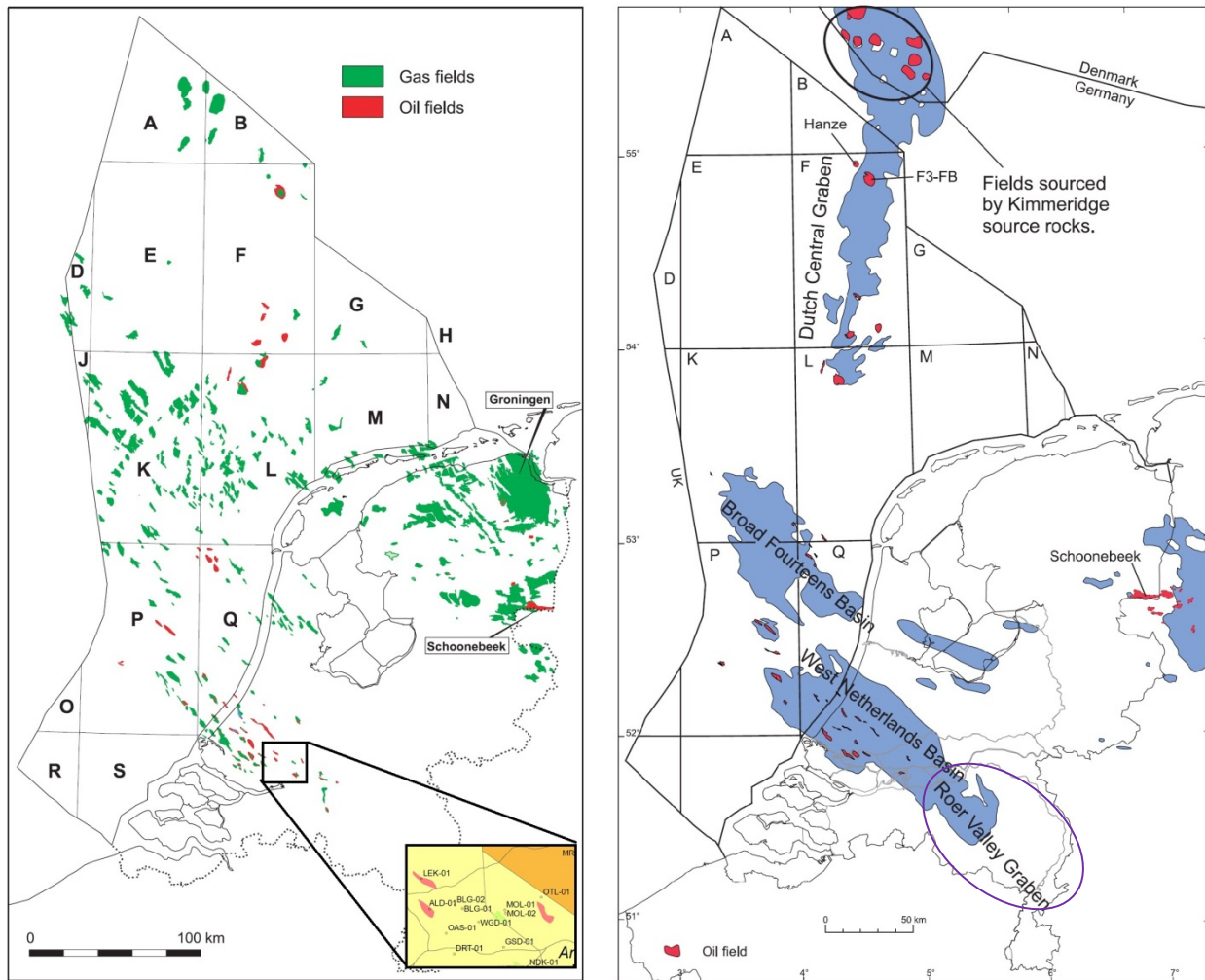


Figure 1.1: Gas and oil field in the Netherlands (left) and the present-day distribution of the Posidonia Shale Formation in blue (right). From: *Geology of the Netherlands* (*de Jager & Geluk, 2007*). The purple contour indicates the study area.

In the northwestern part of the West Netherlands Basin different small oil fields have been encountered in the Jurassic section which have produced. Further to the southeast a combination of oil and gas fields are found. Including several undeveloped oil fields (LekkerKerk, Alblasterdam and Ottoland; figure 1.1) in the southeast of the West Netherlands Basin. In the Fall of 2009 Northern Petroleum drilled the Nieuwendijk-1 well which targeted the Bunter section for gas. The well was dry, however presence of oil was identified on the shakers. Further towards the southeast in the Roer Valley Graben, the Waalwijk and Loon op Zand fields produce a high fraction condensate. The gas field Wijk en Aalburg encountered and produced fluids after a short period of production, including oil.

These observations pose the question if Jurassic source rocks, which include the Posidonia Shale, are mature enough to have generated economic amounts of producible oil in the vicinity of the Roer Valley Graben, as this is a southeastern extension of the West Netherlands Basin. However, the Roer Valley Graben does have a different burial history. It was only mildly inverted during the Sub-Hercynian tectonic pulse (*de Jager, 2007*) and has had much stronger Tertiary and ongoing subsidence, related to the European Cenozoic Rift system.

With the increased interest in shale gas, studies have been performed on the maturity of the Posidonia Shale Formation in the vicinity of the West Netherlands Basin and the Roer Valley Graben. The observation from these studies (which include maturity maps with sweetspots) identified mature areas within the Roer Valley Graben. The Posidonia Shale is currently believed to be at or near maturity level, hence the interest for the shale play in this area. So far interest in the Roer Valley Graben has been low for oil and is under explored compared to the other major basins in the Netherlands except for some activity at the western margin of the basin near the Waalwijk Field. The area has been largely neglected by the E&P industry for the past 20 years. The reason for the lack of interest in this area is believed to be the lack of a potential seal or trapping structure. Thus data in the area is sparse and generally old for E&P standards. The seismic data available is usually 2D, only a small area is covered by 3D seismic (Waalwijk area). Few wells have been drilled. The last exploration wells in the southeastern part of the graben were drilled in the late 80's, all of which did not encounter any hydrocarbons.

The scope of this study is to re-evaluate the available 3D and 2D seismic, well data and literature on the Roer Valley Graben to review its prospectivity, particularly focusing on oil and trapping style or potential reservoir which may have been overlooked in the past. The main focus lies on:

1. Creating a high resolution structural framework for the Roer Valley Graben
2. Identification of potential reservoir (Trias) and structural traps with a favorable configuration for oil accumulation generated from the Posidonia Shale Formation.
3. Evaluate the seismic digitization workflow; are there any quality losses when converting a paper copy to a digital SEG Y file?

2. Geological Framework of the Roer Valley Graben

The NNW-SSE trending Roer Valley Graben is part of a 250 km long and 50 km wide Mesozoic basin system stretching in a NW-SE direction (figure 2.1). It is an asymmetric fault bounded graben which initiated upon pre-existing sedimentary basins of Carboniferous, Triassic to Early Jurassic and Late Jurassic age (*Geluk et al., 1994*). The Graben is bounded by the Peel Boundary Block (Peel Boundary Fault) and Maasbommel High in the north and the Campine Block and London-Brabant Massif to the south. To the northwest, the Graben is bounded by the West Netherlands Basin, which shares a similar tectonic origin and Mesozoic evolution. Today the Roer Valley Graben forms the northwestern extension of the European Cenozoic Rift system (*Ziegler, 1990*) and is one of the most prominent onshore Cenozoic structures in the Netherlands. The Cenozoic graben is closely related to the Late Jurassic basin and the inversional structures at the end of the Cretaceous (*Geluk, et al., 1994*). It is still subject to tectonic activity, as demonstrated by regular mild seismic activity.

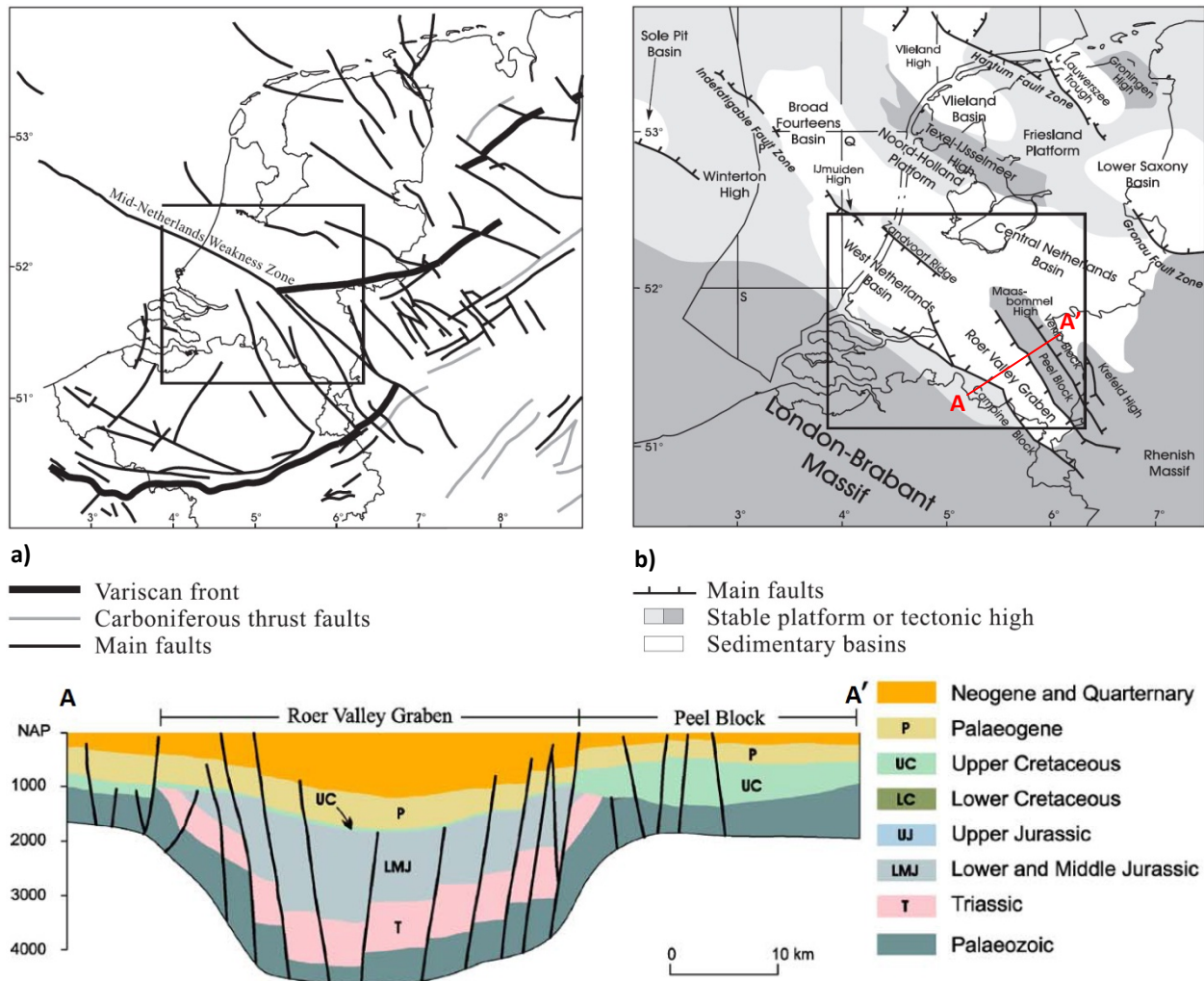


Figure 2.1: Main tectonic features of the Netherlands and its surroundings after the Variscan Orogeny (a) and in the Mesozoic (b) including a geological cross section through the Roer Valley Graben (c). Source: *Worum et al., 2005, after Lokhorst, 1998*; *TNO-NITG, 2002*; *De Mulder et al., 2003*.

2.1 Structural evolution of the Roer Valley Graben

The initial framework for the structural outline of the Mesozoic Roer Valley Graben formed during the Permian upon an ancient NW-SE tectonic lineament, referred to as the Mid-Netherlands Weakness Zone (figure 2.1a), related to wrench movements induced by the Late Carboniferous-Early Permian Variscan Orogeny (Worum *et al.*, 2005). Its evolution is illustrated by the tectonic subsidence curves of three representative wells in figure 2.2. The relevant tectonic phases have also been indicated of which the most important are the Late Permian, Late Triassic and Late Jurassic-Early Cretaceous rifting phases (Worum *et al.*, 2005), induced mainly by the Pangea break-up (Ziegler, 1990). In figure 2.3 an overview of the structural evolution of the Roer Valley Graben from Permian to recent is schematically summarized.

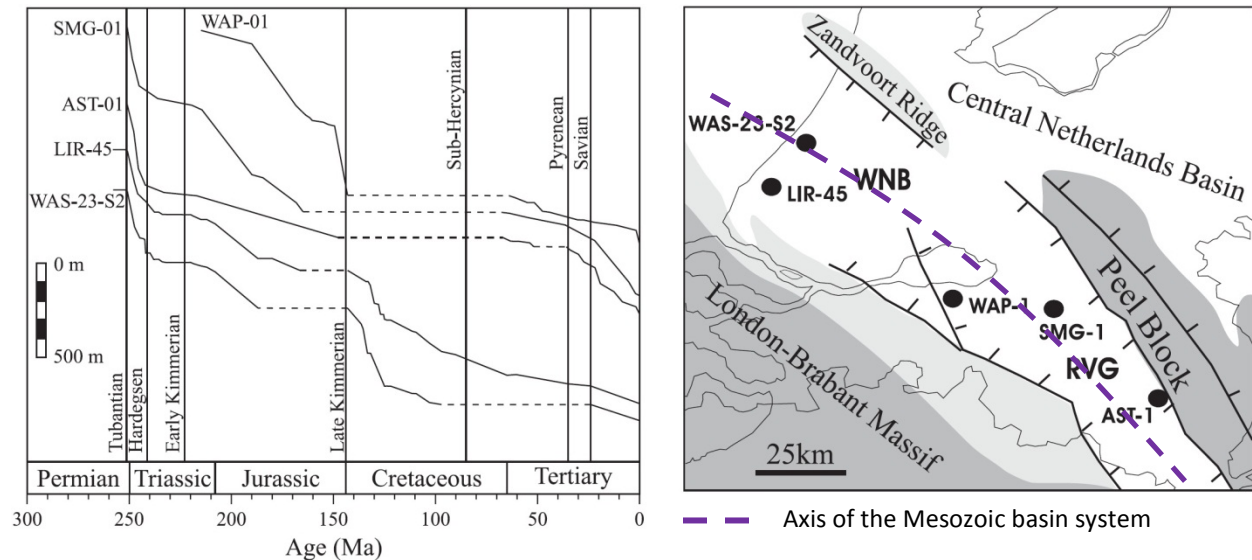


Figure 2.2: a) Tectonic subsidence curves of 5 representative wells located in the WNB-RVG system. b) Location of the wells. Source: Worum *et al.*, 2005, after Zijerveld *et al.*, 1992; Van Balen *et al.*, 2000.

The Permian succession in the Roer Valley Graben is characterized by a large hiatus from Early Permian towards the start of the Late Perm. This hiatus was the result of the Saalian and Altmark tectonic pulses of the Variscan Orogeny (NITG, 2001) and is referred to as the Base Permian Unconformity (Geluk, 2007). Only the youngest Permian is represented by sediments within the graben (NITG, 2001). During the Late Permian the first of the three important tectonic pulses reached the Roer Valley Graben, the Tubantian I and II tectonic rift pulses, modifying the highs and lows in the area (NITG, 2001) further initiating the structural outline for the Mesozoic Roer Valley Graben. No differential subsidence occurred during the Permian. It only acted as a fault bounded platform (Geluk, 1994).

From Late Permian to Early Triassic the Roer Valley Graben was characterized by rapid subsidence. Little syn-depositional faulting and thick homogenous sedimentation occurred. The first tectonic pulse of the Triassic, the Hardegsen mainly effected the areas to the north and east of the Roer Valley Graben eroding parts of the Main Buntsandstein Subgroup (NITG, 2001). It comprises up to four short-lived rift pulses (Geluk & Röhlting, 1997, 1999) alternated with periods of regional thermal subsidence. In the study area only the strongest first pulse effected the graben as differential subsidence was initiated, preserving a thick Volpriehausen sequence (NITG, 2001). As tectonic activity in the area declined, deposition of Triassic sediments continued (Röt and Muschelkalk Formations).

The second Triassic tectonic pulse, the Early Kimmerian commenced during the Anisien and cumulated in the Carnien. The effects were limited within the graben as only differential movements occurred in the vicinity of

the Peel Boundary Fault. Here tectonic movements took place along reactivated NW-SE orientated Variscan faults (*Geluk et al., 1994*). During these times the Roer Valley Graben formed a large-scale NE dipping halfgraben, bounded by faults in the north (*Geluk, 1999b*).

In the Rhaetian (youngest Triassic) and Early Jurassic times a period of relative tectonic quiescence occurred with a uniform sheet-like deposition of pelitic, open-marine sediments (*Herngreen et al., 2003*). Later on, structural complexity gradually increased as a third phase, the Mid-Kimmerian (Aalenian – Callovian/Oxfordian) commenced, reaching its maximum during the Callovian.

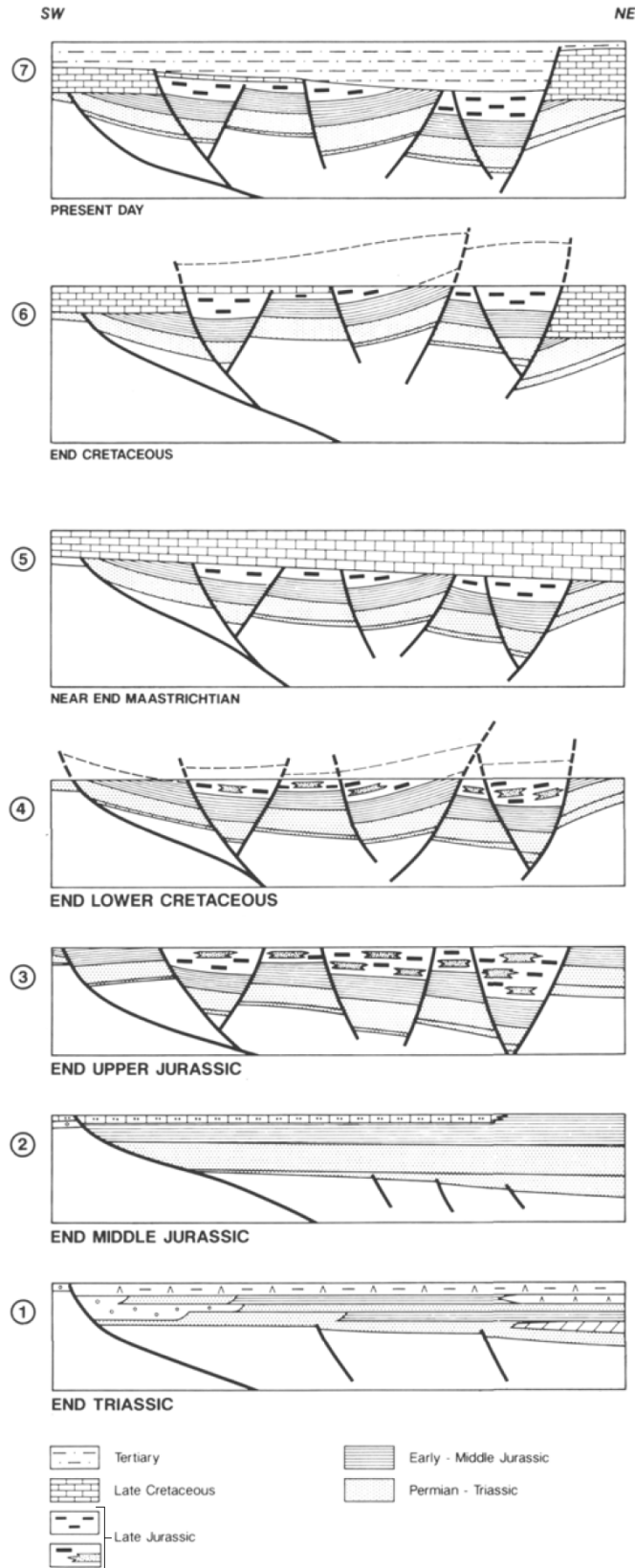
The mid-Kimmerian tectonic pulse of the Middle Jura initiated differential fault movements. The structuration of NE dipping halfgrabens during the Triassic continued. However, the western boundary of the Waalwijk structure also became active during this period initiating the development of a series of grabens (figure 2.3; *NITG, 2001*). This period of tectonic activity is also marked by thermal uplift of surrounding source areas such as the London-Brabant Massif.

The structural modification of the Roer Valley Graben continued as the Late Kimmerian tectonic phase commenced. It comprises two major tectonic pulses: (i) the Late Kimmerian I, occurring at the onset of the Late Jurassic (Oxfordian) and (ii) the Late Kimmerian II during earliest Cretaceous (Ryazanien-Valanginien; *NITG, 2004*). The tensional movements were accommodated by transtensional, dextral strike-slip of reactivated NW-SE trending faults. Thermal uplift occurred along the shoulders of the graben as well as in the London-Brabant Massif towards the south (*Vercoutere & van den Haute, 1993*). This resulted in Middle Jurassic to Cretaceous erosion which strongly reduced or even completely removed the Permian-Triassic-Jurassic sequence outside the graben and near its shoulders (figure 2.3).

In the Graben the complexity of the sub-grabens and fault blocks increased as each unit underwent a differential subsidence pattern (figure 2.3). At regional scale, the Mid-Netherlands Weakness Zone within the basinal system (figure 2.3) together with the E-W extension related to the different tectonic pulses also contributed to the increasing complexity of the Roer Valley Graben as the combination of these factors result in the narrow, concentrated zones of deformation controlled by NNW-oriented faults (*Worum et al., 2005*). In the northwestern part of the graben, the Late Kimmerian I and II pulses initiated a pull-apart basin which was delineated by E-W trending strike-slip faults (*Geluk et al., 1994*). The pull-apart structure formed as a result of the transtensional forces along the NW-SE oriented boundary faults. Within this basin the Waalwijk structure originated.

After this tectonically active period, a period of tectonic quiescence commenced with regional subsidence as the previously disturbed crust recovered. Combined with a regional rise in sea-level which initiated in the Valanginian, a large scale transgression spread across the basinal system expanding the depositional areas across adjacent platforms and highs (*Herngreen & Wong, 2007*) which allowed the deposition of the carbonate sediments of the Late Cretaceous (Chalk group). By Late Cretaceous times the transgression culminated in a regional single open-marine basin that covered large parts of NW Europe (*NITG, 2004*).

The regional subsidence and sea-level rise was followed by Late Cretaceous and Early Palaeocene inversion (Sub-Hercynian and Laramide phases). The Sub-Hercynian phase within the Roer Valley Graben initiated during or possibly before the Early Campanian and ceased during the Maastrichtian. (*Geluk et al., 1994*). The onset cannot be exactly dated as pre-Campanian strata is absent (*Geluk et al., 1994*). Faults active during the Late Kimmerian reactivated as reverse faults. The inversion is a result of a regional plate reconfiguration related to the convergence or early collision of the Alpine-Carpathian Orogen (*de Jager, 2007*). Recently, an alternative hypothesis has been presented by Kley & Voigt (2008), proposing that the Sub-Hercynian event reflects the onset of Africa-Iberia-Europe convergence and that Alpine collision with southern Europe did not commence until the Paleocene or Eocene (*Pharaoh et al., 2010*). The inversion throughout the Roer Valley Graben varies in strength. The effects were strongest in the northwestern sector of the graben. It is expressed by folding and erosion of the Jurassic and Lower Cretaceous Altena and Nieuwerkerk formations that are truncated by a major unconformity



Early Palaeocene: *Laramide phase*, second pulse of inversion and erosion.

Late Oligocene – Quaternary: initiation of the European Cenozoic Rift system and related tectonic activity.

Late Cretaceous: *Sub-Hercynian* tectonic pulse which results in varying amounts of inversion and erosion throughout the basin, strongest in the northwestern sector.

Early Cretaceous: period of tectonic quiescence with regional subsidence as previously disturbed crust recovered. Thick Chalk deposition.

Earliest Cretaceous: second pulse of the Late Kimmerian rift phase (*Late Kimmerian II*). Strong uplift basin shoulders plus erosion. Tilting of fault-bounded blocks.

Upper Jurassic: strong uplift basin shoulders, including the London-Brabant Massif (*Late Kimmerian I*). Tensional movements accommodated by transtensional, dextral strike-slip of reactivated NW-SE trending faults.

Early – Middle Jurassic: period of relative tectonic quiescence with uniform sheet-like deposition. Some differential subsidence related to the *Mid-Kimmerian phase*.

Late Permian - Early Triassic: rapid subsidence, little syn-depositional faulting, thick homogenous sedimentation. Differential subsidence first pulse of the *Hardegsen phase*.

Late Triassic: differential movements occurred in the vicinity of the Peel Boundary Fault. (*Early Kimmerian phase*).

Figure 2.3: Schematic structural evolution of the Roer Valley Graben from the Permian to Recent times. Modified from Winstanley (1993)

(Luijendijk et al., 2010 on cit., Michon et al., 2003; Winstanley, 1993) as well as erosion of the chalk in most of the basin.

During the Tertiary the Peel Boundary Fault continued to be active and this resulted in the Roer Valley Graben resuming its half-graben form (Winstanley, 1993). Gentle regional subsidence occurred during the Eocene. It is proposed to be related to the contraction of the lithosphere after Early Cretaceous rifting or the elastic relaxation of the lithosphere following the Sub-Hercynian and Laramide inversional phases (Worum et al., 2005; after De Lugt et al., 2003; Michon et al., 2003). In the Late Oligocene and onwards the Roer Valley Graben was reactivated as part of the Northwest European rift system and became a major Neogene-Quaternary depocentre (Worum et al., 2005). The structural trend of this depocentre slightly differs from the Mesozoic trend as it has a more NW-SE orientation.

2.2 Stratigraphy

The stratigraphic record in the Roer Valley Graben can be sub-divided into four mega-sequences (based on Winstanley, 1993): a foreland basin, pre-rift, syn-rift and post-rift mega-sequence (see figure 2.4).

2.2.1 Foreland basin mega-sequence

The first sequence comprises the Carboniferous Coal Measures of the Limburg Group. These sediments were deposited in a marginal marine environment of the Variscan foreland basin. The sedimentary succession shows a largely regressive sequence of Namurian marine shales, grading to a more fluvial facies of the Westphalian A-C and terminates in the Neeroeteren Formation; a sandstone of Westphalian D age deposited in a braided river system (Winstanley, 1993). South of the Roer Valley Graben a total thickness of approximately 2500m is observed for the Westphalian A, B and C (Geluk et al., 1994). Based on poorly controlled interpretation of the seismic signal from deeper horizons it is estimated that this thins towards 1000-1500 m in the Roer Valley Graben (Winstanley, 1993). The foreland basin mega sequence is topped by the Base Permian Unconformity.

2.2.2 Pre-rift mega-sequence

The second sequence, the pre-rift mega-sequence comprises sediments deposited during Permian to Middle Jurassic age. These include: (1) the sandstones and conglomerates of the Upper Rotliegend Group (0-10m), (2) younger deposits of the Zechstein Group (10-60m); mainly a sequence of shoreline clastics with only marine carbonates present in the northeast of the graben, (3) evaporitic, playa lake, mudstone of the Lower Buntsandstein Formation, (4) alluvial fan deposits of the Main Buntsandstein and Röt Formations, (5) marginal marine anhydrites and dolomitic mudstones of the Upper Germanic Trias Group, (6) the lower part of the Altena Group; a shale dominated sequence, including the Sleen, Aalborg and Posidonia shales deposited initially under increasingly anoxic conditions, and lastly (7) the upper part of the Altena Group; comprising a regressive sequence of bioclastic and oolitic limestones of the Brabant Formation. The total thickness of the Permo-Triassic sequence (Upper Rotliegend to Upper Germanic Trias Group) locally reaches a total thickness of 900m (Winstanley, 1993). For the Altena Group this varies from 1200-2000m, with the depocentre showing a northwesterly trend (Winstanley, 1993).

2.2.3 Syn-rift mega-sequence

The third mega-sequence in the Roer Valley Graben is separated from the previous sequence by an unconformity. It deposited during the major rift phase, the Late Kimmerian phase of the Late Jurassic to earliest Cretaceous. The succession comprises the Delfland Group, a deltaic sequence of Late Jurassic age deposited in NW-trending, fault controlled sub-basins of the Roer Valley Graben (Winstanley, 1993). Due to the inversion that followed in the Late Cretaceous, the depositional thickness prior to inversion is difficult to estimate. In the Waalwijk area thicknesses of 1000m are observed. This, together with the angular subcrop of the Delfland Group

and the Brabant Limestones underneath the Tertiary unconformity, *Winstanley (1993)* postulates that locally maximum thicknesses of 2000m could have been reached.

2.2.4 Post-rift mega-sequence

The final post-rift mega-sequences comprises: (1) the Upper Cretaceous Chalk Group; deposited in a marine setting as a consequence of the regional transgression that culminated in a single open-marine basin and (2) the marine Lower North Sea Group grading into fluvial clastics of the Upper North Sea Group. The Upper Cretaceous

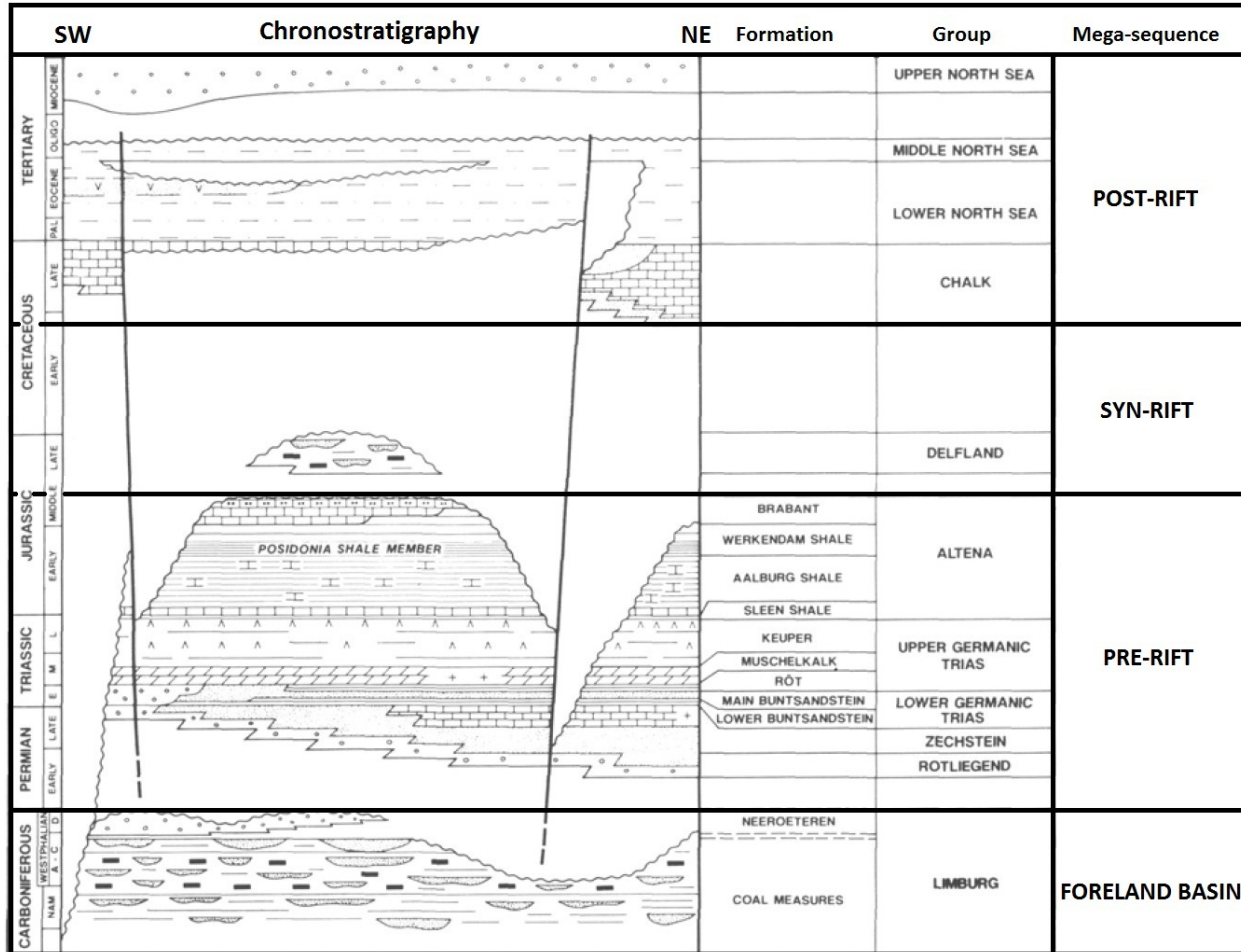
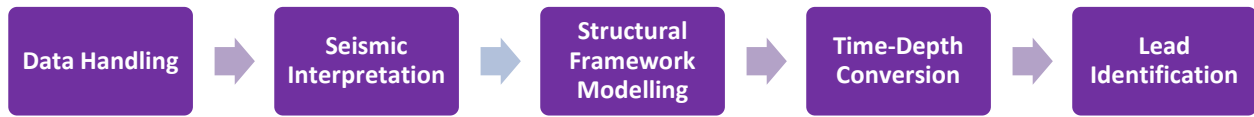


Figure 2.4: Chronostratigraphy of the Roer Valley Graben. Each mega-sequence has been indicated. Adapted from *Winstanley, 1993*.

Chalk Group most probably reached thicknesses of up to 1000m in the north of the graben (*Winstanley, 1994*). Wells on the flanks of the graben indicate that the Chalk deposition had also overstepped the margins of the graben onto the basinal shoulders to an extent where communication between fossil fauna occurred (*Winstanley, 1994 after Bless et al., 1983*). In the graben virtually most of the Chalk deposits have been eroded. In the Late Oligocene and onwards strong subsidence occurred in the area as the graben became part of the Northwest European rift system giving way to the deposition of the marine Lower North Sea Group and the fluvial clastics of the Upper North Sea Group. The North Sea Group can reach thicknesses of up to approximately 1700m in the center of the graben (*Geluk et al., 1994*).

3. Workflow



3.1 Data Handling

For the construction of a regional structural framework of the Roer Valley Graben all available seismic and well data has been incorporated into one Petrel work project. Most data is obtained from the oil- and gas portal of the Netherlands managed by TNO (nlog.nl). This includes well top interpretations by TNO, composite well logs, check shots, two-way-time grids of nine key horizons and velocity data from the Veldmod-2 model constructed by TNO for the Dutch on- and offshore. The seismic data obtained consists of mainly 2D seismic lines of different vintages, varying in age from the 60's to the 90's as well as varying polarities of the seismic signal. The available data included previously digitized seismic sections. Only a relative small part of the study area is covered by 3D seismic of which two surveys were available, one from the 80's and another from the 90's. The dataset that was used forms a part of the large *Terra Cube* project by Fugro. A project that combined and 'glued' all available 3D seismic on- and offshore into one data set (figure 3.1). The different 2D surveys at first did not match well. This was resolved by performing mis-tie corrections between the different surveys to find a best fit. To extend the seismic coverage in areas of low data density, several analog 2D seismic lines have been selected for digitization. These steps and results of this process are summarized below.

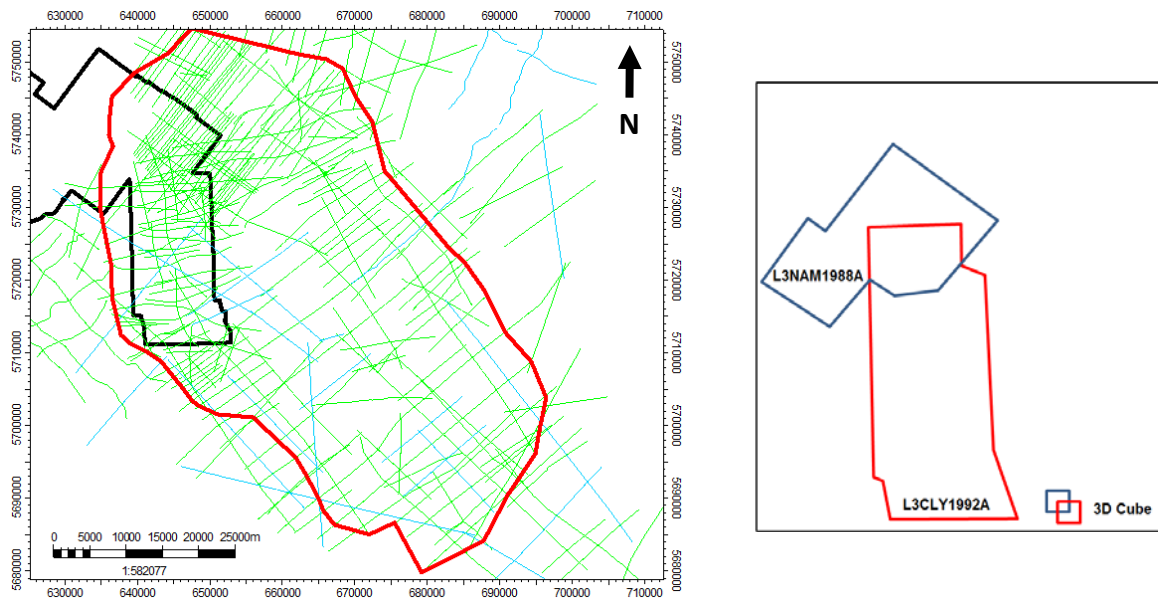


Figure 3.1: Overview of the available seismic data in the Roer Valley Graben, grid ED50 UTM31. The black outline indicates the 3D seismic outline of the Terra Cube by Fugro, the green lines digital available 2D seismic, and the blue lines 2D seismic that have been digitized for this project. In red the boundary of the study area is given.

3.1.1 Mis-tie corrections & Phase shifts

The workflow to ensure a uniform seismic dataset in these corrections was to first check if the mis-tie could be resolved by a simple time shift between the lines, simply shifting one line up or down with respect to another. In this way the initial recorded structure remains intact. In this process the available 3D seismic cubes were taken as the base case dataset to which the miss fitting lines had to be shifted. Thus first a best fit was found between

the 2D lines that cross-cut the 3D seismic cubes to further extend these corrections away from the 3D seismic cubes. During this process it became evident that there consist a 180° phase shift between the 3D seismic cubes and the 2D seismic lines. The 2D lines that showed this miss-match were shifted to fit with the 3D seismic

In situations where several seismic lines cross each other a simple time shift was difficult. Here the mis-tie manager of Petrel has been used. This tool allows you to select different surveys and the program finds a best fit between the selected lines based on user-specified criteria. A range of settings can be used, such as the vertical time range on which the tool should focus for the correction and an option which allows constant or variable corrections along a seismic line. The favorable option here is to use constant correction to avoid changing the initial structure of the seismic line (figure 3.2). During the correction process there were also situations were two seismic lines fitted perfectly at a certain time range but not below or above this level. Usually, the upper part fitted nicely which represents the Tertiary and Late Cretaceous sediments. However, the deeper levels which have a mis-tie are the sedimentary succession of interest in this study. So in these scenarios a best fit situation was found between both levels at the expense of the upper level.

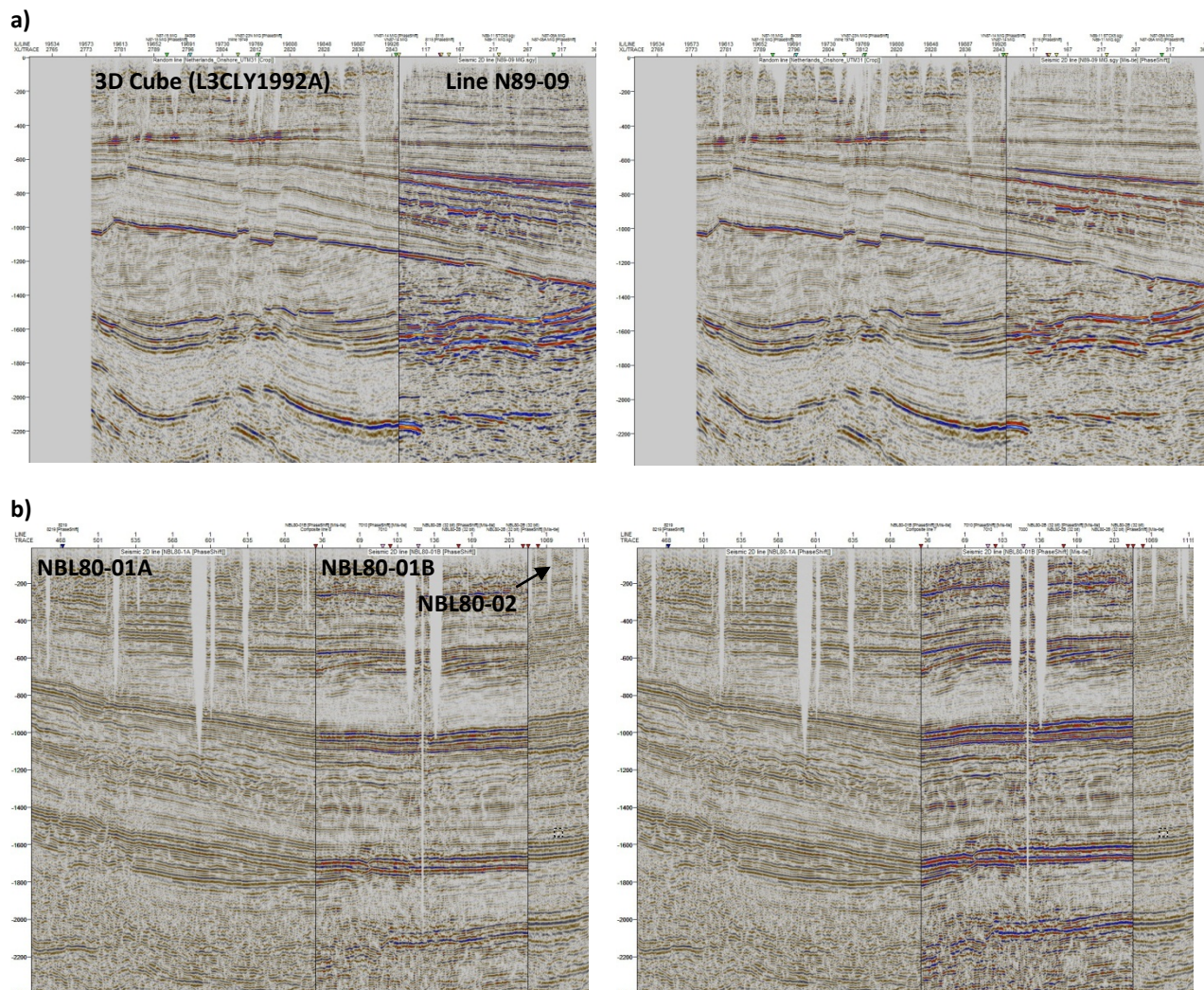


Figure 3.2: a) Example of an uncorrected mis-tie between the L3CLY1992A cube and the N89-09 Line of the L2BP1989A survey (left) and the end result after performing corrections; 8ms time shift and a 180° phase shift (right). b) Example of an uncorrected mis-tie with three seismic lines (left) compared with a variable mis-tie correction to indicate the change in initial structure of the seismic (right).

3.1.2 Hydrocarbon shows & pseudo show logs

To get a good overview of the encountered hydrocarbons in the Roer Valley Graben all available well logs of the drilled wells in the area have been re-evaluated to identify the different formations in which hydrocarbons have been encountered. An overview of the shows that have been identified on the logs are presented in Appendix A. These shows have been loaded into Petrel to be able to identify in which formation the shows have occurred. In addition to this data, hydrocarbon shows that were identified by the NAM have been converted to pseudo well logs (figure 3.3). Green indicates oil shows and red gas shows. The shows identified range from poor, fair to good which corresponds to a value of 1, 2 and 3 on the pseudo show logs.

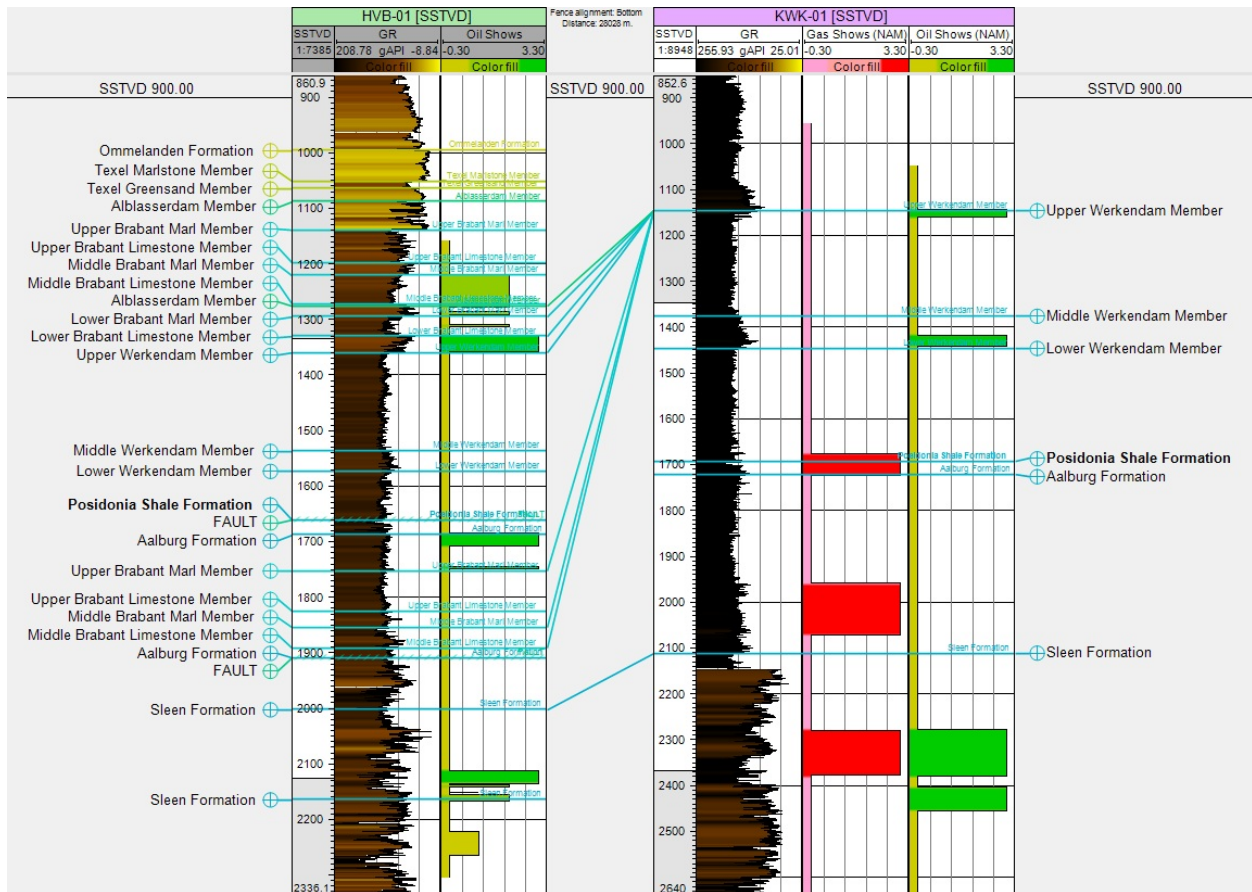


Figure 3.3: An example of a pseudo show log for the Hilvarenbeek-1 and Kerkwijk-1 wells.

3.1.4 Digitization 2D seismic lines

Several seismic sections only available on paper copies have been digitized to increase data density. After digitization the full spectrum of the seismic signal can be used in the interpretation on a workstation. This offers several advantages. It allows the digitized data to be re-displayed in different scales and color settings, improving the visual quality of the section as well as the option to apply post stack processes such as filtering, migration, deconvolution and noise attenuation.

In this study, the digitized lines are successfully incorporated into the digital dataset of the project. Mis-tie correction could be performed, including variable corrections across one seismic line as well as automated tracking utilities for seismic interpretation. In figure 3.4 two examples of lines that have been digitized are given. It is evident that there is rather an increase than a decrease in the visual quality of the lines. The digitization process does not seem to be effected by pre-existing manual interpretation with pencil on the paper copies or the dark stains visible in figure c. The rather prominent horizontal and vertical time grid lines also do not pose a problem.

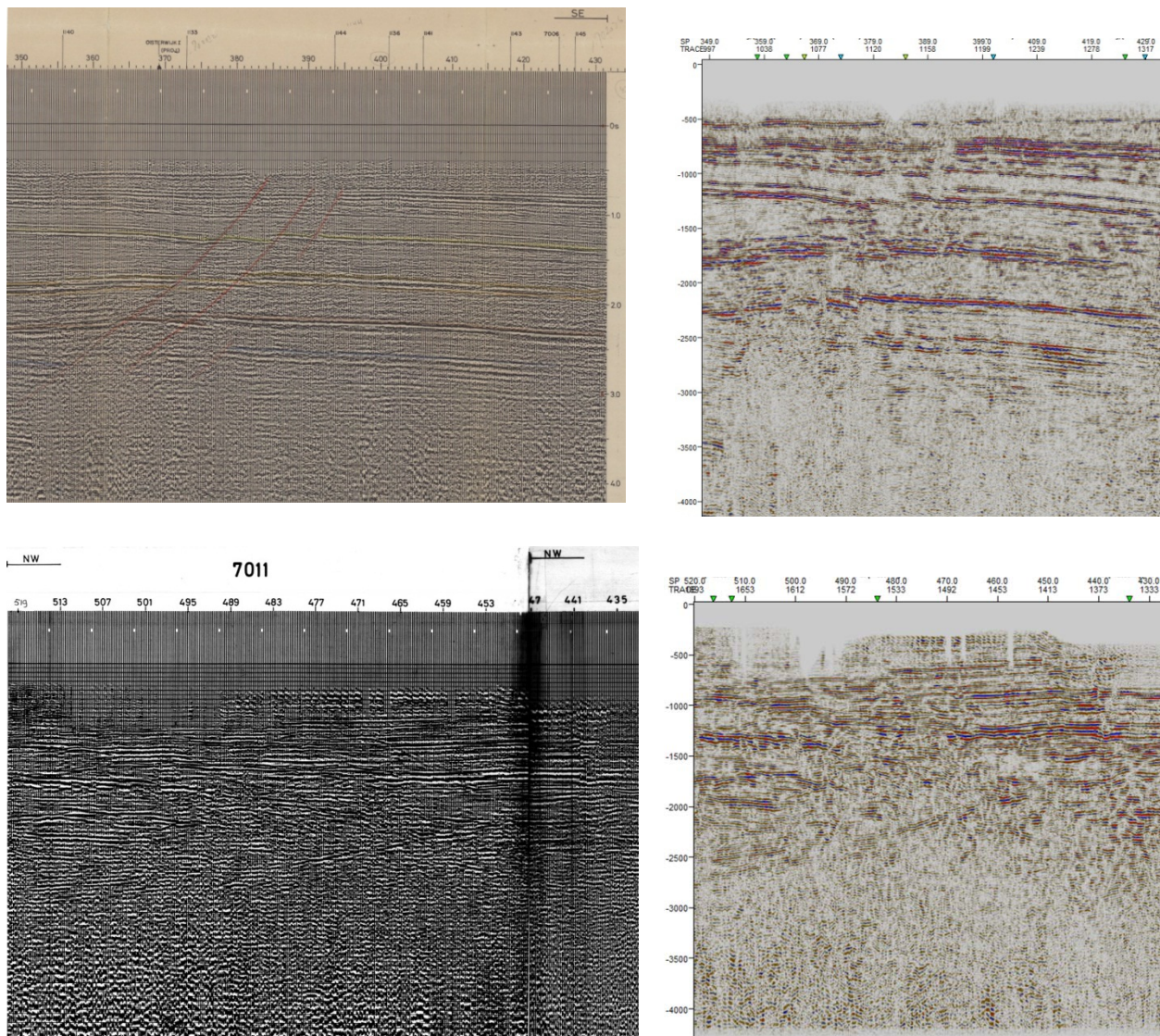


Figure 3.4: a) Section of a paper copy of line 2445 survey L2NAM1964A. b) Digitized section corresponding to the section presented in (a). c) Section of a film copy of line 7011 survey L2NAM1969A. d) Digitized section corresponding to the section presented in (c).

3.2 Seismic Interpretation

The main focus of this study lies on the Lower Triassic play in the Roer Valley Graben. The key horizons that are important for the review of this play are the top Posidonia Shale, base Altena Group, top Main Buntsandstein Sub Group and the base Buntsandstein Subgroup. However, due to the low quality of the seismic data, horizon interpretation is very difficult below a certain level. The deepest horizon which is mappable to a greater extent is the base of the Altena Group, although in certain areas interpretation of this horizon becomes difficult. To guide the interpretation in these areas, an estimation of the base Altena is made by subtracting a time isochore from the interpretation of the top of the Posidonia Shale Formation. This time isochore was constructed by converting a depth isochore of the Posidonia Shale to the base of the Atena Group with the use of velocity data from the Veldmod-2 model. TNO two-way-time grids of the key horizons, available on www.nlog.nl have also been used as a guide in the interpretation in low quality areas to help validate picks for the Posidonia Shale and the base Altena Group. These picks were also cross-checked with synthetics constructed from checkshot data of several wells (figure 3.5).

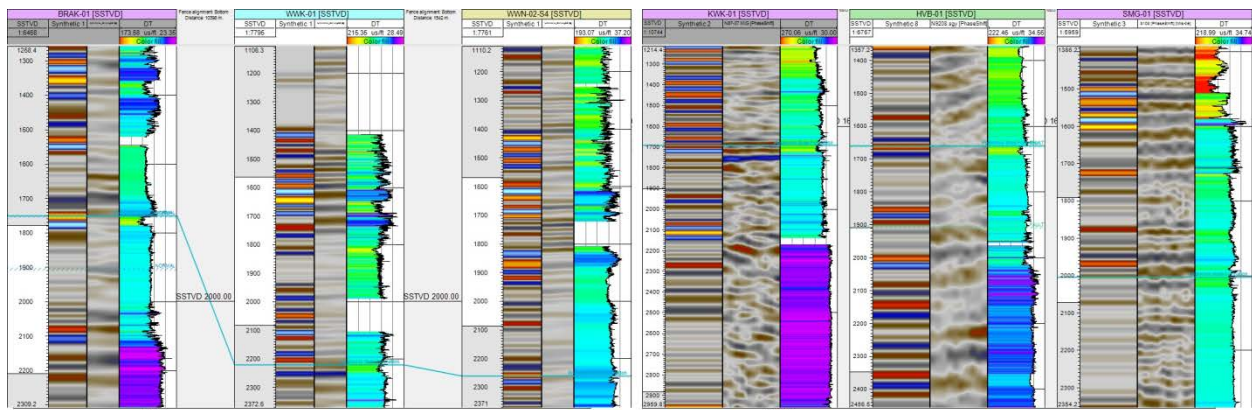


Figure 3.5: Overview of some of the synthetic logs used in this study. The first three wells are located in the 3D seismic area and the last three on different 2D seismic lines. On the log the pick for the Posidonia Shale has been indicated, a red positive reflector.

The amount of wells with available checkshot data is low, particular in the area covered with 2D seismic only. Thus the main workflow in the seismic interpretation of the two key horizons of the Posidonia Shale and the base Altena Group was to extend the 3D seismic interpretation of these horizons via cross-cutting 2D lines into the basin (see figure 3.1). The initial picks of the key horizons are presented in figure 3.6a are picked on the L3CLY1992A cube. The Posidonia Shale has been interpreted on the top red positive reflector of a series of three relative strong reflectors and the base Altena on a somewhat strong blue negative reflector. Throughout the area the character of the reflectors does change, especially for the base Altena Group as seismic quality of the 2D lines is low. The contrast between the different reflectors is low, which makes it hard to distinguish between characteristic successions of seismic reflectors and to validate the picks. As presented in figure 3.6b, the pick for the base Altena interpretation had to be changed to a red positive reflector in the L3NAM1988A cube as the blue reflector becomes less prominent throughout this 3D seismic dataset. It also shows the change in character of the Posidonia Shale pick. It changes from being the top dominant reflector in a series of three to the base dominant reflector in a series of three. This might indicate a phase change between these cubes. However, in this study the Terra Cube is seen as a correct dataset.

As mentioned before, the seismic quality particularly in the area of old 2D seismic greatly decreases with depth making it hard to interpret beyond the base of the Atena Group. To get a best estimate of the extend of the Main Buntsandstein Subgroup, depth and time isochores were constructed which were combined with the interpretation of the base Altena Group to shape an interpretation for the top and base Main Buntsandstein

Subgroup. It is an acceptable workflow, since no major hiatus or unconformity exists between those horizons tops (figure 2.4; *Winstanley, 1993*). This was done with the Structural Framework module (see next section). The end result of this process is presented further on in this report (section 5.1 and 6.1). For the other key horizons in the area, namely the base Middle/Upper North Sea Group, base Lower North Sea Group, base Chalk Group and base Schieland Group, the low resolution two-way-time grid interpretations of TNO are used from the Dutch Oil- and Gas Portal (*nlog*). These horizons were of good enough quality for the purpose of this study, since this study focused on the much deeper horizons.

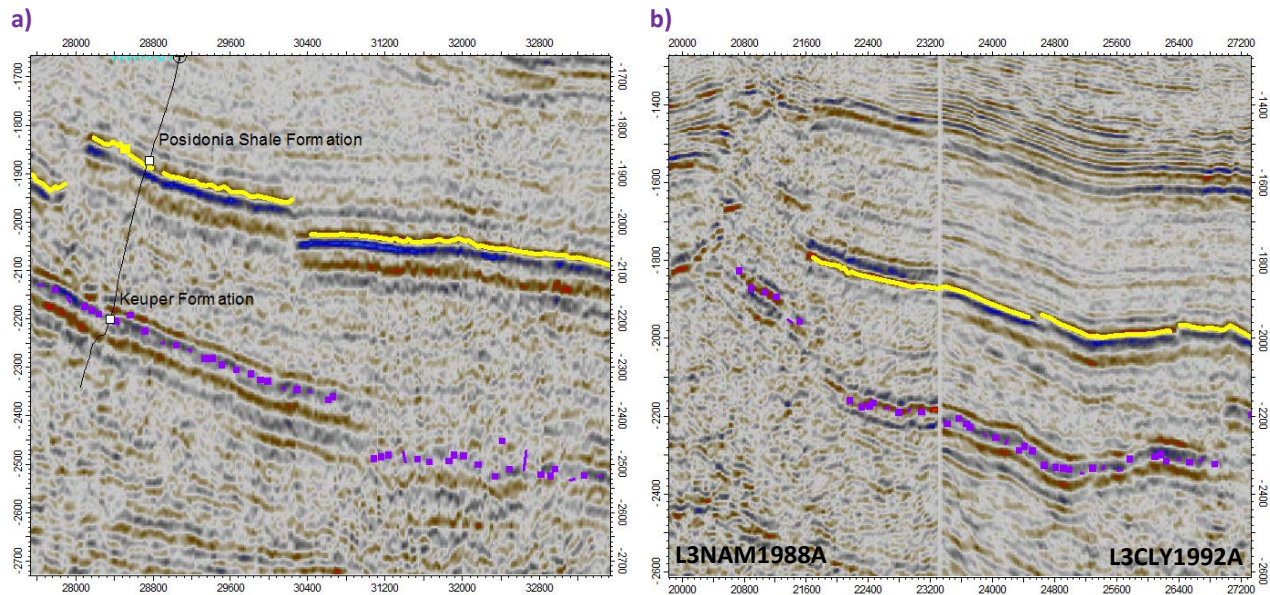


Figure 3.6: a) Example of the validation of the seismic picks of the top Posidonia Shale Formation (yellow) and the base Altena Group (top Keuper Formation; purple) with well WWK-01, Xline 2957 L2CLY1992A. b) Picks at the boundary between the two 3D seismic cubes, Xline 3107. The character of the surrounding reflectors of the Posidonia Shale changes. The blue negative reflector of the base Altena becomes less prominent so the prominent red reflector had to be picked to continue interpretation. Red indicate a positive reflector and blue a negative reflector.

During the workflow of horizon interpretation, faults have also been identified. In the area of 3D seismic this was relatively easy as the lateral extend of the different faults could be visualized in great detail. In the area of 2D seismic this was more difficult. The approach here was to interpret the faults per seismic line and afterwards connect them laterally. In this process a general fault trend of NW-SE was assumed and faults were connected if they were in line with a general displacement profile for a fault. In several situations the seismic line was of low quality making fault interpretation difficult. Here, surrounding 2D seismic lines were used to guide the interpretation. Also fault trace maps of TNO from the Dutch Oil and Gas Portal (*nlog.nl*) were used as a guide in this interpretation workflow.

3.3 Structural Framework Modeling (Petrel)

Recently, Slumberger has introduced a new module in Petrel which allows both fault and horizons interpretation data to be combined together to construct a structural model. This module can be seen as a different approach to the traditional fault modeling and pillar gridding workflow. It allows models to be built on the fly in a 'Modeling while interpreting' workflow. The structural framework module consists of three processes: (1) *geometry definition* (2) *fault framework modeling* and (3) *horizon modeling*. In the geometry definition process, the area of interest is defined as well as the grid resolution of the model. The latter two are the main processes of the structural framework modeling workflow. These will be discussed below.

3.3.1 Fault framework modeling

In the fault framework modeling, faults are modeled from their seismic inputs into individual smoothed surfaces and bound by a fault tip loop, representing the edge of the fault. This edge can be modeled at or beyond its initial interpretation with a set of extrapolation distances (10, 50, 100, 200, 500 and 1000). The latter is ideal in situations where data density is low such as in parts of the study area with limited 2D seismic coverage, allowing the construction of a fault with a smooth fault displacement profile. Another advantage of this modeling workflow compared to the traditional fault modeling and pillar gridding is that when you make changes in the seismic interpretation these can directly be updated into the model instead of having to reconstruct the fault pillars through the fault modeling process. An important aspect of the fault framework modeling workflow is the definition of fault truncation relationships. This is a critical step in the overall process as this may lead to problems during horizon modeling if these are not correctly defined (more on this in the discussion). The process of getting these truncations right is a useful tool as it makes one think if the fault interpretation makes good geological sense or if its structurally feasible. In situations where it is difficult to correctly connect two truncating faults or it does not give the desired end result, this might be an indication that the initial interpretation of the faults is geologically not feasible.

3.3.2 Horizon modeling

The next step in the workflow is adding horizons to the model. The horizons modeling process will first create horizons individually honoring the fault surfaces. If the option ‘apply geological rules and create zone model’ is toggled on, the process will apply horizon truncation rules following the horizon type that has been selected (figure 3.7). It is recommended to run this option at the final stage in the modeling procedure as it greatly increases the calculating time of the model. Input for the horizon modeling process can vary from seismic interpretation to points sets, (fault) polygons, surfaces and isochore maps (figure 3.7). Horizon interpretations with only sparse data may be guided by another surface, with the use of the ‘conforms to’ option. The horizon will then be shaped by another horizon, which can be manually selected. The latter option was very valuable in this study.

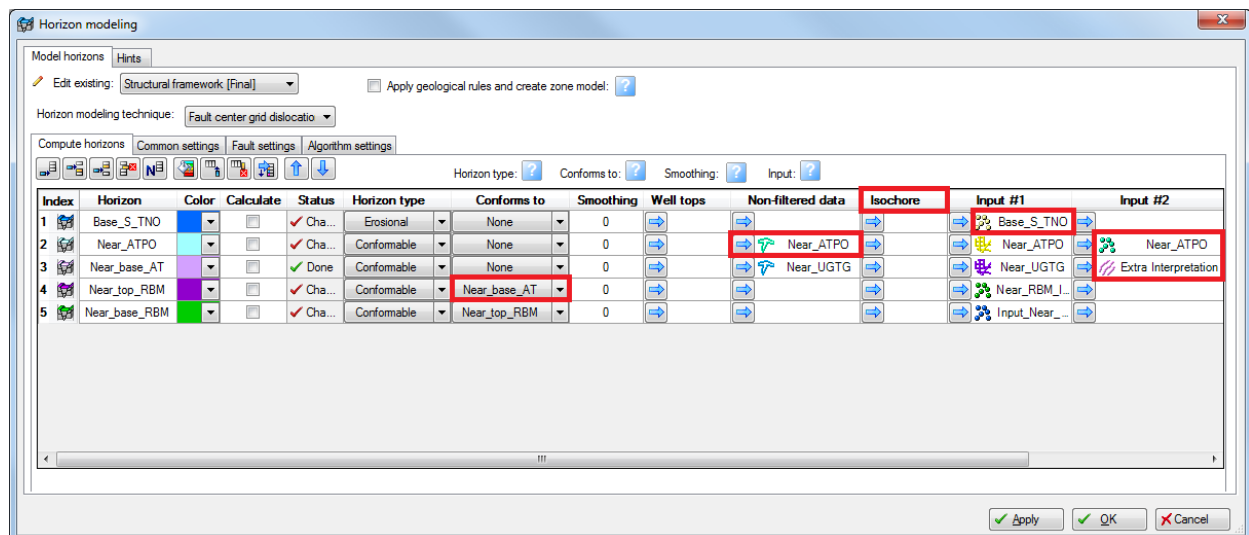


Figure 3.7: Horizon modeling pane. The red boxes indicate different input settings such as the ‘conforms to’ option, fault polygons as non-filtered data input, isochore map input, point sets and seismic interpretation (Input #1) and additional point and polygon input (input #2).

3.3.3 Depth Structural Framework

As a final step, it is possible to create a structural framework in depth using input data that has already been depth converted. Direct time-depth conversion of a structural framework is not possible. Rather, the input

data is depth converted and the model reconstructed based on this depth converted input data. For this purpose, a velocity model is needed. To get a good structural framework in depth, a lot of quality control is needed as due to the depth conversion process, fault plane geometries tend to change. Fault truncation relationships have to be redefined. Also this change in shape causes data spill across faults. This leads to a lot of inconsistencies and glitches in the model when left untouched. To remove these inconsistencies is a time consuming process.

3.4 Velocity Model and Time-Depth Conversion

After seismic interpretation and construction of the Structural Framework Model, the next step was to construct a velocity model to convert the time model to depth. In the Roer Valley Graben there are only eight wells with checkshot data making it difficult to construct a good velocity model. The velocity model available for the area is the Velmod-2 model, a velocity model that covers the Dutch on- and offshore, constructed by TNO in corporation with eleven E&P companies in the Netherlands (*Van Dalfsen et al., 2007*). This model includes V_0 maps, V_{int} maps and K-values for the key horizons in the Roer Valley Graben. For the construction of the velocity model, the detailed interpretations that came out of the structural framework modeling process were used (base Altena and top Main Buntsandstein) in combination with the available two-way-time-grids from TNO for the base Upper North Sea Group, base Lower/Middle North Sea Group, base Chalk and base Schieland. The base of the model was defined by a horizontal surface ($Z = -4000$ ms) being the lower interval of the Lower Germanic Trias Group. In the workflow of finding a best fit velocity model with the well tops, firstly the Velmod-2 model was run and the results cross-checked. This was followed by a run in which Petrel calculated the V_0 and K-values relationship from the available checkshot data, the results were again cross-checked with the well tops. A third step was to check the results of a hybrid velocity model with input from the Velmod-2 model and well time-depth relations calculated by Petrel (figure 3.8). This resulted in a better approximation of the time-depth relation with respect to the well tops compared to the previous velocity models. As a final step this hybrid velocity model was run with well corrections. By definition, the residuals between the wells were reduced to zero. The corrected well top residuals are presented in table 1.

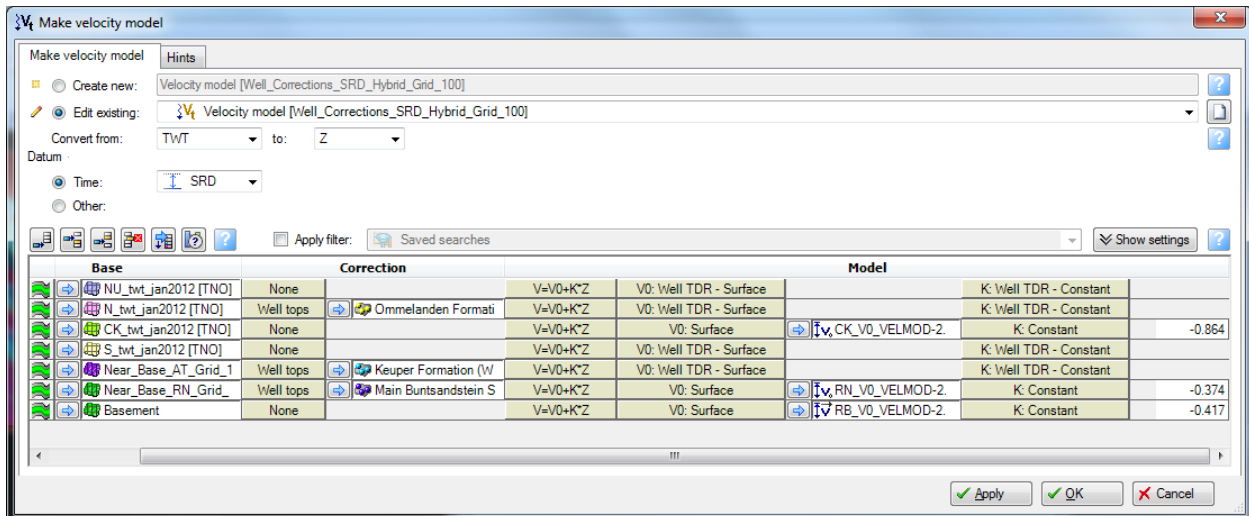


Figure 3.8: The hybrid velocity model used with corresponding settings in Petrel. The K-values used are from the Velmod-2 Velocity model.

Well	Base AT	Near top RBM
	Before	Before
SPC-01	189	198.23
WAA-01	88.17	46.02
HSW-01-S1		13.21
WWN-03	103.02	116.47
BUM-01	212.38	464.47
GWD-01	280.79	
BKZ-01	126.22	165.90
WWS-01-S1	-56.63	-24.40
SPG-01-S2	-20.63	9.82
SMG-01	-92.18	-61.17
WWN-01-S2	211.58	82.99
VRK-01	58.23	22.24
WWS-02	-40.48	9.24

Well	Base AT	Near top RBM
	Before	Before
GWD-01-S1	273.56	
WWK-01	18.50	33.57
HVB-01	-23.49	-16.40
AND-06	-22.86	-32.65
KDK-01	3.15	19.25
HBV-01	397.36	427.09
KWK-01	-124.64	-108.28
WWN-02-S4	133.53	89.93
BRAK-01	-94.77	-84.90
LOZ-01	41.44	
WAA-01-S1	88.13	42.06
HSW-01	64.97	
AST-01	138.26	301.44

Table 1: The well residuals of the depth conversion of the base Altena Group and the near top Main Buntsandstein.

3.5 Lead identification

After the construction of the structural framework and the velocity model, the framework was converted to depth. The near top depth map of the Main Buntsandstein Subgroup was used to identify potential structures which could accommodate accumulation of hydrocarbons. This was done by creating a general Z slice intersection which could be moved up and down to identify spill points of different structures. An example for the Waalwijk Field is given in figure 3.9. Both the top and base Buntsandstein Subgroup were used to calculate the gross-rock volume of each structure.

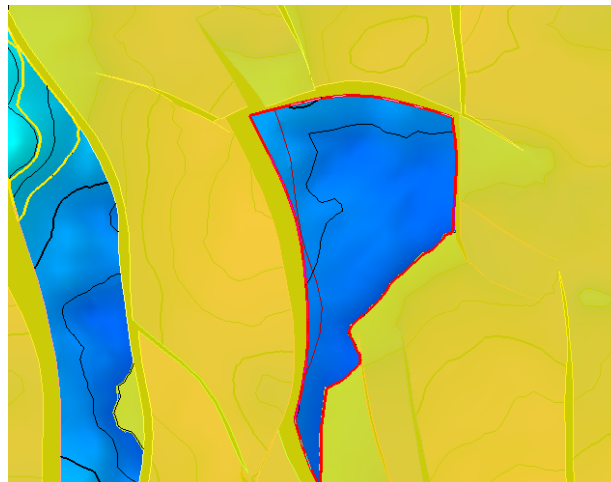


Figure 3.9: Example of a Z-slice intersection through the Waalwijk Field (in red) at a depth of 3000m. The surface surrounds the structure meaning no spill occurs, if the side faults are sealing and top seal is present.

4. The hydrocarbon system of the Roer Valley Graben

The first discovery in the vicinity of the Roer Valley Graben is the Waalwijk area. Here gas was found in Waalwijk-1 (BP, 1987), Kerkwijk-1 (NAM, 1988) and in Loon op Zand (Waalwijk-Zuid-1, Clyde Petroleum, 1991) in which the Triassic Röt and Main Buntsandstein Formations were targeted. (*van Hulst, 2009*). This was followed by some other discoveries like the Andel (NAM, 1991) and Brakel (Northern Petroleum, 1992) fields.

Within the Roer Valley Graben two different plays have been identified, an oil and a gas play. The gas play is a proven play mechanism with gas charge from the Westphalian Coals (and possibly Namurian Shales) into tilted fault blocks of the Triassic (figure 4.1). The play mechanisms for the oil occurrences is still unproven. The most probable mechanism is charge from the Posidonia Shale into juxtaposed reservoirs of the Triassic (figure 4.1). However, these configuration are limited within the Roer Valley Graben and maturity is questionable. Another option are the Namurian Shales.

This section will discuss the hydrocarbon system with respect to the five major components: the reservoir, source, seal, trapping mechanisms and timing. In figure 4.2 an overview of the encountered fields in the Roer Valley Graben (and West Netherlands Basin) is given. For each field the reservoir formation (figure 4.2a) and source rock signature (figure 4.2b) has been indicated.

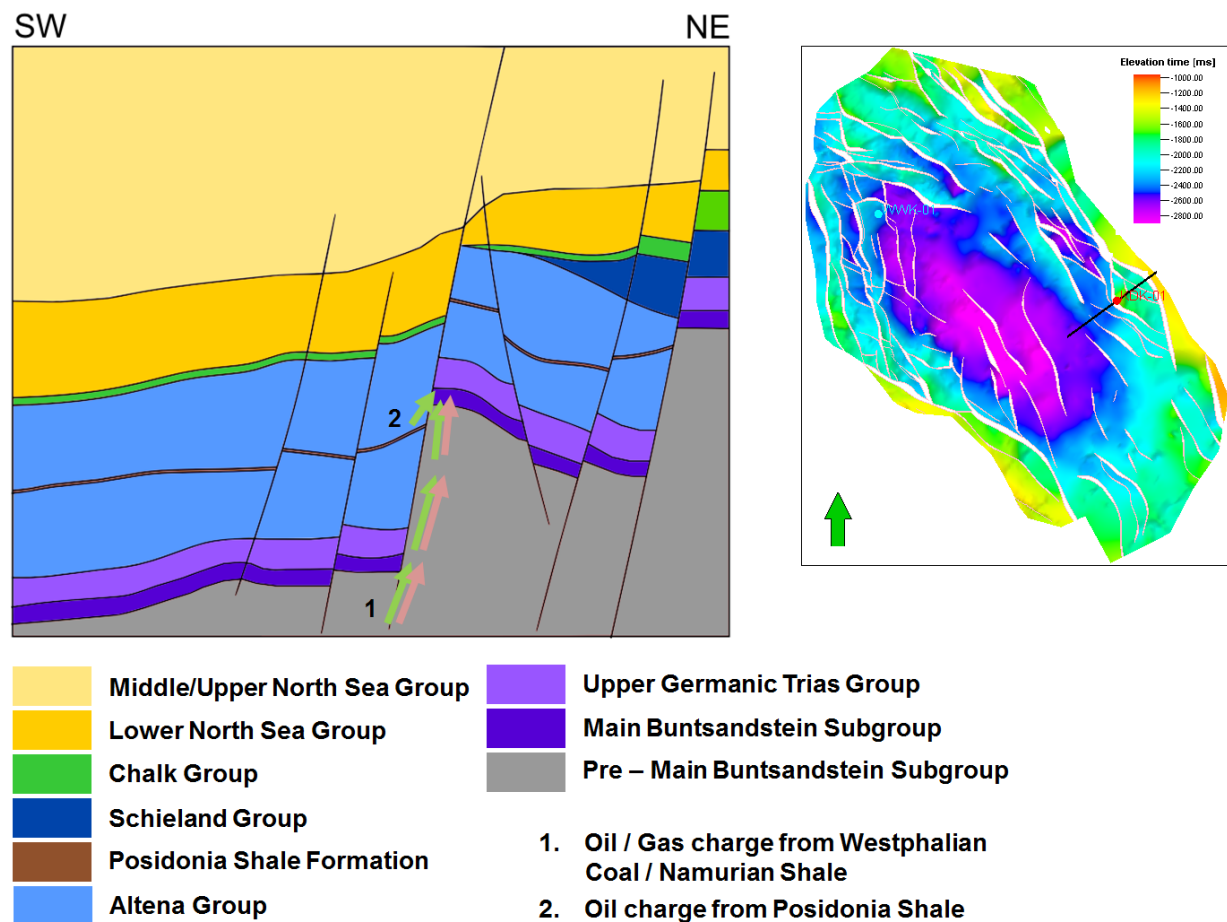


Figure 4.1: Example of the play mechanisms in the Roer Valley Graben.

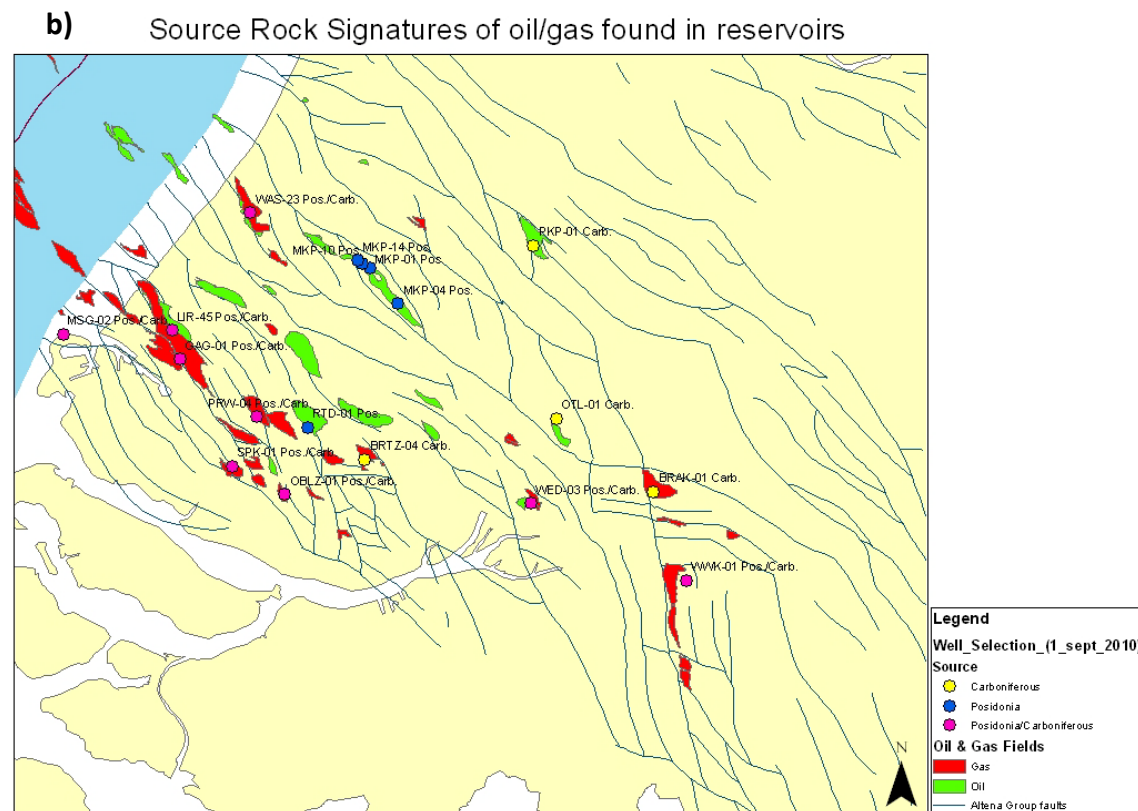
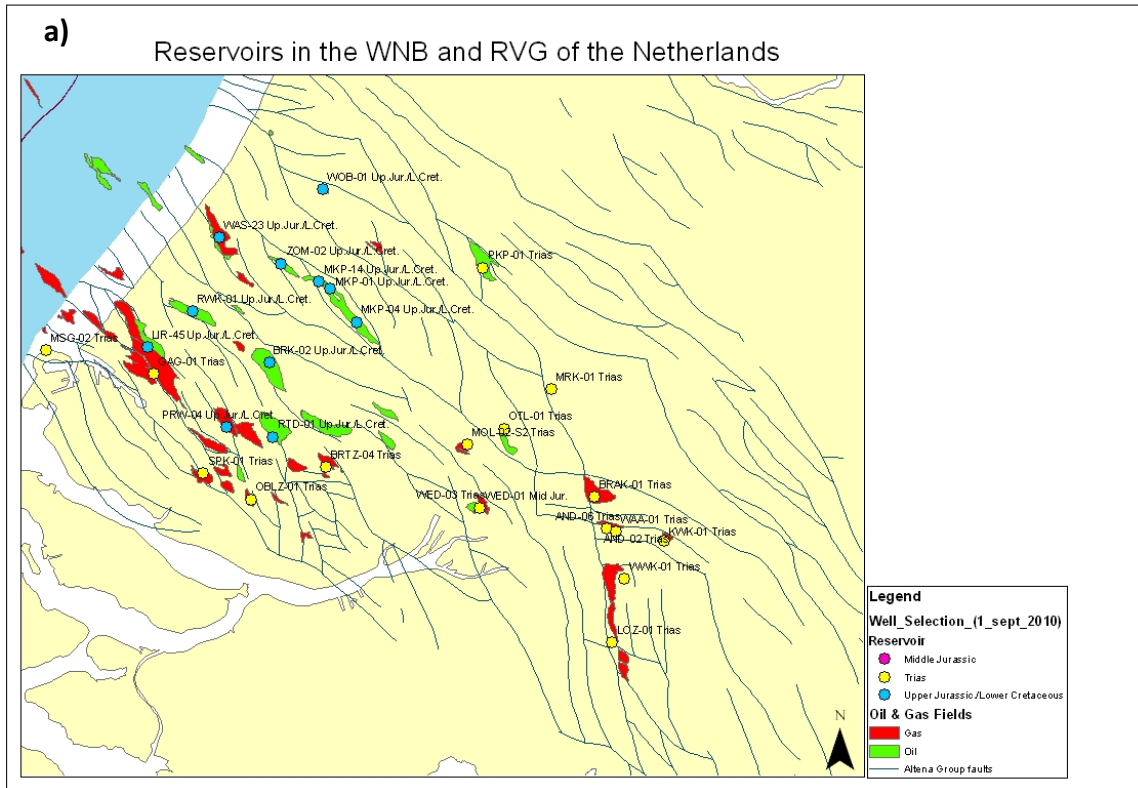


Figure 4.2: Maps of the West Netherlands Basin and the Roer Valley graben with their respective oil and gas fields. For each field the reservoir formation (a) and source rock signature (b) has been indicated. Source: *EBN (2012)*.

4.1 Reservoir

The current gas fields of the Roer Valley Graben are situated in the Upper Germanic Trias Group (Röt Fm) and the Lower Germanic Trias Group (the Main Buntsandstein Subgroup) belonging to the pre-rift mega-sequence in the Waalwijk license area. They are composed of alluvial fan deposits formed at the confluence of alluvial fan systems emanating from the southwest and southeast (*Winstanley, 1993*). Four distinct cycles of fan development can be recognized, three in the Main Buntsandstein Subgroup and one in the Röt Formation. The division between sandstones and shales is not very precise due to the proximal setting of the graben during time of deposition (*Winstanley, 1993*). In figure 4.3, a plot of porosity versus burial depth for the Triassic reservoir is presented. Measured porosities vary between 4 and 24%. The average net-to-gross in the Waalwijk North Field is 53% (*Winstanley, 1993*). A cross-check on the gamma-ray indicated a average net-to-gross of 57%.

Well correlation (figure 4.4) of the Triassic reservoirs indicate a relatively constant thickness for the Röt Fringe sandstones, however thickness is low compared to the Main Buntsandstein equivalents. The Volpriehausen seems to have the most favorable thickness and distribution throughout the graben.

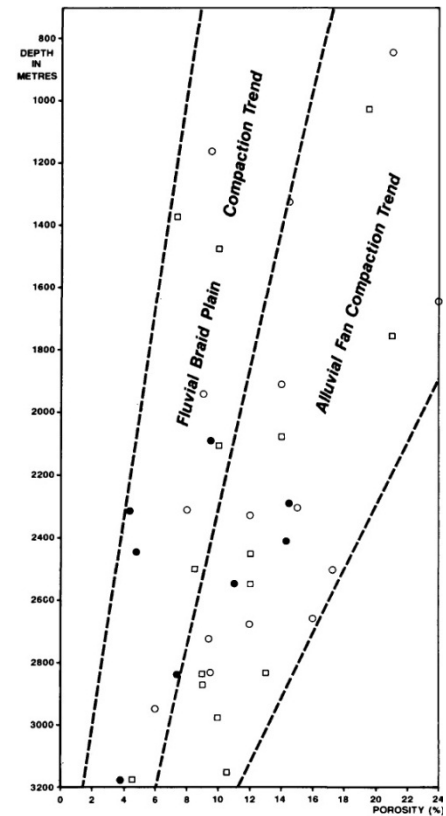


Figure 4.3: Plot of porosity versus depth of burial for the Triassic reservoir in wells within the Roer Valley Graben. Source: *Winstanley, 1993*.

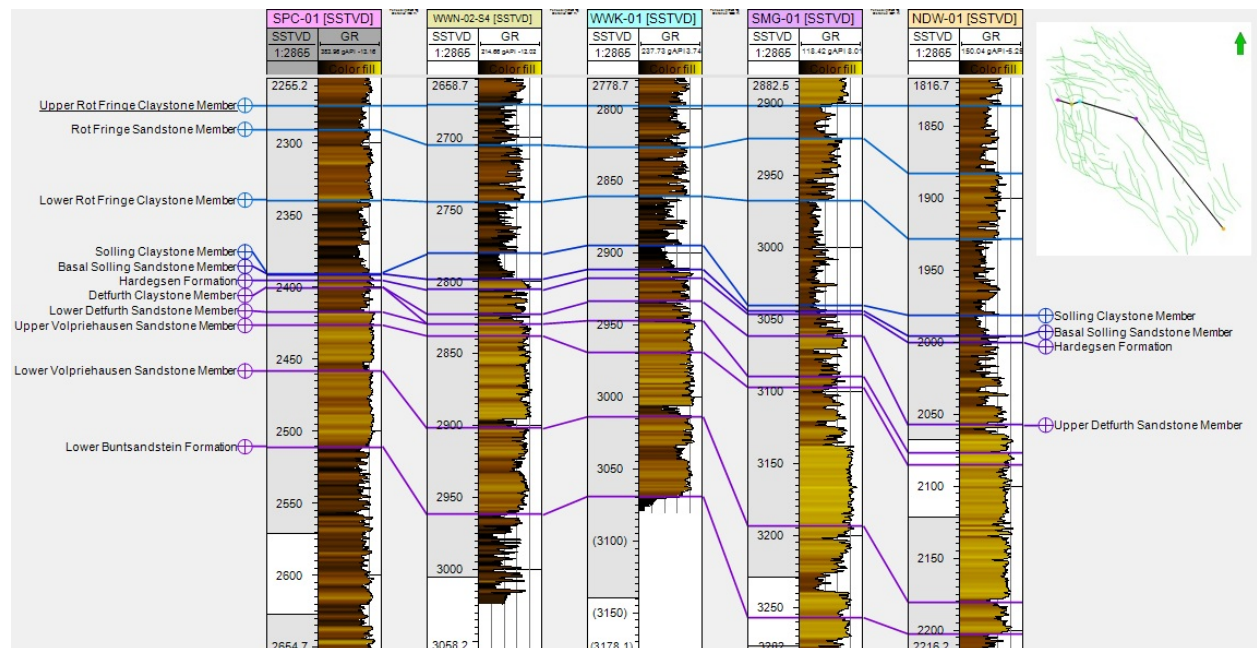


Figure 4.4: Log correlation of the reservoir section between SPC-01, WWN-02, WWK-01, SMG-01 and NDW-01, respectively from west to east. The green lines indicate the fault center lines at top Main Buntsandstein level.

4.2 Source

In the study area of the Roer Valley Graben there are several source rocks present that (may) have contributed to the encountered oil and gas shows. These include, the Namurian Shales (Geverik Member), the Westphalian Coal measures (Caumer Subgroup) and the Jurassic oil-prone marine shales of the Altena Group (Sleen, Aalburg and Posidonia Formations) of which the Posidonia Shale is deemed the most probable (*Bouw & Lutgert, 2012*). As the focus of this study lies on the oil prospectivity of the Posidonia Shale this source rock will be discussed in more detail in a separate section.

The Namurian Shales have been suggested as the second most probable option as a possible contributor to the oil encountered (*Winstanley, 1993*). Data on these shales is virtually absent in the area and a correlation between shows and source rock have never been proven. *Van Balen et al., 2000* identified the Namurian Shales as a Type II Kerogen source rock with a TOC of up to 8%. Vitrinite reflectance modelling has indicated that the Namurian Shales are currently over-mature. The Caumer Subgroup has been identified as the most important source rock for gas in the western part of the Roer Valley Graben, responsible for most of the generated and accumulated gas in the Waalwijk area. The second contributor of gas may have been the Namurian shales. This type of source rock would initially start with oil generation.

The oldest shale of the Altena Group, the Sleen Formation is characterized by its relatively thin deposition compared to the other Jurassic marine shales, Total Organic Content levels below 2% with an average of 1.3% with a standard deviation of 1.1% (*EBN, 2012*) and its classification as a Type IV Kerogen. Correlation of the geochemical signature of the oil occurrences with the Sleen Formation, indicate that this might be the source rock (*NITG, 2001*). However, the characteristics of the Sleen Formation in the Roer Valley Graben are insufficient to have produced the amounts of oil that have been encountered near Loon op Zand (*Winstanley, 1993*). The younger Aalburg Formation is much thicker with an average thickness of 250m. The organic-rich sections of this formation, mainly located in the basal sections can reach TOC levels of up to several percent (*van Leverink & van Bergen, 2008*). However, the majority of the Aalburg Formation is of Type IV Kerogen and shows corresponding low TOC levels, approximately 1% (*EBN, 2012*). Thus based on these observation it is unlikely that this is the main oil source in the area, leaving the Posidonia Shale Formation as the most prolific source.

4.2.1 Posidonia Shale Formation

The Toarcian Posidonia Shale Formation is one of the most important oil source rocks in the Netherlands as it is mainly the source of most oil fields found in the Dutch subsurface. As shown in figure 1.1 the onshore distribution of the Posidonia Shale is mainly limited to the West Netherlands Basin and the Roer Valley Graben. The latter is related to the inversion events during the Late Cretaceous and Early Paleocene (as described in the previous chapter), eroding the formation outside the basinal areas.

The Posidonia Shale Formation, deposited in a marine, anoxic environment and is characterized by its organic-rich black shales, an average thickness of 30 to 60 m and is classified as a Type II Kerogen with average Total Organic Content (TOC) values of 5 to 10% (*Nelskamp & Verweij, 2012*). It forms a very distinctive interval throughout the Netherlands and can be easily recognized on wire-line logs and seismic sections by its high gamma-ray and resistivity readings (*Adrichem Boogaert et al., 1993-1997*), and the low acoustic speeds caused by the organic richness of the formation, forming a clear reflector on seismic.

A recent study re-evaluated the thermal and structural evolution of the West Netherlands Basin and Roer Valley Graben by basin modelling (*Nelskamp & Verweij, 2012*). From this study (and others) it can be concluded that the temperature and maturity calibration within the Roer Valley Graben is difficult (see figure 4.5). In the northwest only several wells with Vitrinite reflectance and temperature measurements are available of which the quality is questionable. In the southern part only data for one well of varying quality is available, namely the Nederweert-1 well (NDW-01). This complicates the reliability of the model as calibration of maturity and temperature is not possible because the measured vitrinite reflectance values are too low to be calibrated using

the measured present-day temperatures which are deemed more reliable (Nelskamp & Verweij, 2012). As an explanation for these observations Nelskamp & Verweij (2012) postulate that the present-day temperature is not equilibrated due to Pleistocene cooling or that large scale fluid flow influences the system. This inability to calibrate maturity and temperature thus has to be taken into account when evaluating interpreted maturity maps of the Posidonia such as the ones presented in figure 4.6. The maturity indicated might be lower than expected. The maturity maps (figure 4.6) indicate the highest maturities in the center of the Roer Valley Graben and west of the Waalwijk area. Here the modelled maturity can vary between 0.8% R_0 up to 1.2% R_0 but mostly a maturity of 0.6 to 0.8% R_0 is modelled which means that the Posidonia Shale is currently at or near maturity for oil in the deeper parts of the graben. Several wells drilled in the area have encountered oil occurrences at the level of the Posidonia Shale Formation (LOZ-01, BKZ-01, HVB-01, VEH-01, KWK-01 and WAP-01) and thus this can be seen as an indication that the Posidonia Shale generated hydrocarbons.

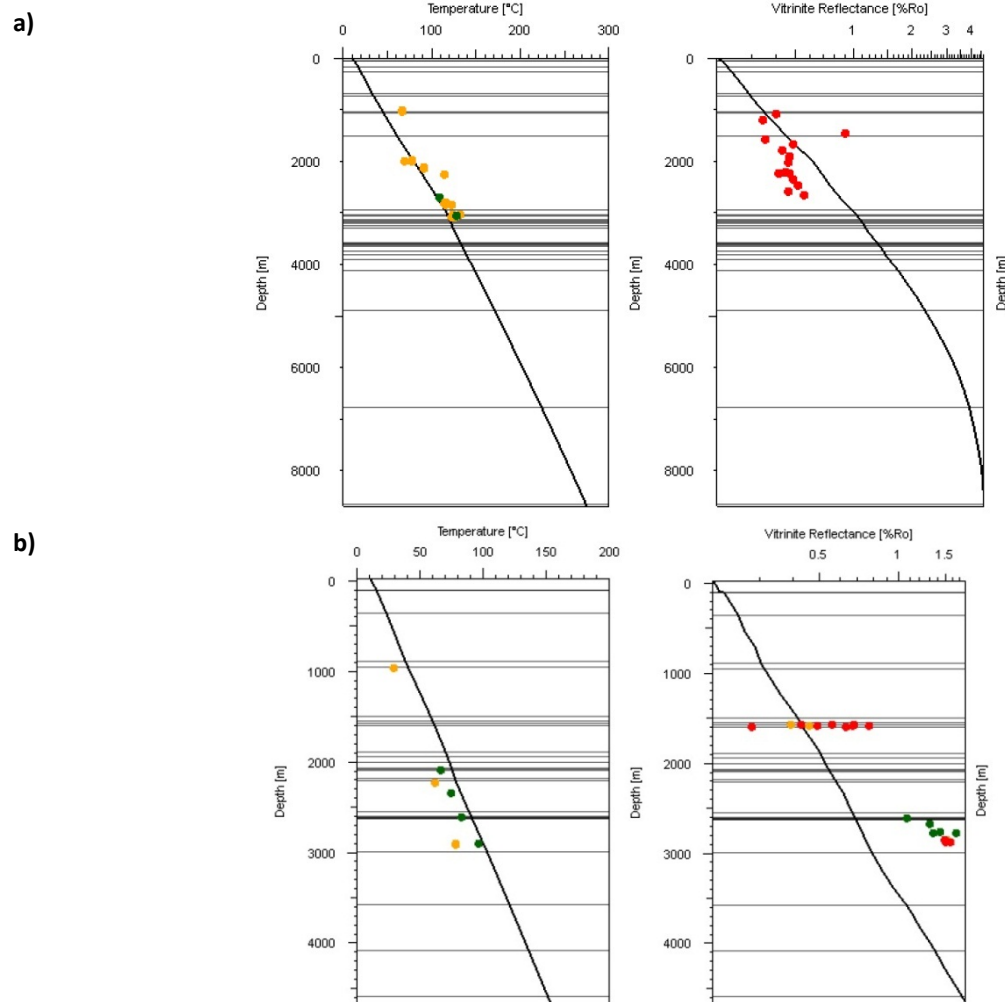


Figure 4.5: Temperature and Vitrinite reflectance calibration of well WWK-01 (a) and NDW-01 (b). Source: Nelskamp & Verweij (2012).

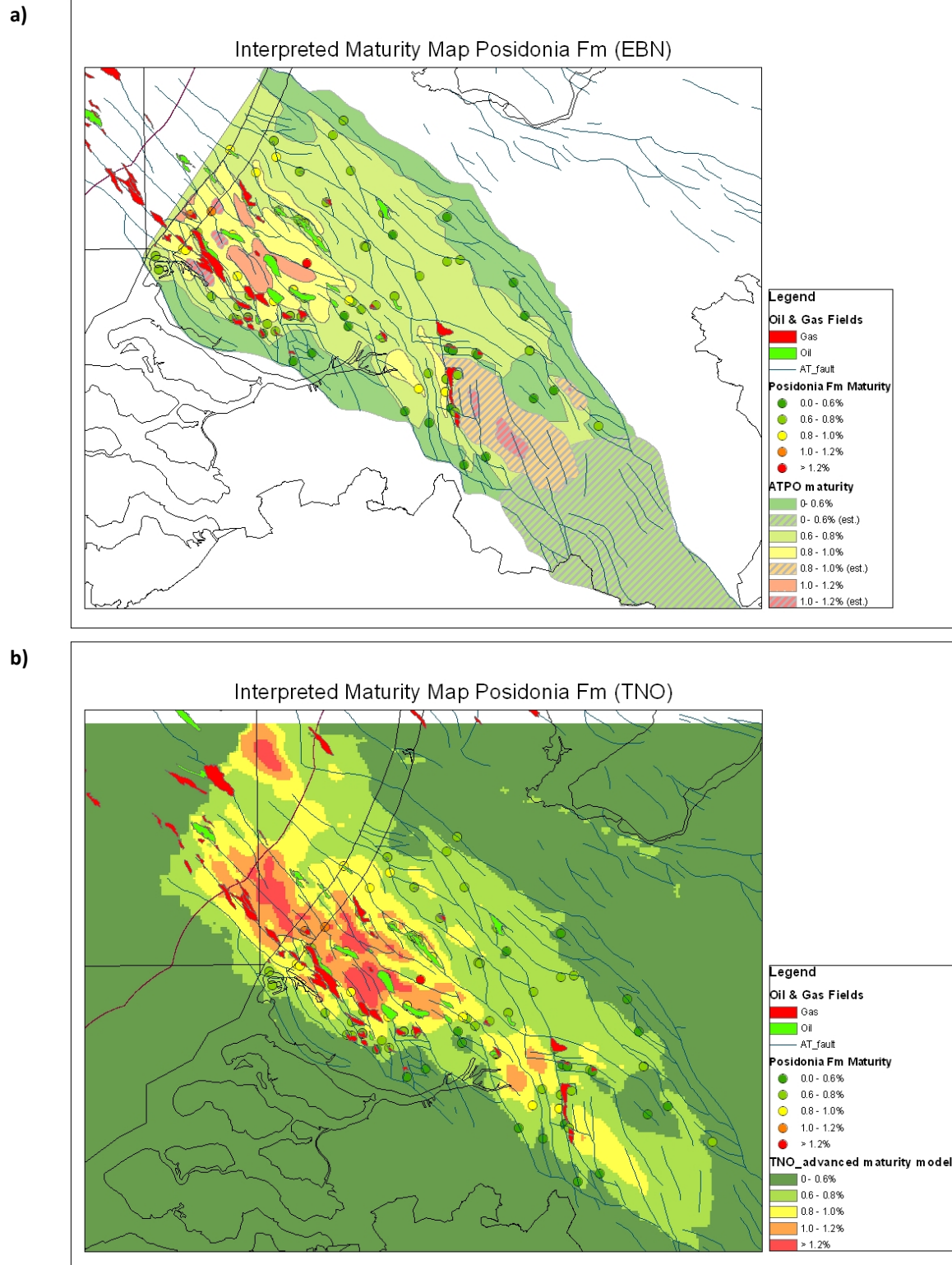


Figure 4.6: Interpreted maturity maps of the Posidonia Shale Formation by Kee, 2010 (a) and TNO (b). The wells which provide maturity data have been indicated. Maturity scale: immature $< 0.6 R_0$, oil $0.6 < R_0 < 0.8$, oil and gas $0.8 < R_0 < 1.0$ and dry gas $1.0 < R_0 < 2.5$. The TNO Map (b) uses a enhanced heat flow of around 80 mW/m^2 . Source: Kee (2010), TNO.

4.3 Seal

The vertical seal for the Lower Triassic play in the Roer Valley Graben is believed to be the shales (and anhydrites) of the Upper Germanic Trias Group and the lateral seal, the Lower Jurassic shales of the Altena Group (Winstanley, 1993). In the area, not much is known on the sealing capacity of these formations due to limited well data. However, they have been proven seals in the Waalwijk area (the Waalwijk, Brakel, Andel and Kerkwijk fields). Here Triassic intra-formational shales of the Solling and Röt Formations act as vertical seals and the Jurassic shales of the Sleen and Aalburg Formations of the Altena group as lateral seals. The latter can also act as the ultimate top seal in the area. The intra-formational shales of the Werkendam Formation (Upper part of the Altena Group) may also act as a lateral seal. However, in several of the previously drilled structures which had the Werkendam juxtaposed next to the reservoir sections proved to be dry (see section 4.4). This is probably the cause of local sandy intervals within the Formation, not the lack of sealing potential of the shales.

4.4 Trapping mechanisms

So far several structural traps have been drilled, mainly fault-dip closures of which the Waalwijk structure is most successful as here gas has been found and is being produced. Kerkwijk is currently marked as an undeveloped field. The trap structures are vertically sealed by the shales of the Upper Germanic Trias Group and laterally by the shale formations of the Altena Group (Lower Jurassic). The structures that proved to be dry at the level of the Triassic reservoirs is most probably explained by the presence of local sandy intervals within the sealing Formations of the Solling Claystones, Röt Claystones and Altena Group or the lack of charge. This chapter will discuss the structural traps that have been drilled so far (figure 4.7), to identify proven trapping mechanisms in the play system of the Roer Valley Graben.

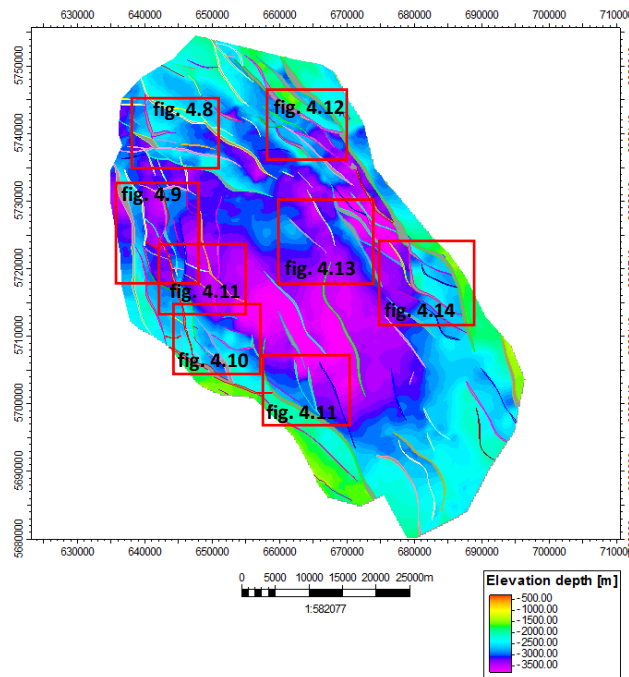


Figure 4.7: Depth map of the Main Buntsandstein Subgroup. The red boxes indicate the different sectors in which previously structural closures have been drilled, discussed in the following sections.

4.4.1 Brakel, Andel & Kerkwijk

The primary objective of the Brakel-1 well (1992) was to test the Middle and Upper Bunter reservoirs for gas in an independent fault block, which forms part of a large regional high dissected by an orthogonal fault system

(figure 4.8a-b) just 3 km north of the Andel structure, a different enclosure on the same regional high. To the east the Kerkwijk-1 well (NAM, 1998) was drilled in a different titled fault block (figure 4.8c).

Brakel-1 tested gas in the Upper and Middle Bunter (Upper Volpriehausen and Detfurth Formation) and consists of two blocks; the drilled main block and a small Southern, undrilled block (NPN, 2008). The Brakel-1 well has also encountered minor amounts of oil in the Delfland, Röt (Röt Fringe Sandstone Member) and Buntsandstein Formations (Detfurth and Upper Volpriehausen Formation). Andel-6 encountered a fair to good significance of oil in the Delfland, Middle Werkendam, Röt (Röt Fringe Sandstone) and Bunter Formations (Detfurth). Kerkwijk-1 encountered good oil shows at the Rogenstein Member (Lower Buntsandstein Subgroup), Detfurth Formation, Röt Fringe Formations and the Middle/Upper Werkendam Formation. Good gas shows were encountered in the Röt , Aalburg and Posidonia Formations.

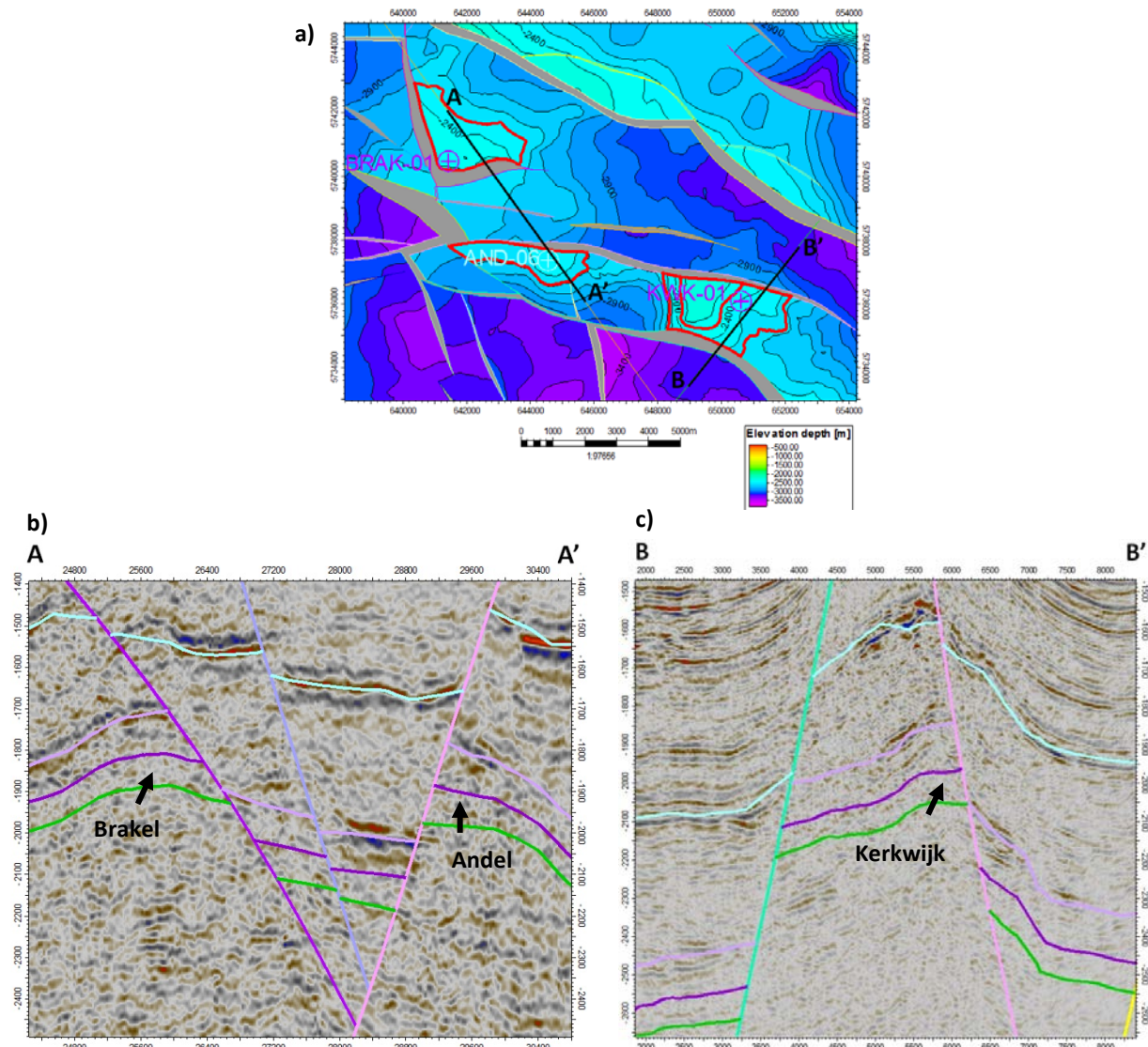


Figure 4.8: Depth map of near top Main Buntsandstein Subgroup (a). Indicated in red are the structural closures. Kerkwijk-1 shows two outlines, a minimum and a maximum. The cross-section through Brakel and Andel (b) is a random seismic line from the 3D Terra cube. The line through Kerkwijk is represented by line 871912 from the L2NAM1987J survey (c). green = near base Main Buntsandstein Subgroup, dark purple = near top Main Buntsandstein, light purple = near base Altena Group, cyan = near top Posidonia Shale and dark blue = base Schieland Group (TNO).

4.4.2 Waalwijk Area

The Waalwijk-1 well's (1987) main target was the large fault-dip closed high (figure 4.9a-b) at both Brabant Formation (oil) and Bunter Group (gas) level. Only minor oil shows were encountered while drilling in the Brabant Formation and the Middle Werkendam Member. The Bunter target yielded commercial gas accumulations with subordinate amounts of condensate (BP, 1987). More of this fault-dip closed high was successfully targeted by the Waalwijk North-1 and Waalwijk North-2 wells at Upper and Middle Bunter level. This was followed by the further expansion of the Waalwijk Gas Field with the Sprang-1 well (Clyde Petroleum 1994) which targeted additional sandstones of the Triassic Röt and Main Buntsandstein Formations just to the south of the Waalwijk-1 well and the Waalwijk North-3 (Clyde Petroleum 1998) which targeted additional Triassic sandstones north of wells Waalwijk North-1 and Waalwijk North-2 (Clyde, 1999). The Waalwijk South-1 (Clyde Petroleum 1991) and Waalwijk South-2 (Clyde Petroleum 2005) wells were drilled in different fault compartments of the Waalwijk structure, namely the Loon op Zand Structure which was first drilled by the NAM in 1953 (figure 4.9a). However, this fault block proved to be dry, although good oil significance was encountered in the Upper and Middle North Sea Supergroup (Oosterhout Fm. and Breda Fm.) and the Upper Brabant Limestone, Middle Werkendam, Posidonia Shale and Aalburg Formations. Waalwijk South-1 encountered a good oil shows in the Delfland, Röt and Main Buntsandstein Formations.

To the west of the Waalwijk structure two other prospects have been drilled, namely the Sprang Capelle-1 (BP 1987) and Huibeven-1 (Clyde Petroleum 2002) which targeted two other tilted fault blocks (figure 4.9c-d) with the Triassic reservoir sections as the main target. These structural closures proved to be dry. However, the wells did encounter signs of hydrocarbons. The Sprang Capelle-1 well encountered fair to good gas shows in the Röt Fringe Sandstones and the Upper Volpriehausen. The Huibeven-1 well encountered weak oil shows in the Röt Fringe Sandstone Mb., Röt Fringe Claystone Mb. and the Detfurth Formation.

4.4.3 Hilvarenbeek & Broekzijde

Further southward of the elongated Waalwijk structure, two other prospects have been drilled (figure 4.10), the Hilvarenbeek-1 (Clyde Petroleum 1995) and Broekzijde-1 (BP 1989). Both wells targeted the Triassic reservoirs in tilted fault blocks. Hilvarenbeek-1 encountered good reservoir quality in the Lower Detfurth Sandstone Mb. with porosities of 20 to 23%. Unfortunately, the structure proved to be dry and log evaluation indicated that the Triassic sandstones are 100% water saturated (Clyde, 1996). However, the well did encounter weak oil shows in the Röt Fringe Sandstone and Claystone Member, the Lower Muschelkalk Member, the Brabant Formation and the Posidonia Shale. Weak signs of gas were encountered in the Aalburg and Posidonia Shale Formations. The Broekzijde-1 well was plugged and abandoned dry with weak to good oil shows in the Lower Werkendam Member, Sleen Formation, Röt Fringe Sandstone Member, several good oil shows in the Detfurth and Volpriehausen Formations and hydrocarbon potential was recognized within Jurassic Brabant limestones in a small four-way dip-closure (BP, 1989).

4.4.4 Oisterwijk & Veldhoven

The wells Oisterwijk-1 (NAM 1959) and Veldhoven-1 (1959 NAM), respectively did not drill further than the Jurassic Lower Werkendam Formation and the Jurassic Aalburg Formation. They did not reach the Main Buntsandstein Subgroup. It is unclear what the main target of both wells was. Documentation on the Dutch Oil and Gas Portal is limited, no well reports are available. It is postulated that it was initially thought that the Main Buntsandstein Subgroup was interpreted at a shallower level. It is also plausible that the small folded structures on the seismic were targeted. A review of the composite logs which were available through the Dutch Oil and Gas Portal, indicate poor oil shows at the level of the Posidonia Shale, Aalburg Formation, Upper Werkendam Formation and the Brabant Formation for the Veldhoven-1 well. Oisterwijk-1 shows poor oil shows at the Lower Werkendam, Upper Werkendam and Brabant Formations. A review of the composite logs which were available through the Dutch Oil

and Gas Portal, indicate poor oil shows at the level of the Posidonia Shale, Aalburg Formation, Upper Werkendam Formation and the Brabant Formation for the Veldhoven-1 well. Oosterwijk-1 shows poor oil shows at the Lower Werkendam, Upper Werkendam and Brabant Formations.

4.4.5 Varik & Gewande

Varik-1 (NAM 1995) and Gewande-1 (NAM 1991) were both two promising structural closures on the Northeastern flank of the graben (figure 4.12). Unfortunately, both tilted fault blocks were dry at the targeted Triassic reservoirs. The Varik-1 well did not drill further than the Lower Röt Fringe Sandstone Member, the Main Buntsandstein Subgroup was not reached. Poor to good oil shows were encountered in the Upper Röt Fringe Claystone and Röt Fringe Sandstone Members. Several good shows were observed in the Hardeggen Formation. The Gewande-1 well encountered fair gas shows in the Upper North Sea Group (Breda Formation) and poor to fair oil shows in the Aalburg Formation, Upper Muschelkalk Member and Upper Röt Fringe Claystone Member.

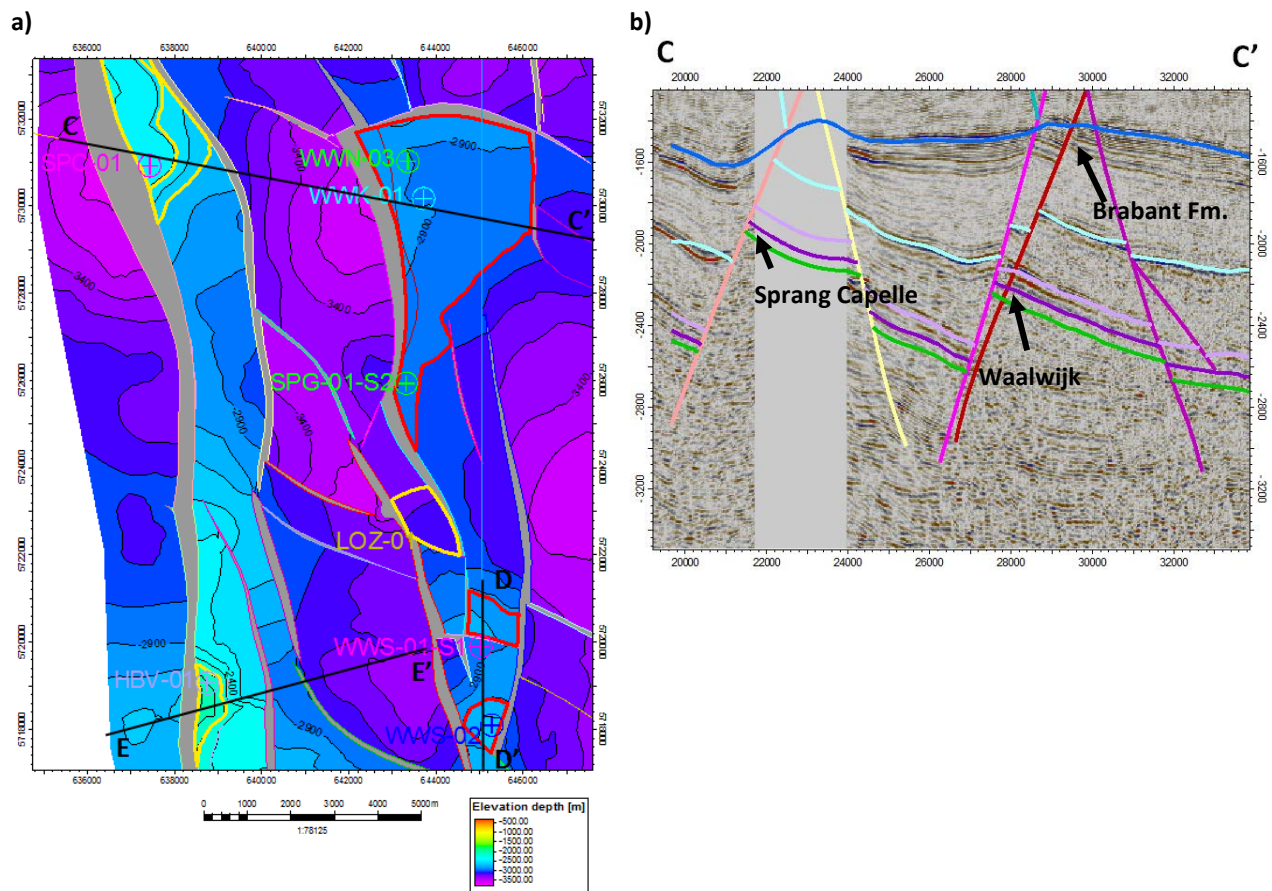


Figure 4.9: Depth map of near top Main Buntsandstein Subgroup (a) for the area around wells WWK-01, WWN-03, SPC-01, SPG-01, LOZ-01, WWS-01, WWS-02 and HBV-01. Indicated in yellow are the structural closures which proved to be dry and in red found gas reserves. The cross-section through Sprang Capelle-1 and Waalwijk South (b) is on a random seismic line of the 3D Terra Cube and Inline19813, respectively. The line through Huibeven-1 is represented by line 8407 survey L2BP1984A (c). Horizon colours same as in figure 4.8.

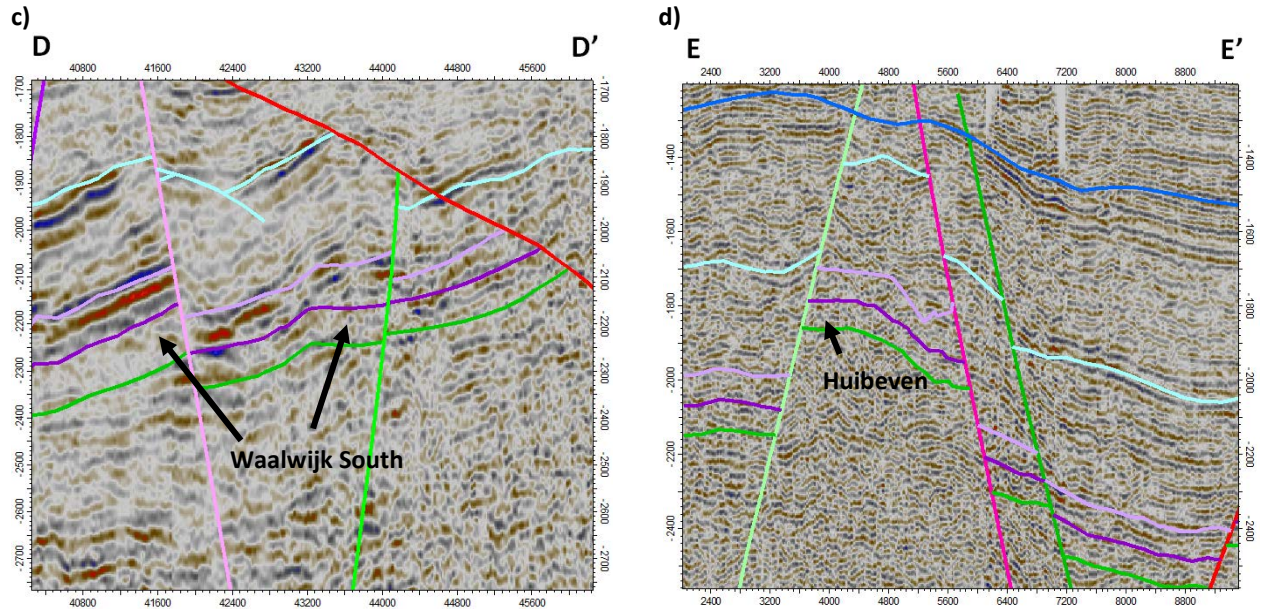


Figure 4.9 (continued)

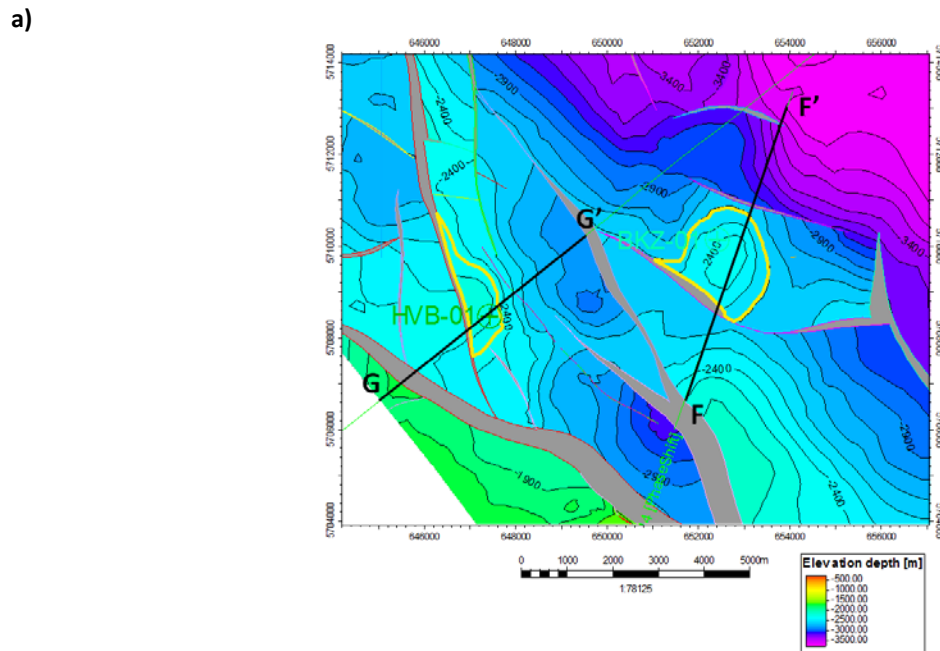


Figure 10: Depth map of near top Main Buntsandstein Subgroup (a) for the area around wells HVB-01 and BKZ-01. Indicated in yellow are the structural closures which proved to be dry. The cross-section through Hilvarenbeek-1 (b) is on seismic line 7006 survey L2NAM1969A. The line through Broekzijde-1 is represented by line 8414 survey L2BP1984A (c). Horizon colours same as in figure 4.8.

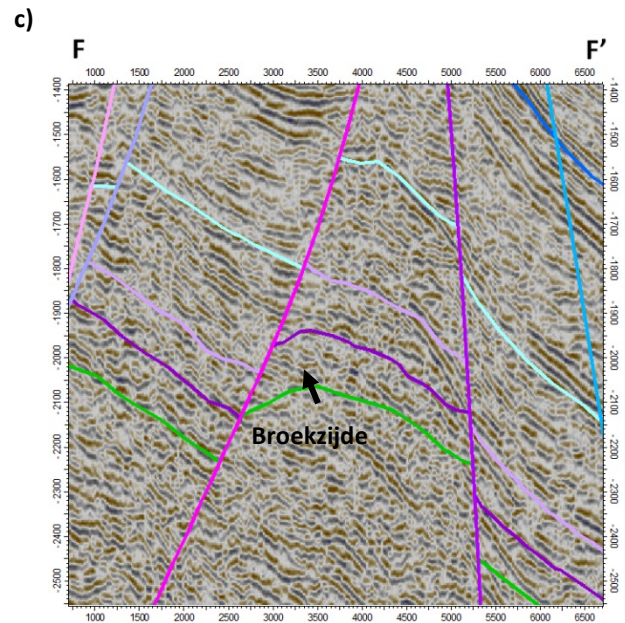
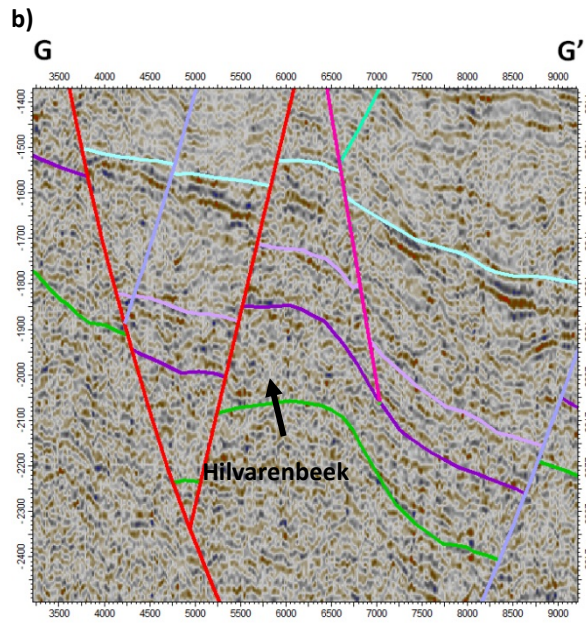


Figure 4.10 (continued)

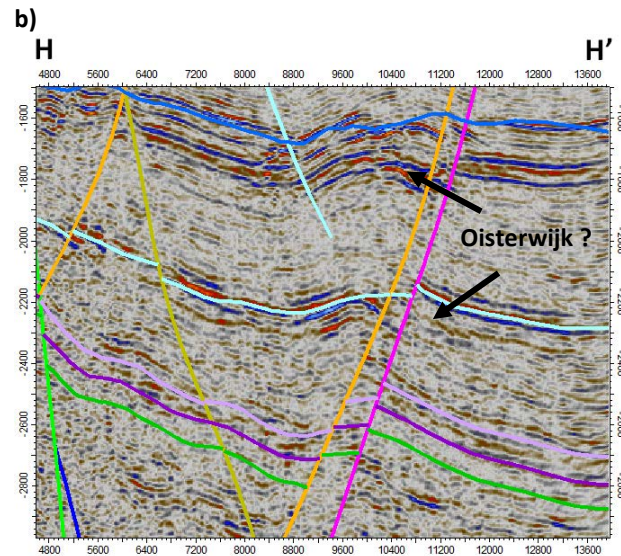
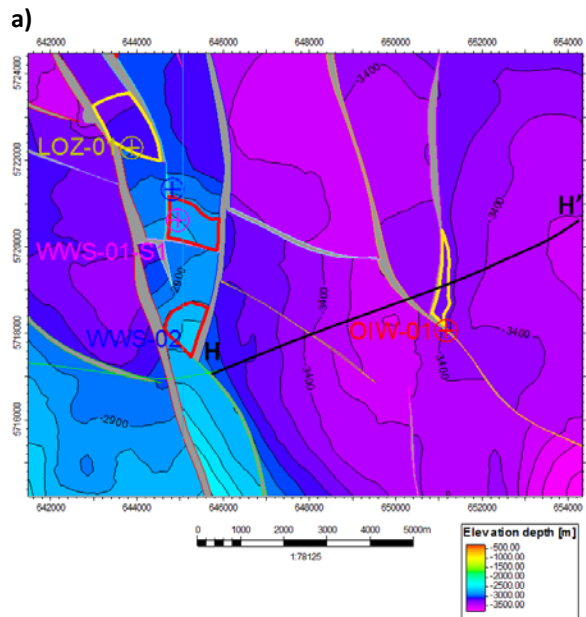


Figure 4.11: Depth map of near top Main Buntsandstein Subgroup (a & c) for the area around wells OIW-01 and VEH-01. Indicated in yellow are the structural closures which proved to be dry and in red found gas reserves. The cross-section through Oisterwijk-1 (b) is on seismic line N89-02 survey L2BP1989A.. The line through Veldhoven-1 is represented by line NBL80-1A survey L2CHE1980A (d). Horizon colours same as in figure 4.8.

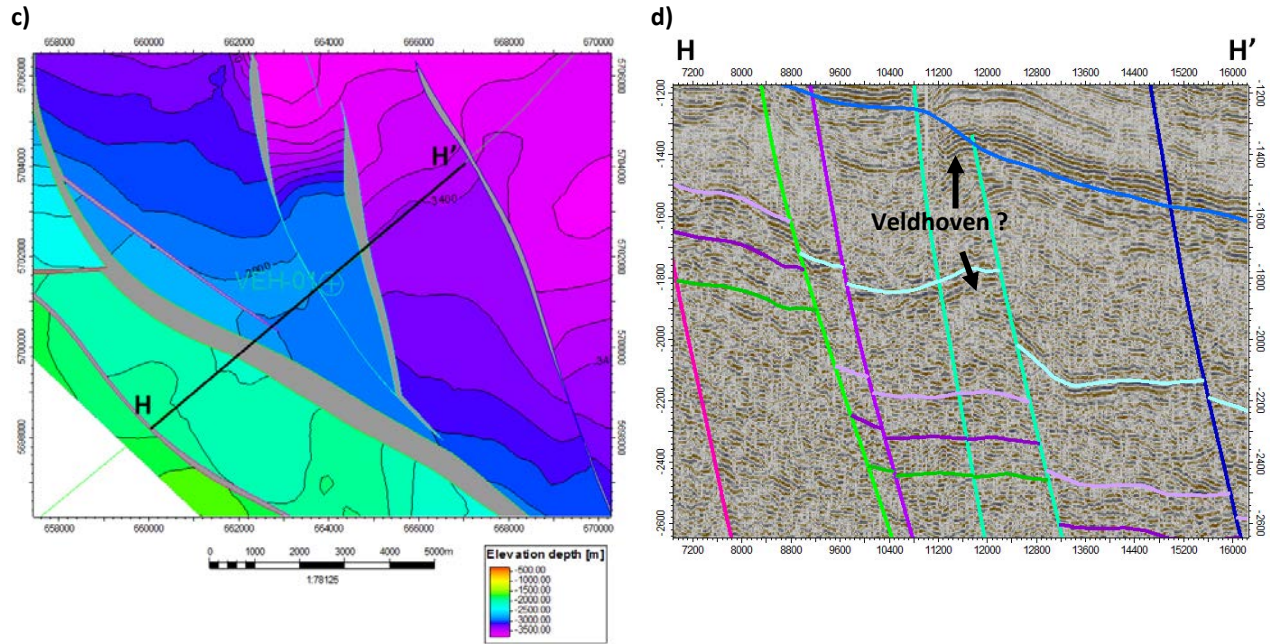


Figure 4.11 (continued)

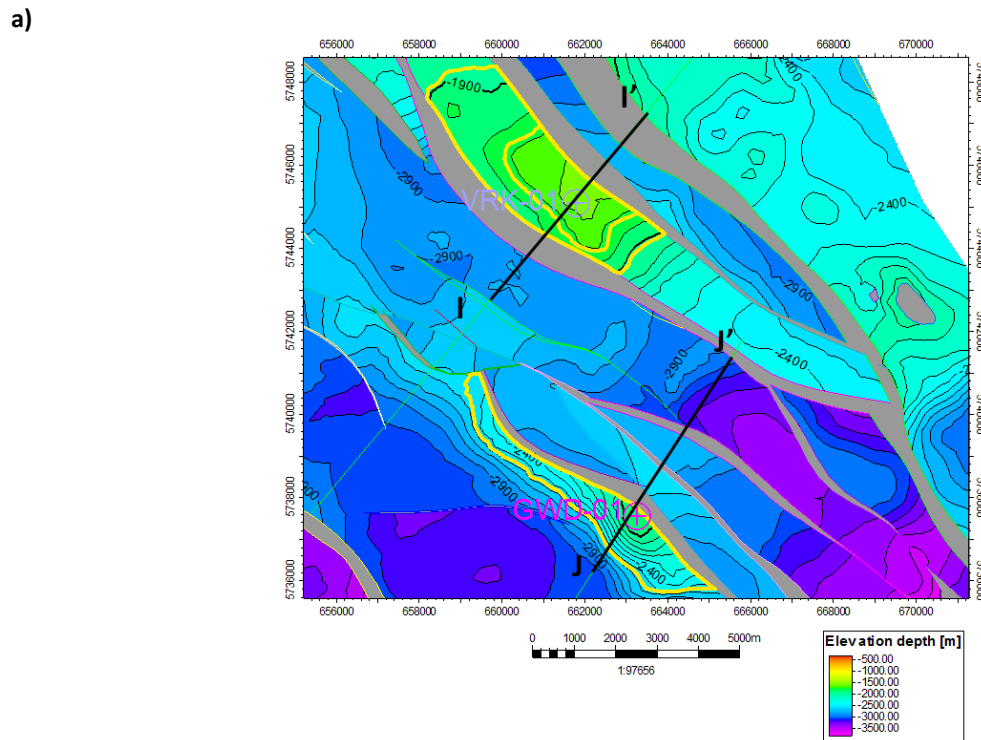


Figure 4.12: Depth map of near top Main Buntsandstein Subgroup (top) for the area around well VRK-01 and GWD-01. Indicated in yellow are the structural closures which proved to be dry. A maximum and minimum case is indicated for VRK-01. The cross-section through Varik-1 (left) is on seismic line 872102 survey L2NAM1987B. The line through Gewande-1 (right) is represented by line 893102 survey L2NAM1989A-2. Horizon colours same as in figure 4.8.

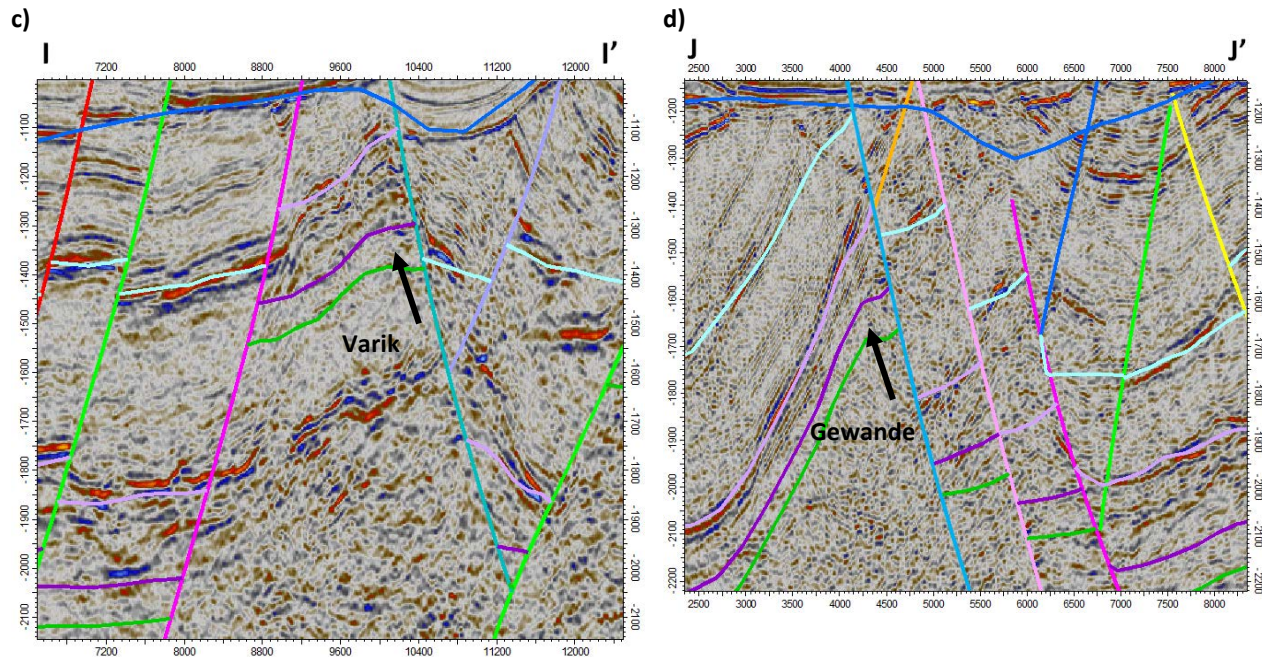


Figure 4.12 (continued)

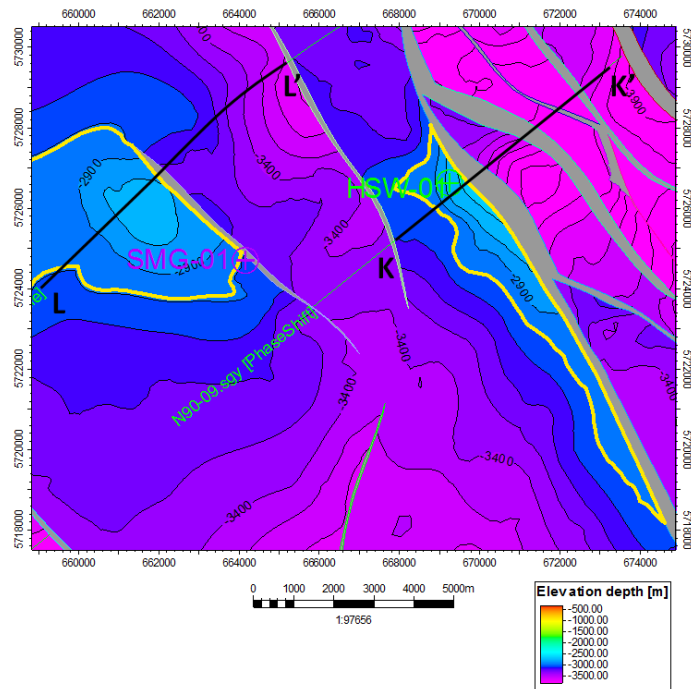
4.4.6 Sint-Michelsgestel & Heeswijk

Sint-Michelsgestel-1 (Fina 1969), located more towards the center of the graben targeted a local high bounded by a fault to the north (figure 4.13). This structure is relatively old compared to the other structures drilled as it is overlain by the Jurassic shales without fault reactivation. The structure is quite large but unfortunately dry. Fair gas shows were observed at the Aalburg, Posidonia Shale and the Breda (Upper North Sea Group) Formations. At the level of the Bunter Formations porosities of 6% were measured (Fina, 1969). Northeast of this structure another large prospect was drilled, the Heeswijk-1 well (Clyde Petroleum 1991). The main target was a tilted fault block forming the flank of a local through (figure 4.13) targeting the Triassic reservoirs (figure 4.13b). The structure proved to be dry and no sign of hydrocarbons were encountered during drilling.

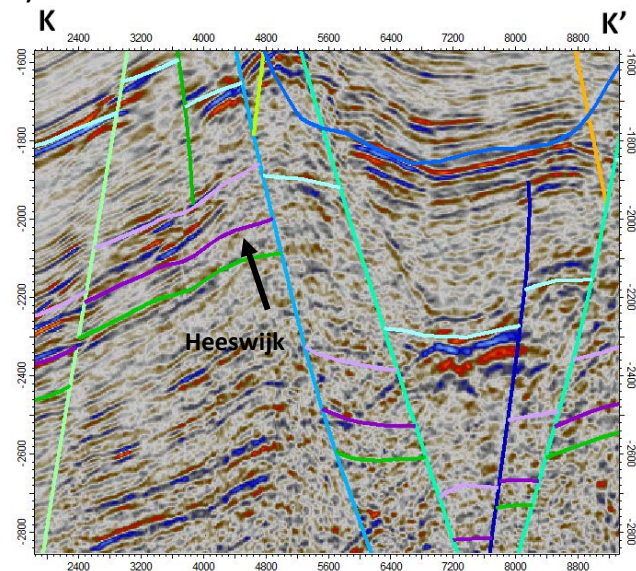
4.4.7 Keldonk

Keldonk-1 (Clyde Petroleum 1992) targeted a prospect in the structure in the eastern sector of the Roer Valley Graben (figure 4.14). Clyde Petroleum identified the structure as a structural closure which initiated by extensional faulting during the Early Jurassic to Early Cretaceous rifting (Sub-Hercynian Tectonic pulses). The Late Cretaceous inversion strongly affected the structure but present day trap geometry is mainly the result of Late Tertiary to Recent extension (Clyde, 1992). The volumetrics were promising but unfortunately dry. However, fair oil shows were encountered in the Upper Werkendam Formation and good shows in the Middle Werkendam Formation, Upper Röt Fringe Claystone Member and the Röt Fringe Sandstone Member.

a)



b)



c)

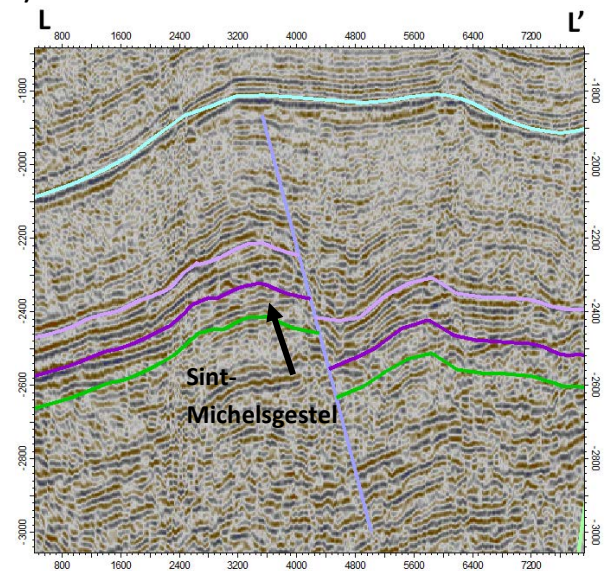


Figure 4.13: Depth map of near top Main Buntsandstein Subgroup (a) for the area around wells SMG-01 and HSW-01. Indicated in yellow are the structural closures which proved to be dry. The cross-section through Heeswijk-1 (b) is on seismic line N90-09 survey L2CLY1990A. The line through Sint-Michelsgestel-1 (c) is represented by line 8223 survey L2BP1982A. Horizon colours same as in figure 4.8.

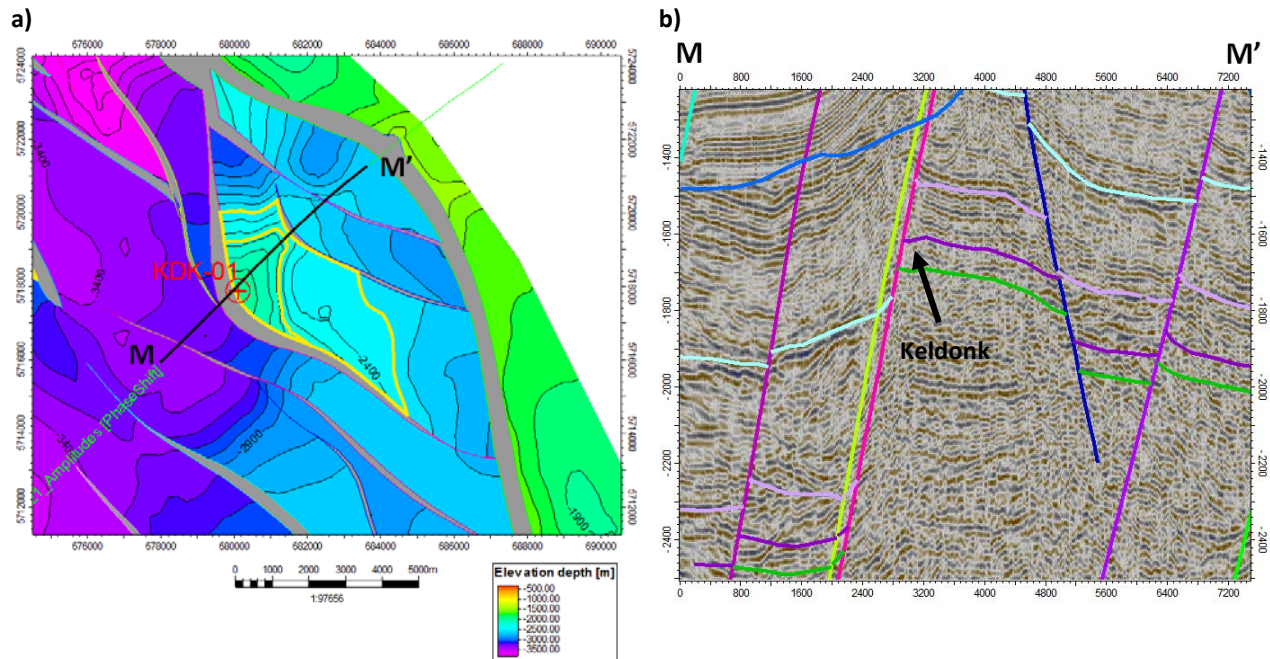


Figure 4.14: Depth map of near top Main Buntsandstein Subgroup (a) for the area around well KDK-01. Indicated in yellow are the structural closures which proved to be dry. A maximum and minimum case is indicated. The cross-section through Keldonk-1 (b) is on seismic line 8221 survey L2BP1982A. Horizon colours same as in figure 4.8.

4.5 Dry Hole Analysis

Now that each drilled structure has been presented, the question remains why most of the structures drilled proved to be dry? There are several possible scenarios:

- 1) The drilled structure is not valid
- 2) A breach in top seal has occurred or no top seal is present
- 3) A breach in side seal has occurred or no side seal is present
- 4) No reservoir
- 5) No charge
- 6) No source

All drilled wells did encounter the Lower Triassic reservoirs except for VEH-01, OIW-01 and GWD-01. Respectively, these wells did not drill further than the Aalburg, Lower Werkendam Formations and Lower Röt Fringe Claystone Member. So the presence of reservoir is not the issue. The coal wells drilled in the area indicate the presence of the Westphalian Coal Measures as well as studies done by Geluk et al., 1994 and Winstanley, 1993 which mention a carboniferous sequence of 1500 to 2000m. Previous research on this source rock indicates that charge has occurred within the Roer Valley Graben (see section 4.6). Thus it can be said that source is present throughout the area as well as charge. All cross-sections and map views of the drilled structures presented in the previous section indicate valid structures that have been drilled, except for VEH-01 and OIW-01 although it is unclear what the main target of these structures was. So of the six scenarios the most plausible explanation for the dry structures is the top or side seal breach of the structures. Local sandy intervals within the Röt Sealing Formations for the top seal and the Sleen, Aalburg and Werkendam Formations for the side seal may have led to seal breach.

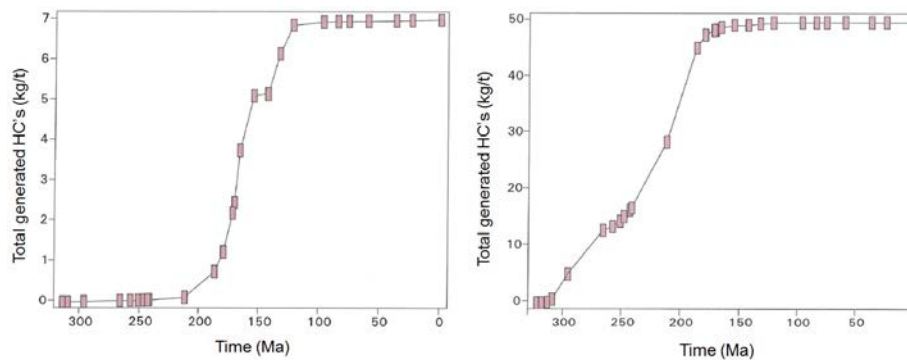
4.6 Timing

The timing of hydrocarbon generation in the Roer Valley Graben has been previously modeled by TNO (NITG, 2001) and to a limited extent by van Balen *et al.*, 2000. The outcome of this model is presented in figure 4.15. The first known source rock in the area that underwent hydrocarbon generation are the Namurian Shales. It commenced during the Late Carboniferous (~300 Ma; Kasimovian) and cumulated at the end of the Early Cretaceous (~100 Ma; Albian). Generation initiated as a result of Carboniferous, Permian and Mesozoic burial. The second source rock which underwent a period of hydrocarbon generation are the Westphalian Coal measures. Generation initiated during the Late Triassic (~210 Ma; Rhaetian) and cumulated during the Late Cretaceous (~120 Ma; Apitian). The quick rise in hydrocarbon generation in the period 180 Ma to 120 Ma is explained by the relative quick burial and high heat flow during the Late Kimmerian tectonic pulses (Late Jurassic to Earliest Cretaceous).

The filling of the Triassic reservoirs with hydrocarbons generated from the Westphalian Coal measures is estimated at 130 to 100 Ma, before the tectonic pulses of the Sub-Hercynian (NITG, 2001). For the Namurian Shales, the model indicates a start of accumulation at the Triassic reservoirs at approximately 160 Ma. This is roughly the same time period as the accumulation from the Westphalian Coals which makes it likely that the gas accumulation of the Waalwijk area are a mixture of both source rocks.

The source rock which has become active most recently is the Posidonia Shale Formation. According to de Jager *et al.*, 1996, oil generation commenced pre-Mid Cretaceous and is still ongoing. Depending on the modelled heat flow, the onset of hydrocarbon generation for the Posidonia Shale can vary. When enhanced heat flow related to possible volcanic heating during Permian is assumed, hydrocarbon generation could have already started during the Jurassic (Nelskamp *et al.*, 2008).

a)



b)

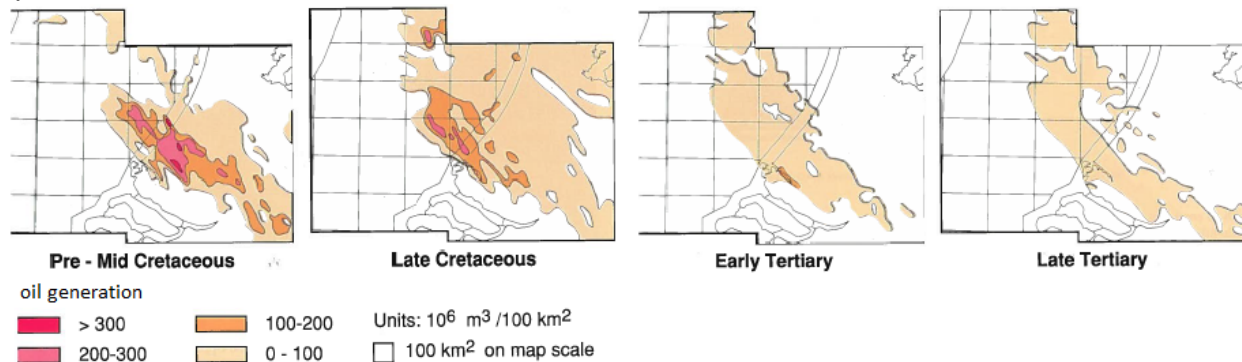


Figure 4.15: a) Graphs illustrating the timing of hydrocarbon generation in the Roer Valley Graben for the Westphalian Coal measures (left) and the Namurian Shales (right), source: NITG, 2001. **b)** Oil generation from the Posidonia Shale. Source: de Jager *et al.*, 1996.

5. Results

5.1 Structural Framework Modeling & Time-Depth Conversion

The main results of the Structural Framework workflow in Petrel are the following:

- A detailed 3D structural framework of the Roer Valley Graben below the level of the base Schieland Group, including the Posidonia Shale Formation, base Altona, top Main Buntersandstein and base Main Buntsandstein. The model is illustrated by several cross-sections in Appendix B.
- Four detailed structural maps in elevation time of the top Posidonia Shale, base Altona, near top Main Buntsandstein Subgroup and the near base Buntsandstein Subgroup (Appendix C).
- Two detailed structural maps in elevation depth of the near top Main Buntsandstein Subgroup and the near base Main Buntsandstein Subgroup (Appendix D).

For the scope of this study the end results of this detailed 3D structural Framework model has been mainly used to map and identify leads at the level of the Main Buntsandstein Subgroup (see section 5.2 and 5.3). To assess the impact of the newly constructed maps on the geology in the area is beyond the scope of this study.

The detail of the model allowed correct interpretation of the key horizons in areas of complex fault populations and narrow fault blocks, this made it easier to identify structural closures and establish migration pathways. As the focus of this study lies on the identification of potential oil leads at the level of the Lower Triassic, the maps most relevant for depth conversion were the top Main Buntsandstein and the base Main Buntsandstein. These maps could be corrected quite easily as only the inconsistencies in the top Main Buntersandstein Subgroup had to be corrected. A depth isochore of the Main Buntsandstein Subgroup and the 'conforms to' option could be used within the Structural Framework model to get a depth interpretation at the level of the base Main Buntsandstein Subgroup.

5.2 Oil Leads

In the study area, a total of seven new leads have been identified which could possibly have accumulated oil generated from the Posidonia Shale (figure 5.1). These leads have a favorable configuration were the Posidonia Shale (source) is juxtaposed in the proximity of the Main Buntsandstein Subgroup (reservoir) in two different structural closures, namely (i) fault-dip closures and (ii) down-thrown fault-dip closures. No four-way dip closures could be identified at the level of the Main Buntsandstein Subgroup. In the following series of figures (figure 5.2-5.5), each oil lead is presented in map view (elevation depth) with the extend of the closure and a cross section through the structure (elevation time). For each lead the spill points have been determined together with the gross rock volume of the structural traps for the Main Buntsandstein Subgroup (table). An average net-to-gross ratio of 53% is assumed, this correlates with the Waalwijk structure (see section 4.1). Porosities have been estimated with the use of the graph presented in figure 4.3, following the alluvial compaction trend. The hydrocarbon saturation has been set at 80% and a formation volume factor of 1.1 was used assuming low shrinkage oil. In table 2 the STOIP calculations are presented for each structural closure. Each lead has been color coded to indicate which leads give the highest STOIP. Lead 5 and 6 seem to be most promising regarding their volumetrics. It should be noted, the volumetric estimates given for each lead provide a static measure of oil in place. The accuracy of the estimate depends on the amount of data available, which is limited in this area. Rough estimates are taken for each of the STOIP parameters.

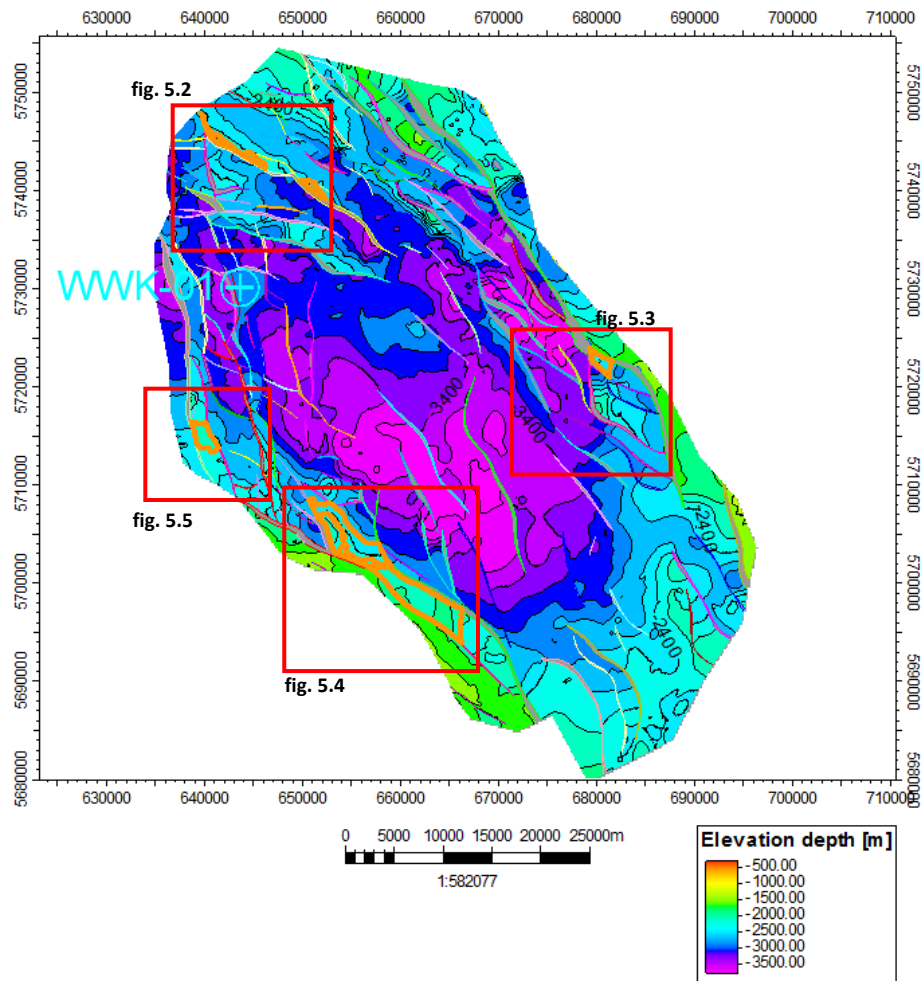


Figure 5.1: Depth map of the near top Main Buntsandstein Subgroup, contour interval is 200m. The red boxes indicate the different sectors in which the different oil leads are presented in the following figures.

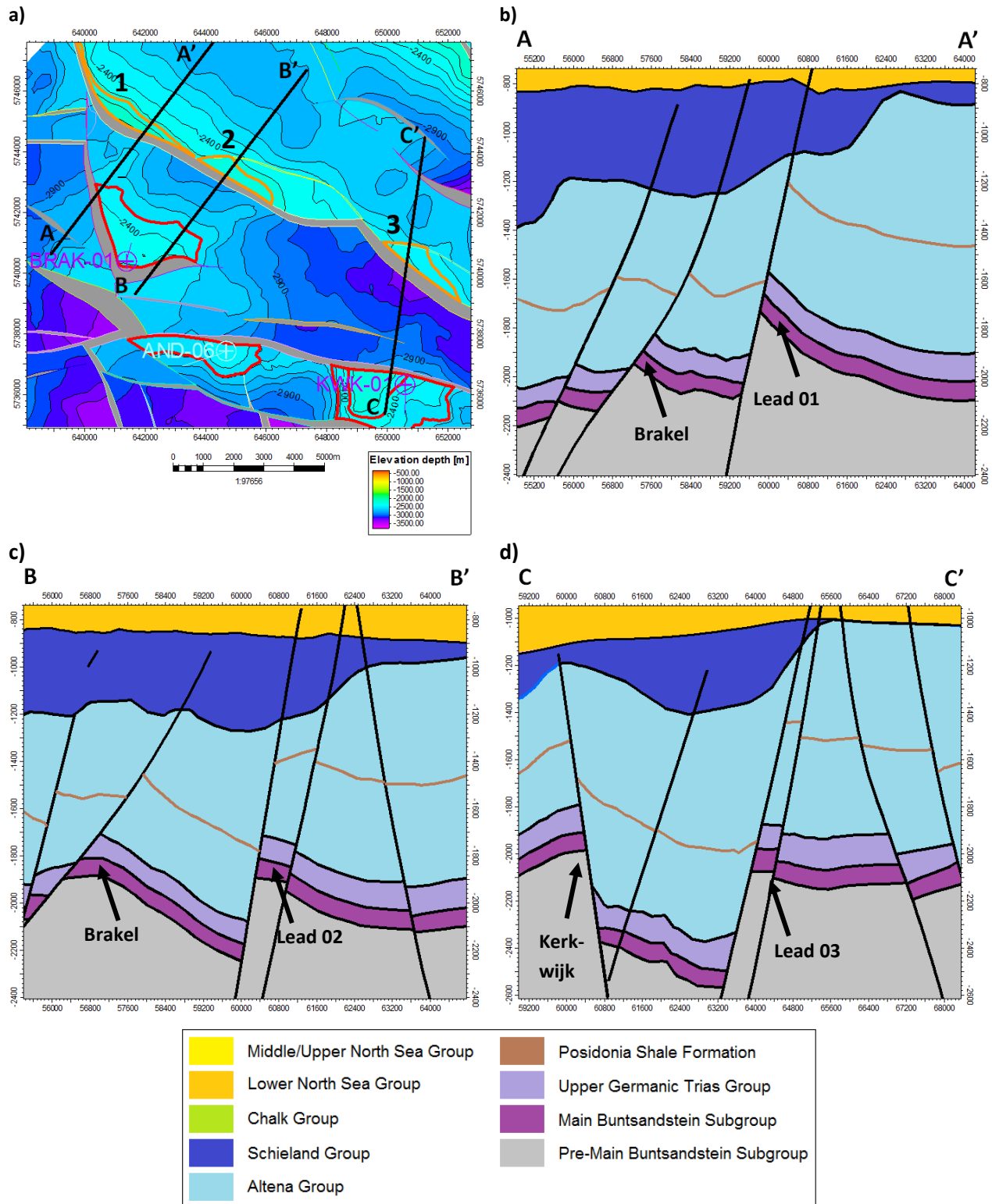


Figure 5.2: a) Depth map of near top Main Buntsandstein Subgroup, see figure 5.1 for the location in the Roer Valley Graben. Contour interval is 100m b) Cross-section through lead 01 in elevation time. c) Cross-section through lead 02 in elevation time. d) Cross-section through lead 03 in elevation time.

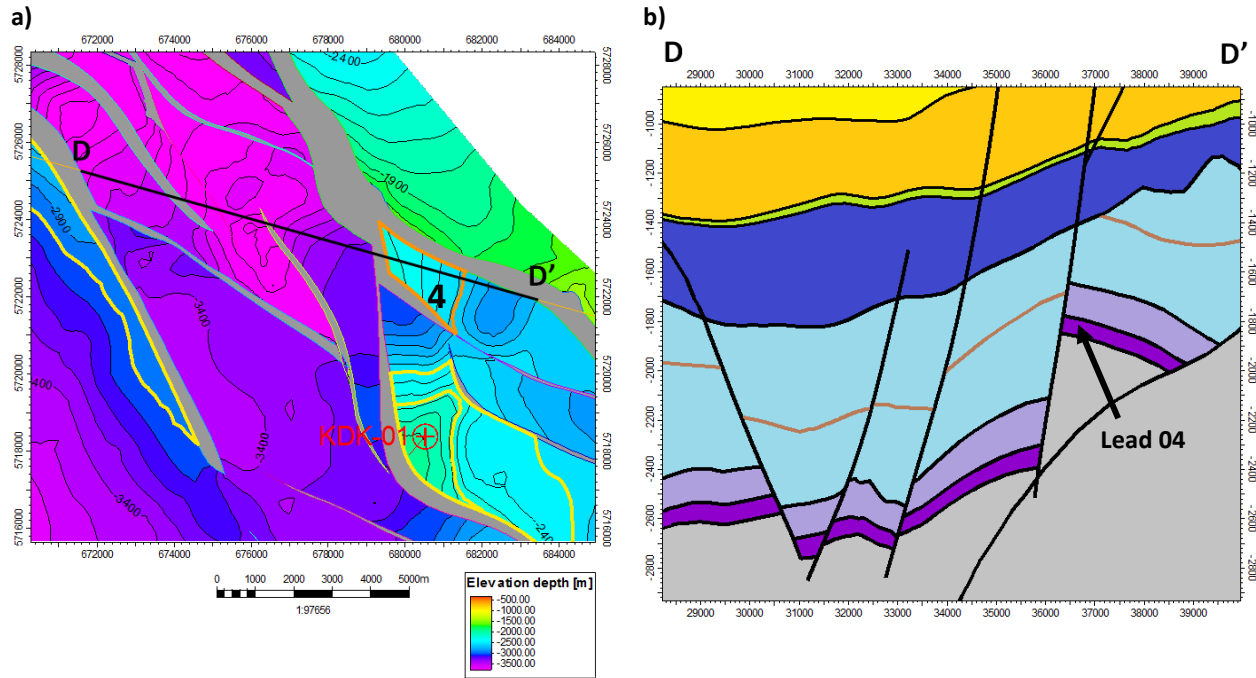


Figure 5.3: a) Depth map of near top Main Buntsandstein Subgroup, see figure 5.1 for the location in the Roer Valley Graben. Contour interval is 100m b) Cross-section through lead 04 in elevation time. Colour index same as in figure 5.2.

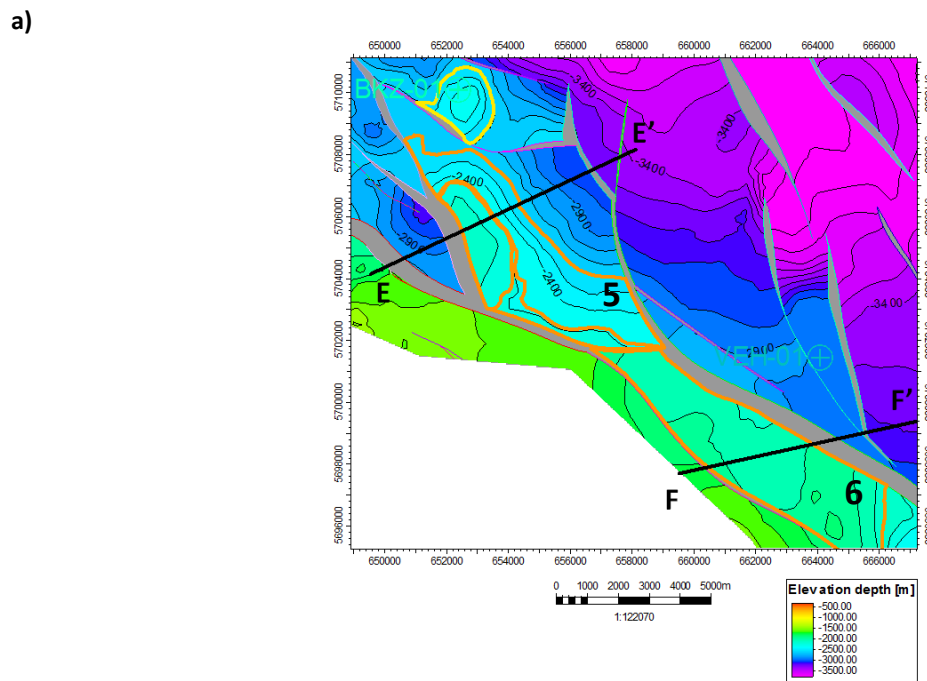


Figure 5.4: a) Depth map of near top Main Buntsandstein Subgroup, see figure 5.1 for the location in the Roer Valley Graben. Contour interval is 100m b) Cross-section through lead 05 in elevation time. c) Cross-section through lead 06 in elevation time. Colour index same as in figure 5.2.

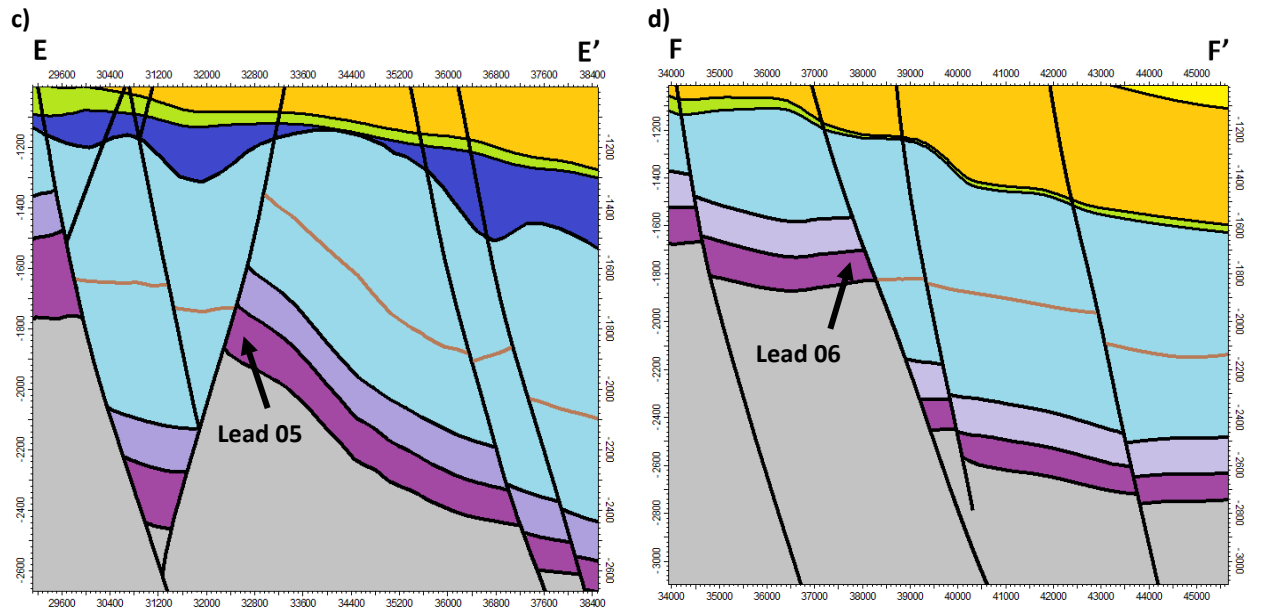


Figure 5.4 (continued)

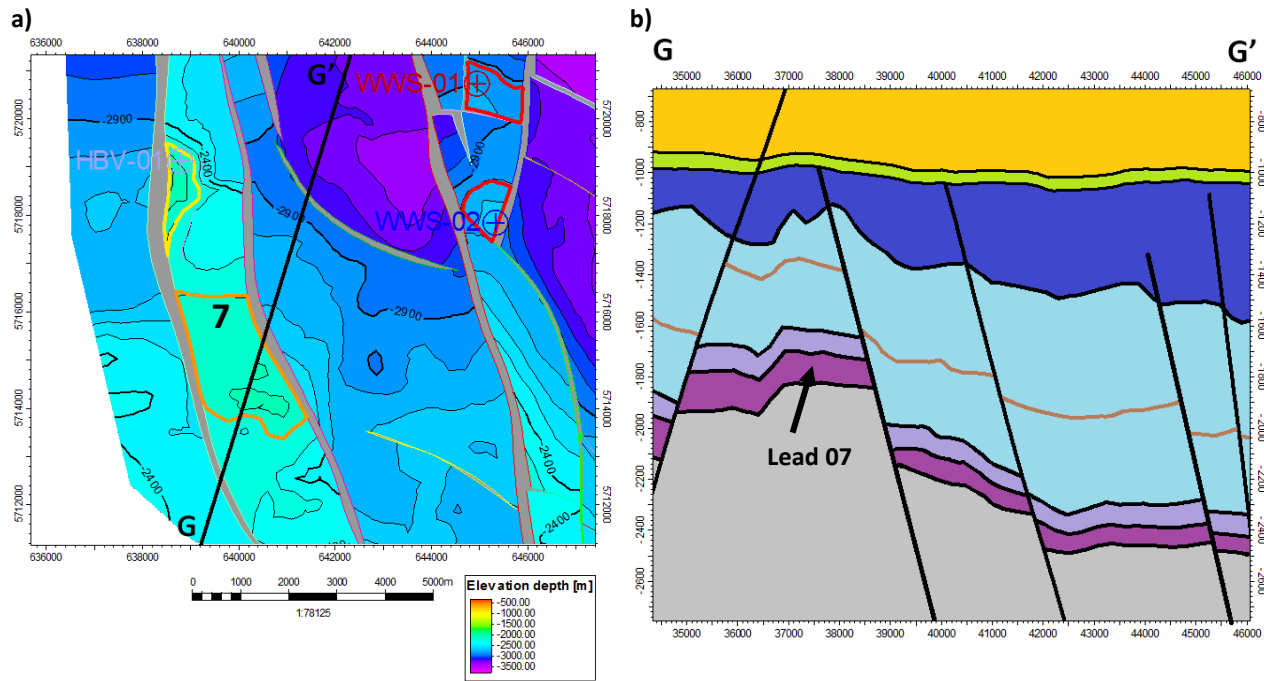


Figure 5.5: a) Depth map of near top Main Buntsandstein Subgroup, see figure 5.1 for the location in the Roer Valley Graben. Contour interval is 100m b) Cross-section through lead 07 in elevation time. Colour index same as in figure 5.2.

Lead no.	Trap Type	SP (m)	GRV (m ³)	N/G	φ	S _o	1/B _o	STOIIP (m ³)	STOIIP (bbl)
1	Fault-dip Closure	2260	1.62E+08	0.53	0.15	0.8	0.91	9.38E+06	5.90E+07
2	Fault-dip Closure	2265	4.90E+07	0.53	0.15	0.8	0.91	2.83E+06	1.78E+07
3	Fault-dip Closure	2455	6.76E+07	0.53	0.14	0.8	0.91	3.65E+06	2.29E+07
4	Down-thrown Fault-dip Closure	2630	3.30E+08	0.53	0.14	0.8	0.91	1.78E+07	1.12E+08
5	Min Fault-dip Closure	2290	3.59E+08	0.53	0.15	0.8	0.91	2.08E+07	1.31E+08
5	Int Down-thrown Fault-dip Closure	2310	5.32E+08	0.53	0.15	0.8	0.91	3.08E+07	1.93E+08
5	Max Down-thrown Fault-dip Closure	2600	4.61E+09	0.53	0.15	0.8	0.91	2.66E+08	1.68E+09
6	Down-thrown Fault-dip Closure	2150	3.10E+09	0.53	0.16	0.8	0.91	1.91E+08	1.20E+09
7	Fault-dip Closure	2210	3.39E+08	0.53	0.15	0.8	0.91	1.96E+07	1.23E+08

Table 2: STOIIP calculations for the seven oil leads that have been identified at the level of the Main Buntsandstein Subgroup. A color scale of green-yellow-red has been applied on the STOIIP values, with green indicating the highest and red the lowest. SP = spill point, GRV = Gross Rock Volume, N/G = Net-to-Gross, φ = porosity, S_o = oil saturation and B_o = oil formation volume factor.

5.3 Gas Leads

The eighteen leads presented in figure 5.6 at the level of the Main Buntsandstein form the structural closures that are identified as only being a gas lead due to their unfavorable configuration with respect to the Posidonia Shale Oil migration into these structures from this source rock is very unlikely. However, gas migration from the Carboniferous is plausible. The latter is also possible for the first eight leads that previously have been identified as oil leads (figure 5.7 - 5.11). So a total of 25 gas leads have been identified at the level of the Main Buntsandstein Subgroup. Two types of structural closures are observed, (i) fault-dip closures and (ii) down-thrown fault dip closures. In figure 5.6 an overview of the different leads is presented in map view. Several promising structures have been selected which are presented in more detail with a close-up map view and a cross-section through the structure. For each lead the GIIP has been calculated (table 3). This also includes the oil leads as these can also be seen as a gas lead. For the net-to-gross, porosity and saturation parameters, the same values have been assumed as in the calculations of the STOIIP. The gas formation volume factor (B_G) is determined by the following equation (see Appendix E for the derivation):

$$B_G = 0.350958 \frac{zT_{res}}{p_{res}}$$

The rough estimates of the GIIP have been color coded to indicate which lead gives the highest GIIP (table 3). Volumetrically, lead 10, 11, 15, 16, 18 and 25 seem to be the most promising structural closures for gas accumulations. Again, it should be noted, the volumetric estimates given for each lead provide a static measure of gas in place. The accuracy of the estimate depends on the amount of data available, which is limited in this area. Rough estimates are taken for each of the GIIP parameters.

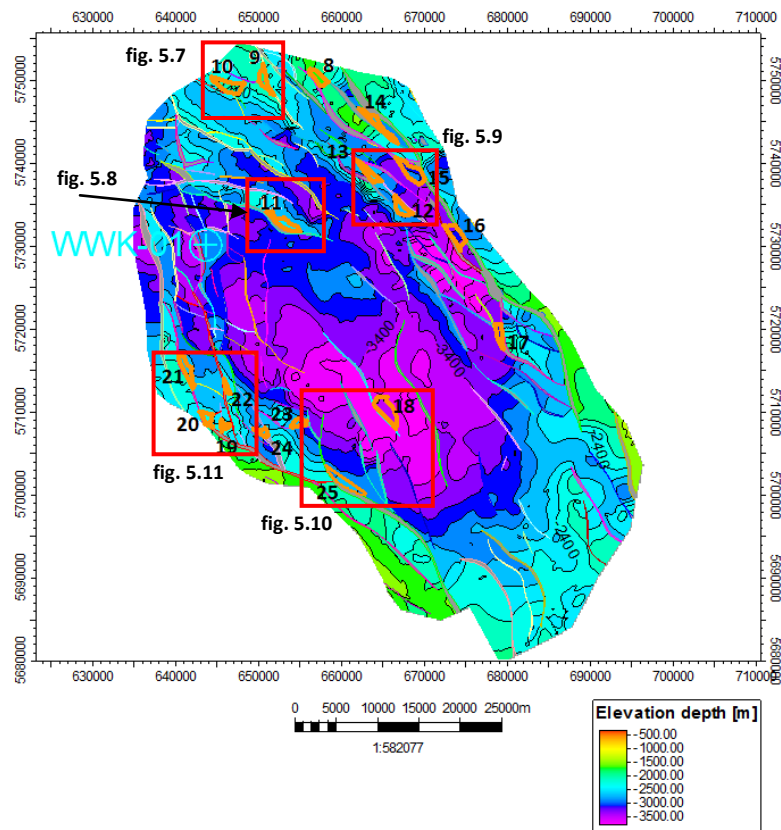


Figure 5.6: Depth map of the near top Main Buntsandstein Subgroup, contour interval is 200m. Indicated in orange are the different leads. The red boxes indicate the different sectors in which the different gas leads are presented in the following figures.

Lead no.	Trap Type	SP (m)	Temp @ SP (K)	GRV (m ³)	N/G	φ	S _G	1/B _G	GIIP (m ³)	GIIP (BCM)
1	Fault-dip Closure	2260	348.15	1.62E+08	0.53	0.15	0.8	199.40	2.06E+09	2.06
2	Fault-dip Closure	2265	348.15	4.90E+07	0.53	0.15	0.8	199.84	6.23E+08	0.62
3	Fault-dip Closure	2455	353.15	6.76E+07	0.53	0.14	0.8	206.72	8.30E+08	0.83
4	Down-thrown Fault-dip Closure	2630	353.15	3.30E+08	0.53	0.14	0.8	219.12	4.29E+09	4.29
5	Min Fault-dip Closure	2290	348.15	3.59E+08	0.53	0.15	0.8	202.04	4.61E+09	4.61
5	Int Down-thrown Fault-dip Closure	2310	348.15	5.32E+08	0.53	0.15	0.8	203.81	6.90E+09	6.90
5	Max Down-thrown Fault-dip Closure	2600	353.15	4.61E+09	0.53	0.15	0.8	216.62	6.35E+10	63.47
6	Down-thrown Fault-dip Closure	2150	348.15	3.10E+09	0.53	0.16	0.8	191.80	4.03E+10	40.34
7	Fault-dip Closure	2210	348.15	3.39E+08	0.53	0.15	0.8	196.06	4.23E+09	4.23
8	Fault-dip Closure	1765	338.15	1.12E+08	0.53	0.18	0.8	163.93	1.40E+09	1.40
9	Fault-dip Closure	2020	343.15	1.22E+08	0.53	0.16	0.8	181.82	1.50E+09	1.50
10	Fault-dip Closure	2240	348.15	4.68E+08	0.53	0.16	0.8	197.63	6.27E+09	6.27
11	Fault-dip Closure	2555	353.15	2.54E+08	0.53	0.14	0.8	214.00	3.23E+09	3.23
12	Fault-dip Closure	2765	358.15	1.20E+08	0.53	0.13	0.8	224.79	1.49E+09	1.49
13	Down-thrown Fault-dip Closure	2655	353.15	1.16E+08	0.53	0.13	0.8	220.05	1.41E+09	1.41
14	Down-thrown Fault-dip Closure	2765	358.15	1.41E+08	0.53	0.13	0.8	224.79	1.75E+09	1.75
15	Down-thrown Fault-dip Closure	3185	383.15	5.55E+08	0.53	0.11	0.8	228.92	5.93E+09	5.93
16	Down-thrown Fault-dip Closure	3265	383.15	2.55E+08	0.53	0.1	0.8	233.52	2.52E+09	2.52
17	Down-thrown Fault-dip Closure	3210	383.15	1.43E+08	0.53	0.1	0.8	230.72	1.40E+09	1.40
18	Fault-dip Closure	3620	393.15	4.12E+08	0.53	0.06	0.8	245.12	2.57E+09	2.57
19	Fault-dip Closure	2355	348.15	6.00E+06	0.53	0.14	0.8	207.78	7.40E+07	0.07
20	Down-thrown Fault-dip Closure	2370	348.15	3.48E+07	0.53	0.14	0.8	207.96	4.30E+08	0.43
21	Down-thrown Fault-dip Closure	2735	358.15	1.53E+08	0.53	0.13	0.8	222.35	1.88E+09	1.88
22	Fault-dip Closure	2380	348.15	4.04E+07	0.53	0.14	0.8	208.84	5.01E+08	0.50
23	Fault-dip Closure	2680	353.15	1.02E+08	0.53	0.13	0.8	222.12	1.25E+09	1.25
24	Down-thrown Fault-dip Closure	2665	353.15	2.68E+07	0.53	0.13	0.8	220.88	3.26E+08	0.33
25	Down-thrown Fault-dip Closure	2875	363.15	2.49E+08	0.53	0.11	0.8	228.14	2.65E+09	2.65

Table 3: GIIP calculations for the 25 gas leads that have been identified at the level of the Main Buntsandstein Subgroup. A color scale of green-yellow-red has been applied on the GIIP values, with green indicating the highest and red the lowest. The color scale has been divided in two between the potential oil (1 to 7) and other leads (8 to 25) indicated by the black line. SP = spill point, GRV = Gross Rock Volume, N/G = Net-to-Gross, φ = porosity, S_G = gas saturation and B_G = gas formation volume factor (expansion factor).

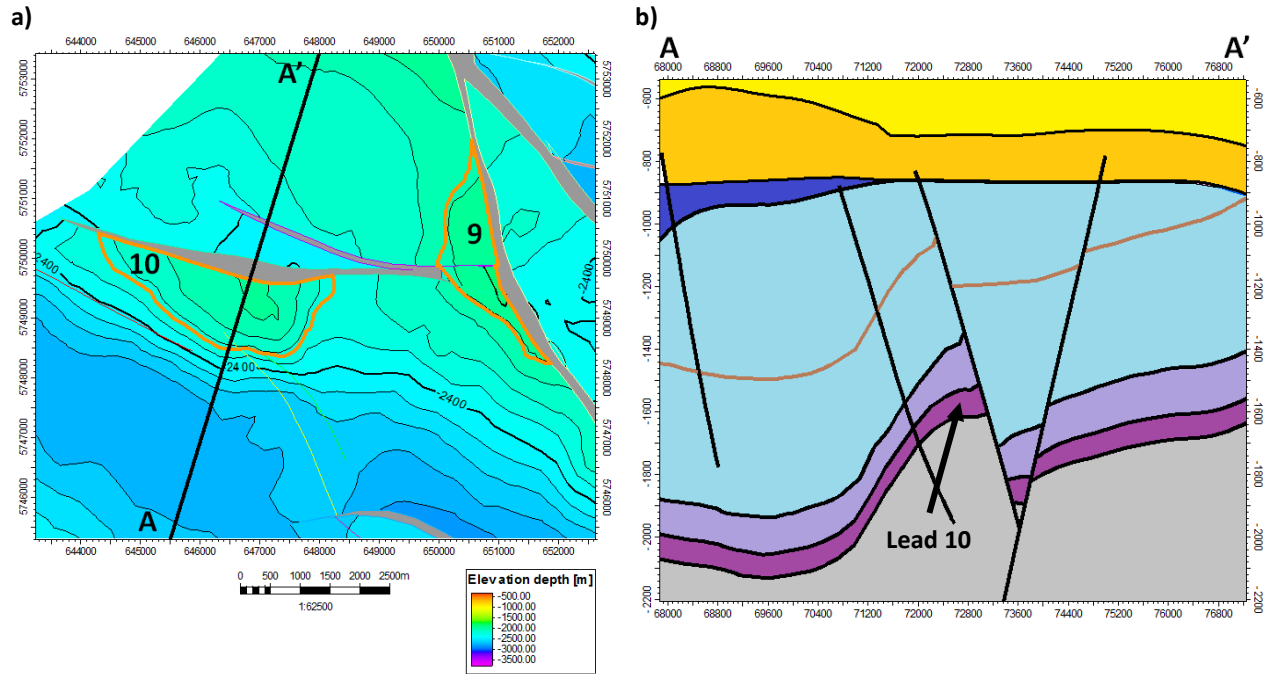


Figure 5.7: a) Depth map of near top Main Buntsandstein Subgroup, see figure 5.6 for the location in the Roer Valley Graben. Contour interval is 100m b) Cross-section through lead 10 in elevation time. Colour index same as in figure 5.2.

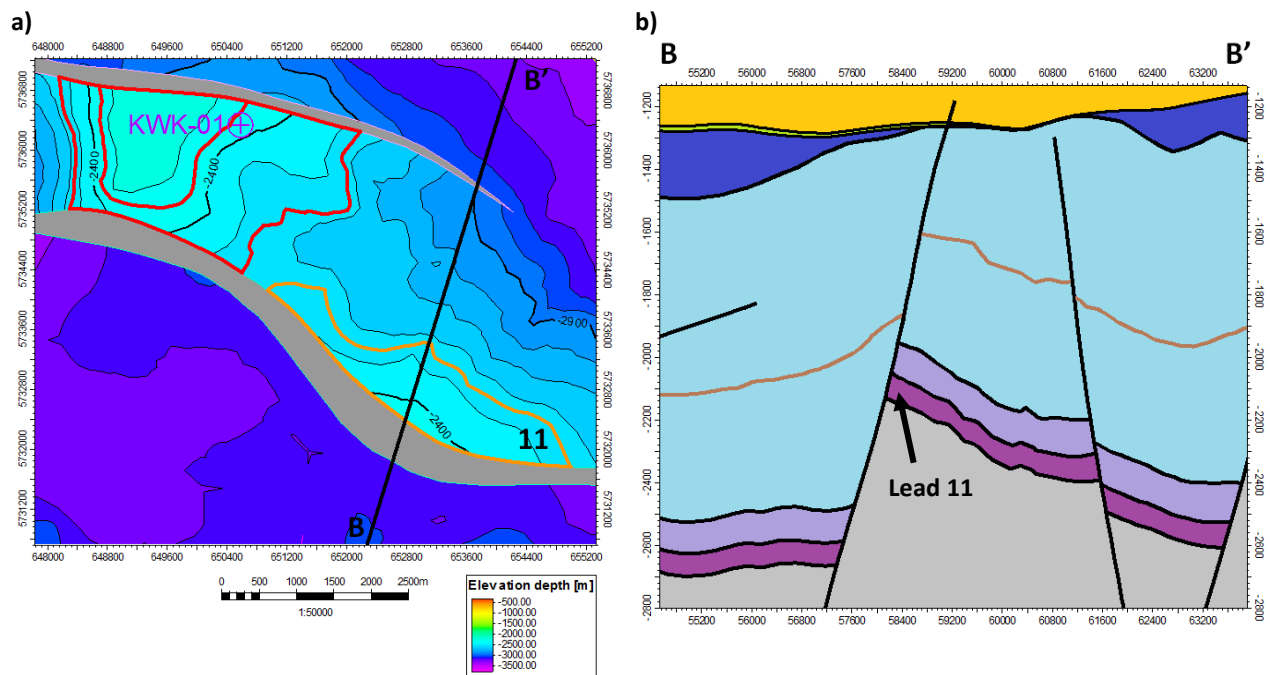


Figure 5.8: a) Depth map of near top Main Buntsandstein Subgroup, see figure 5.6 for the location in the Roer Valley Graben. Contour interval is 100m b) Cross-section through lead 11 in elevation time. Colour index same as in figure 5.2.

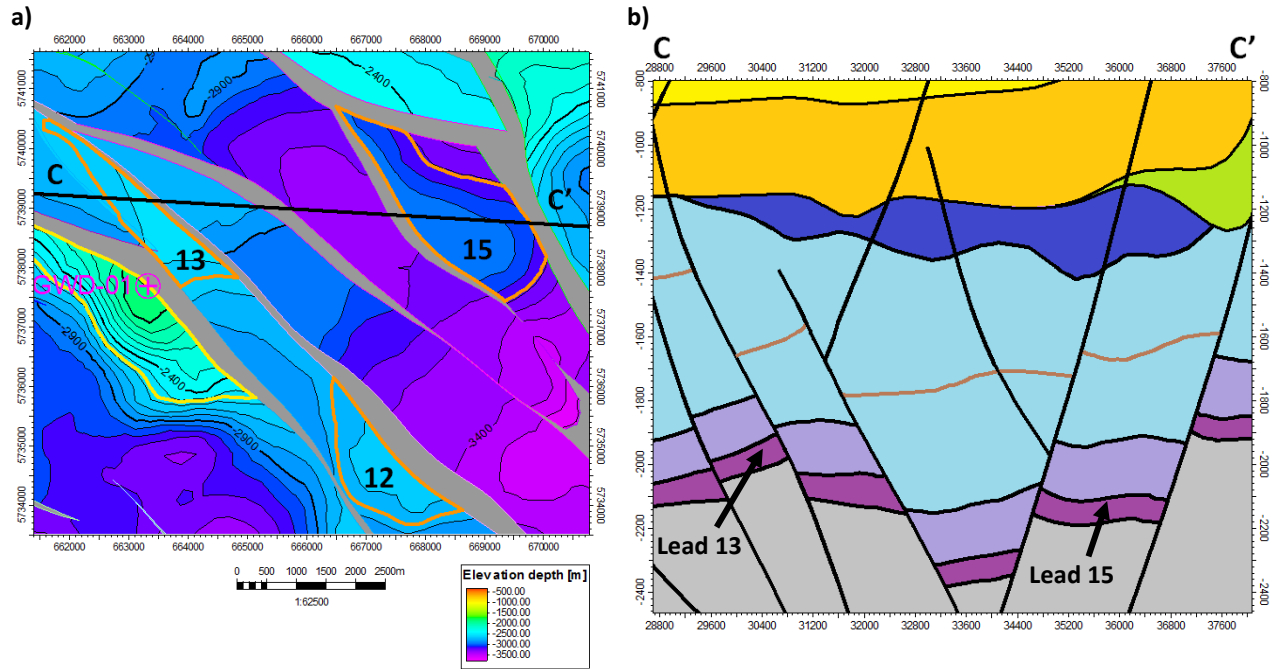


Figure 5.9: a) Depth map of near top Main Buntsandstein Subgroup, see figure 5.6 for the location in the Roer Valley Graben. Contour interval is 100m b) Cross-section through lead 13 and 15 in elevation time. Colour index same as in figure 5.2.

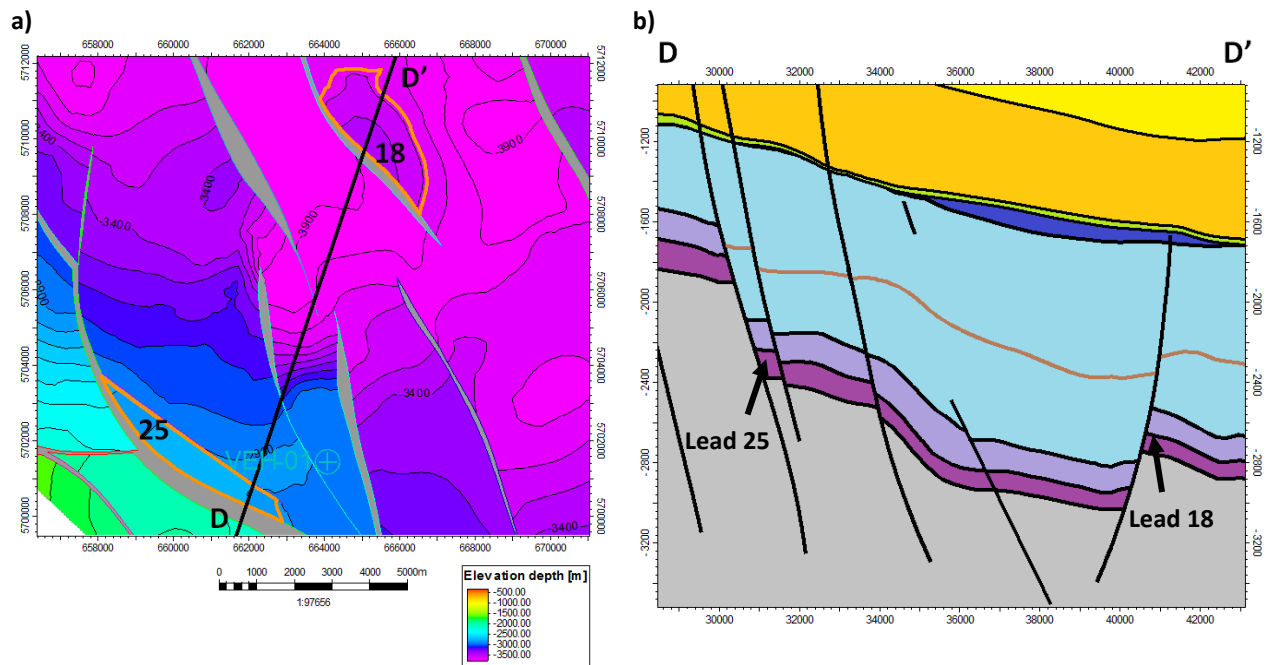


Figure 5.10: a) Depth map of near top Main Buntsandstein Subgroup, see figure 5.6 for the location in the Roer Valley Graben. Contour interval is 100m b) Cross-section through lead 18 and 25 in elevation time. Colour index same as in figure 5.2.

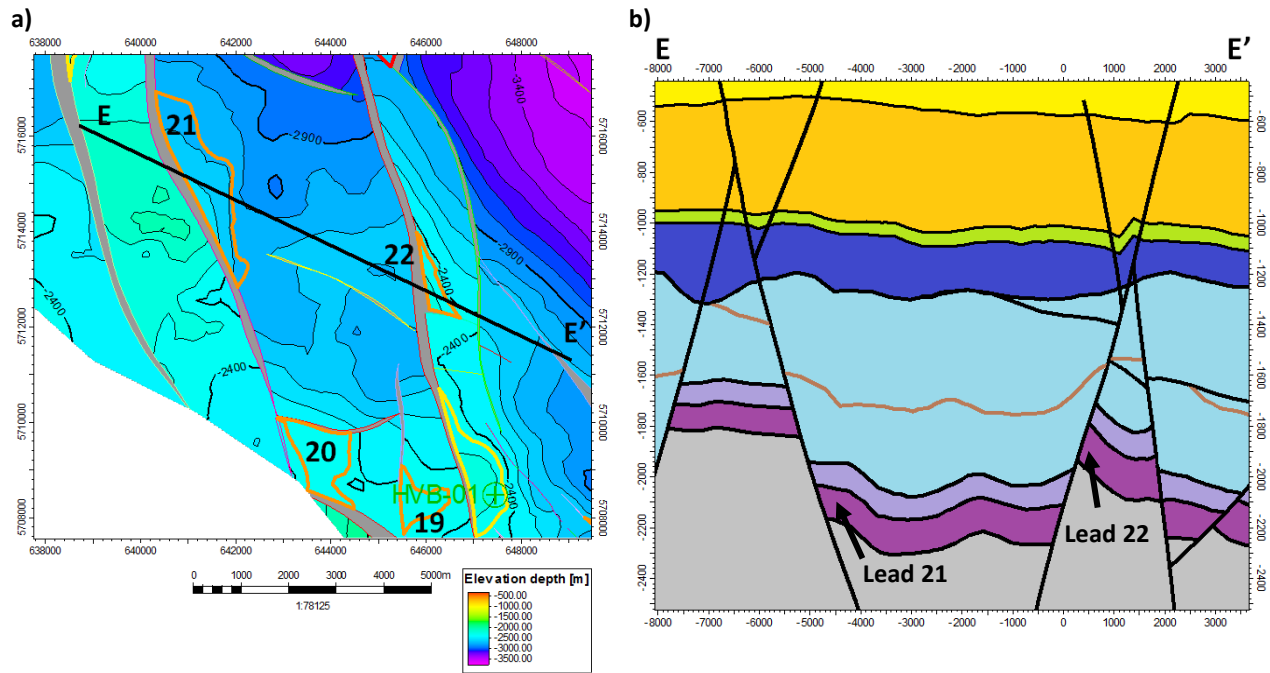


Figure 5.11: a) Depth map of near top Main Buntsandstein Subgroup, see figure 5.6 for the location in the Roer Valley Graben. Contour interval is 100m b) Cross-section through lead 21 and 22 in elevation time. Colour index same as in figure 5.2.

6. Discussion

This section will first outline some of the uncertainties related to the data input and results. Secondly issues and difficulties encountered during the structural framework modeling workflow will be discussed. Lastly, the identified leads will be evaluated on their migration pathways and a risk qualification is made.

6.1 Uncertainties

In the study area data quality and density is limited which affects the seismic interpretation of the key horizons which influences the outcome of the structural framework model. Due to limited checkshot data, synthetic well control is limited in validating the picked seismic horizons and together with the low quality of the seismic signal it influences the certainty of a picked horizon away from a well. The surface with the highest certainty is the Posidonia Shale, as this reflector is the best traceable horizon across the study area. Uncertainty in the mapped horizons increases with depth. It should also be noted that the interpretations of the near top and base Main Buntsandstein group are best estimates based on isochore data from well markers, meaning that in complex faulted areas and areas away from well control the uncertainty in this interpretation increases. It should be mentioned that the isochore maps had to be converted to time maps for which velocity data was needed. For this, interval velocity maps from the Velmod-2 have been used. Nevertheless, with the data availability this is the best option available. Also the used well markers are well top interpretations from TNO, these are treated as correct.

In the depth conversion of the structural framework model also lie uncertainties. As when the model was initially converted to depth without any corrections, each depth map had an offset with the well tops which was quite large in several wells (see table 1). To resolve these residuals between the interpretation and the wells, the velocity model was re-run with well corrections. However, these well corrections have a certain influence range, which can lead to the domal artifacts around the wells creating structures that are initially not there, this should be taken into account when identifying the leads. It should also be mentioned that well data is limited, making it hard to establish a good velocity model in the area.

6.2 Structural Framework Modeling Workflow

The workflow for the structural framework model was new to this study, which resulted in it being a relative time consuming process. The different steps were learned on the fly and this occasionally led to difficulties in the modeling process as discussed below.

One of the major problems during the fault framework modeling process was to correctly define the fault truncation relationships in complex areas where large cross-cutting faults occur. To resolve this issue, the problematic fault interpretations were split into separate fault fragments so that the desired faults could be set as active for each horizon. However, this had a minor setback as in several cases lateral fault fragments did not connect well, not properly cutting of the surface at these intersections (figure 6.1). This issue could not be resolved but is of minor importance for the overall structure of the constructed time and depth maps.

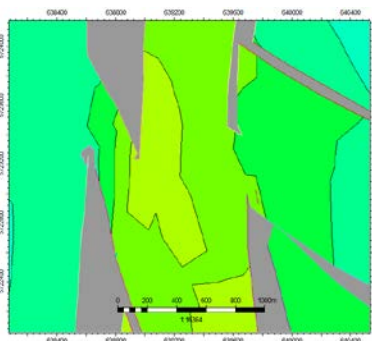


Figure 6.1: Example of two faults where no good connection relation could be established, resulting in not a proper cut-off of the surface at these intersections.

Another reoccurring issue were areas where something went wrong with the horizon modeling process. This usually happened in areas with a dense fault population, narrow fault blocks and limited input data. Here the process had difficulties to correctly extrapolate the interpretation resulting in glitches and weird structures or not honoring the input data (figure 6.2a). In most cases these weird structures occurred at fault intersection where the truncation relationships were not fully and correctly defined to the level of the particular horizon. However, in several cases this was not the problem. To resolve the issue here, several methods were applied: (1) changing the 'distance to fault' parameters, input data closer than this distance to the fault is not used in the modeling process, (2) adding polygon lines to the initial input data to stir the desired result, (3) inserting fault polygons, or a point data set to select areas of the input data that need to be unfiltered during the modeling process or (4) a combination of the three. The latter two could also be applied to resolve issues were the modeled horizon does not honor the input data correctly (figure 6.2b). In the end all leads were cross-checked and identified as glitch-free

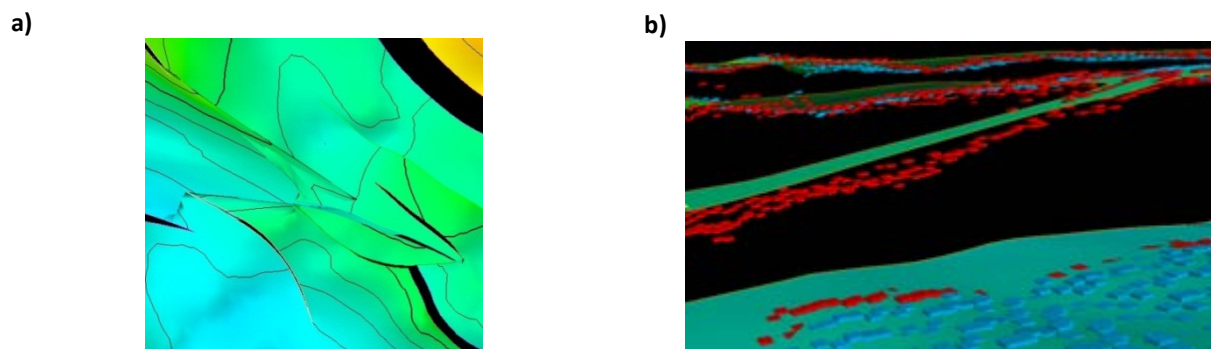


Figure: Example of a glitch/weird structure after horizon modeling (a) and a mismatch between the modeled horizon and the input data (b).

There was also an issues in the modeling process when applying the 'conforms to' option together with a time isochore. For some unknown reason the modeling process did not correctly follow the time isochore which resulted in intersections between the two horizons which should not occur (figure 6.3) as it should lie directly below the horizon that shaped the isochore. To resolve this issue, the time isochore was manually subtracted from the desired surface and converted to a point set which could then be used as initial input for the horizon together with the 'conforms to' option to get the desired result. However, the subtraction does not account for the faults present, resulting in data spill across faults. This has to be manually removed which can become a time consuming process when this has to be done for multiple surfaces.

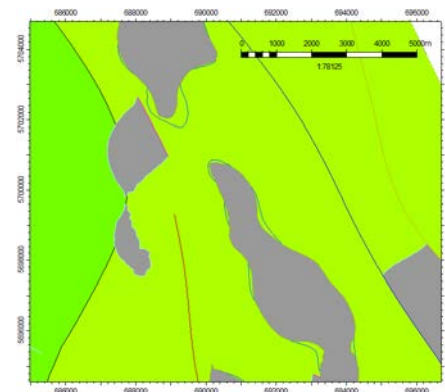


Figure 6.3: Example of an area were the isochored surface cross-cuts the surface from which it was created.

In conclusion, the structural framework module is a nice and reliable tool in constructing a regional structural model in an area where data is limited. The 'conforms to' option proved to be quite useful in constructing interpretations for the top and base Main Buntsandstein Subgroup beyond the limits of the seismic quality. To avoid it being a time-consuming process, it should be used directly at the start of seismic interpretation so that fault relations can correctly be defined as efficiently as possible.

6.2.1 Isochore maps TNO

During the structural framework workflow and the construction of depth and time isochores to extrapolate the base Altona interpretation to the level of the Main Buntsandstein Subgroup it was noticed that the interpretation of TNO for the top Main Buntsandstein Subgroup was situated a lot deeper. To find an explanation for this mismatch a back calculation was done on the two-way-time grids of the base Altona and base Upper Germanic Trias Group to construct a depth isochore with the use of the velocity model. The result is presented in figure 6.4. It becomes clear that away from the 3D cubes a sharp increase in thickness is assumed, approximately twice the size as has been observed in the 3D cubes which is strange as this is not in line with the observed thicknesses in the wells in this area. This makes the interpretation made in this study a better approximation of the top Main Buntsandstein Subgroup which could be used in the identification of potential leads.

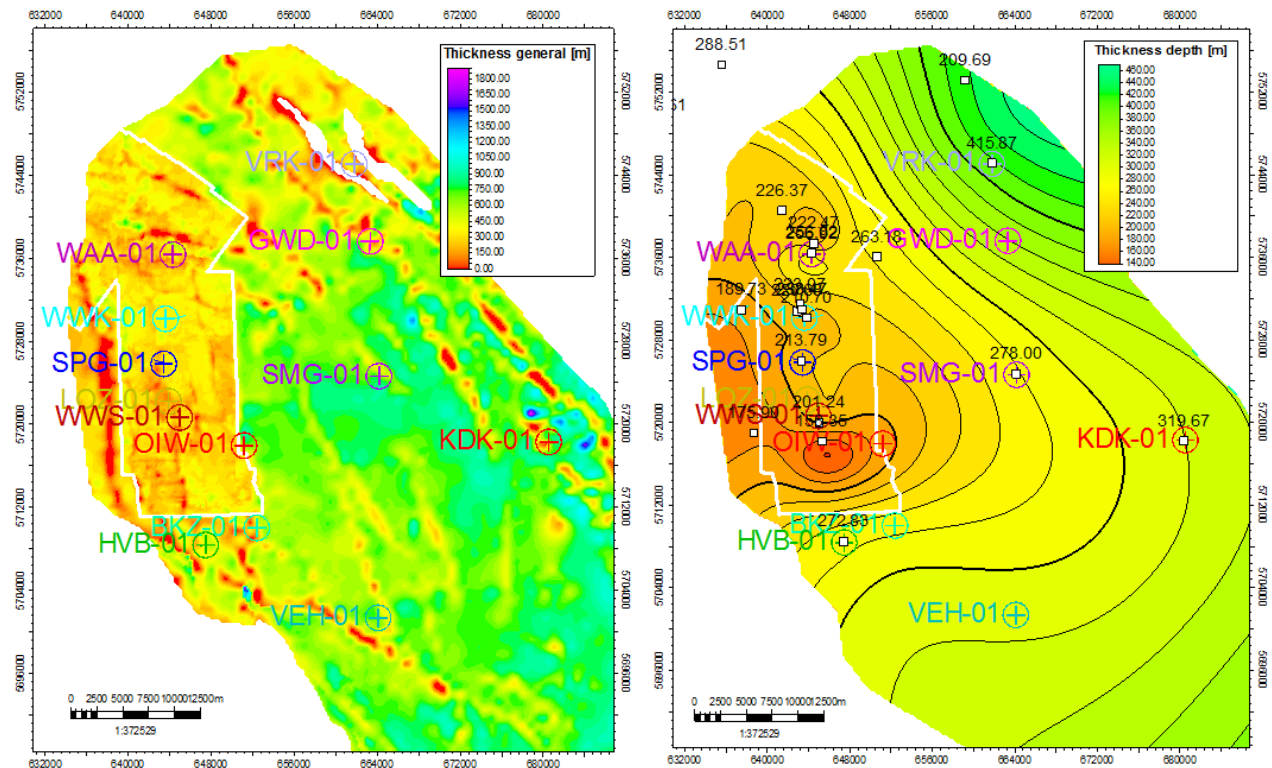


Figure 6.4: A comparison of the isochore map used by TNO and the structural framework of this study for the interpretation of base Upper Germanic Trias Group. The white contour indicates the outline of the 3D seismic cubes.

6.2 Oil Leads

Lead 1, 2 and 3 show a close approximation to a favorable juxtaposition configuration with respect to the Posidonia shale and the Main Buntsandstein Subgroup. The Posidonia Shale has been interpreted slightly above the Main Buntsandstein reservoir. It should be mentioned that lead 2 and 3 are located exactly on the boundary of the 3D seismic and 2D seismic, where both the quality on 2D and 3D is bad (see figure 6.5b). This made it hard to get

a solid interpretation making the structural closure modeled questionable. This makes lead 1, the most solid lead in this area. For the structures to qualify as an oil lead, the Posidonia shale needs to be situated at deeper levels to be mature enough for oil generation. The observed structures are situated in an area which is relatively high in the graben and migration from deeper levels where the Posidonia shale is assumed to be mature (see figure 4.6) is not deemed likely. Thus the probability that these structures are oil filled (based on maturity) is not plausible. However the mapped structures indicate the present-day situation, as inversion has occurred (figure 6.5b) in the area it is expected that the Posidonia shale initially was buried deeper prior to the Sub-Hercynian phase (Late Cretaceous). As no chalk deposits occur in the area it can be assumed that inversion related processes have removed the chalk. If the trap remained intact during the inversional periods than oil could have accumulated in this reservoir (figure 6.5a). This concept is deemed unlikely, as in this case the trap was most probably buried deeper as well. In conclusion, these leads classify better as a gas lead only.

Lead 7 has a similar configuration as lead 1 but is situated more to the south (see figure 5.1). In the area signs of inversion are less prominent making it very unlikely that this configuration works for oil charge. The structure is also situated just southward of the previously drilled Huibeven target which was proved to be dry.

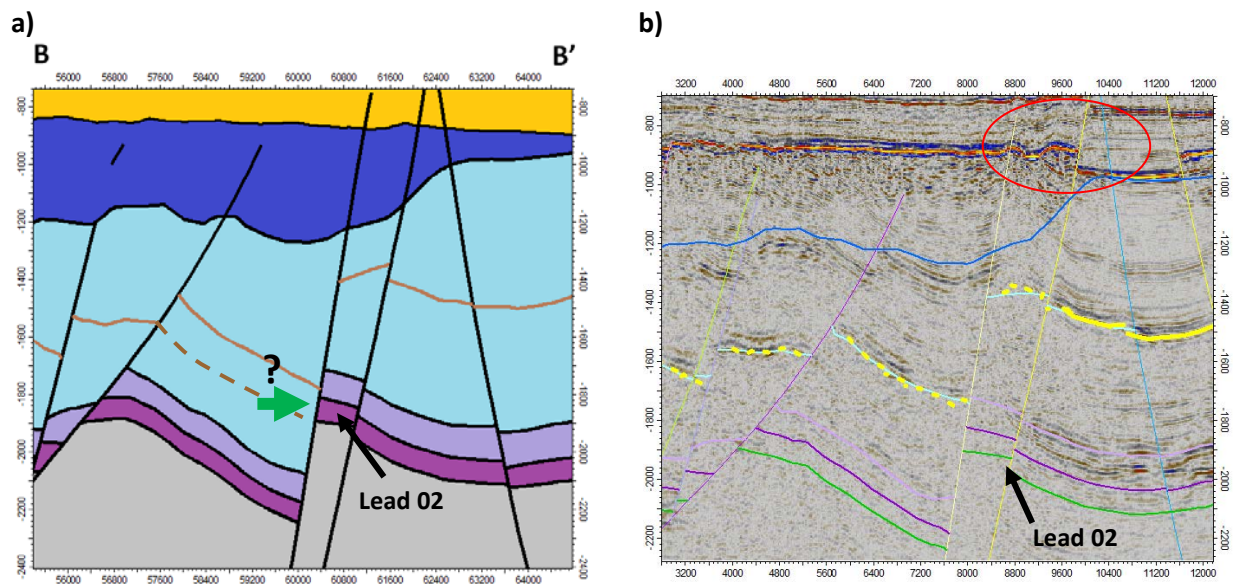


Figure 6.5: a) Cross-section through lead 02 (for location see figure 5.1). The possible migration path way has been identified. Color scale same as figure 5.2 b) Seismic line 871902 of the L2NAM1987J survey indicating inversion in the area. The most clear features occur at the level of the base North Sea Group (red ellipse), no chalk is interpreted here. The yellow interpretation correlates with the interpretation of the Posidonia Shale. The dotted line indicates the part that could be interpreted on the 3D seismic and the solid line corresponds to the interpretation on 2D seismic.

Other structures with a more favorable configurations are lead 4, 5 and 6 of which 4 and 6 are most promising as for these leads migration pathways can be established without the requirement of inversion (figure 6.6). Also for both structures, the migration pathways come from areas which are interpreted to be most mature in the basin (see figure 4.6). These structures however, are identified as down-thrown fault-dip closures and are situated next to the major boundary faults of the graben. This makes trap integrity not plausible. Also lead 4 is in the close proximity of a previously drilled dry structure, namely keldonk-1. Although this well did encounter hydrocarbon shows in the Röt Fringe Sandstone Member but preservation of potentially generated oil remains unrealistic. In lead 5 the Posidonia Shale is directly situated against the top Main Buntsandstein Subgroup making migration questionable. There is also a possibility that oil could have accumulated in the Röt fringe sandstones, which is situated above the main Buntsandstein reservoirs as is illustrated in figure 6.6c. Oil shows encountered in

the Röt Formations of the Andel, Brakel and Kerkwijk structures which lie in close proximity of each other, demonstrate that lateral migration of oil in this formation might work. The position of the Röt Fringe Sandstone Member has been determined in the same way as the top of the Main Buntsandstein Subgroup by construction of an isochore map and shaping the surface with the use of the base Altena interpretation. A quick rough estimate has been made of the STOIP, in the same way as for the other leads. The structure has a gross-rock-volume of $1.95 \cdot 10^8 \text{ m}^3$ and a calculated STOIP of $1.13 \cdot 10^7 \text{ m}^3$. For lead 6 there is a high chance that the lateral side seal (see figure 6.6d) is not sealing as there is a bunter-bunter contact, making this lead high risk. The lateral seal integrity in the northwestern corner of the trap is also questionable, data density here was low and the suggested fault configuration might be unrealistic.

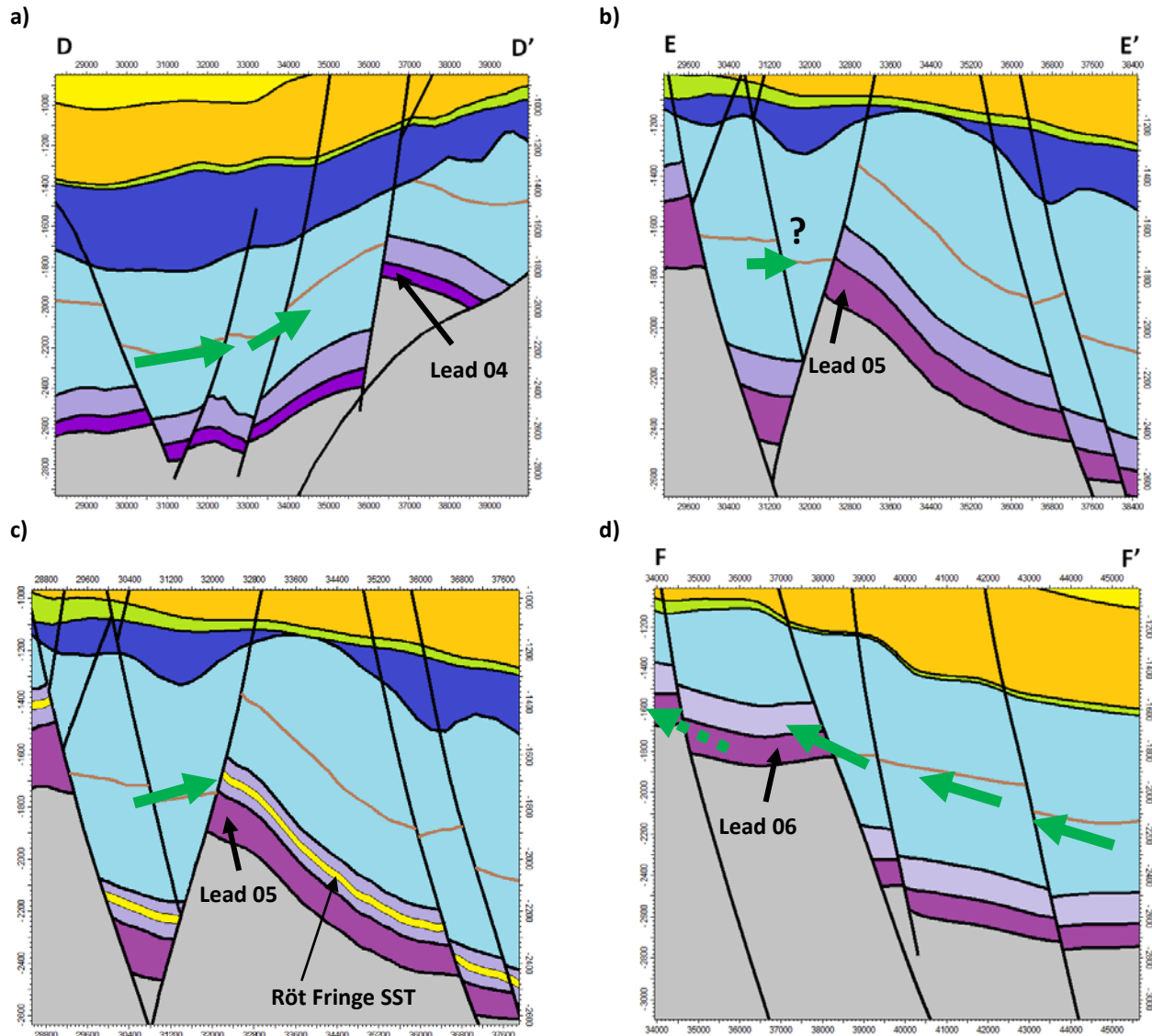


Figure 6.6: Possible oil migration into the structural closures of lead 4 (a), 5 (b-c) and 6 (d). The green arrow indicates oil charge from the Posidonia shale. For the location of the different leads in the graben see figure 5.1. Color scale same as figure 5.2

6.3 Gas Leads

As the main focus of the study lies on the identification oil traps, not much attention has been paid to the possible generation of gas from the Carboniferous Coal Measures and/or the Namurian Shales. The occurring gas fields in the Waalwijk area seem to have gas generated from these coals and shales, proving that this play mechanism works in the area (see section 4). Thus when assuming charge did occur throughout the basin, all identified leads at the level of the Main Buntsandstein Subgroup can be seen as potential leads for gas, including lead 1 through 7 which previously have been identified as potential oil leads. However, a lot of the identified structures are down-thrown fault-dip closures and these structures are seen as high risk due to the high probability of lateral seal breach. Thus in this section the leads that are deemed most promising will be presented with their possible migration pathways (figure 6.7 - 6.9).

In figure 6.7 the possible migration routes for lead 1 to 3 are identified. The migration pathway indicated in the cross-section of lead 1 (figure 6.7a) is similar for lead 2 and 3. The leads are situated just to the north of the proven gas fields Brakel, Andel and Kerkwijk. As these structures shows gas there is a chance that the gas that has been generated in this area could also be trapped in the three identified leads as spill from these fields could have migrated towards these structures or even generation occurred from deeper levels. The same can be postulated for the leads 11 and 22. These structures are situated in the proximity of Kerkwijk and Waalwijk South, respectively (figure 6.8). In the proximity of lead 9 and 10 (figure 6.9) no drilled structures are present, however it shows a favorable trap configuration and is one of the leads with the most promising volumetric.

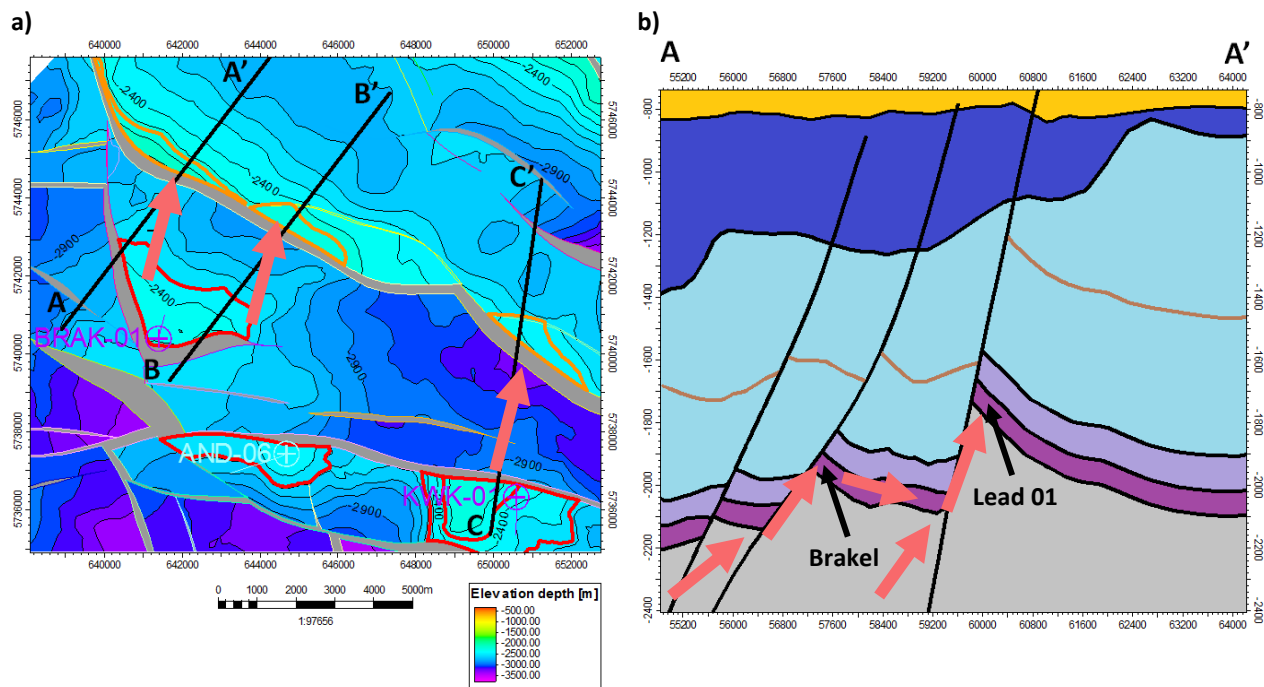


Figure 6.7: Possible gas migration into the structural closure of lead 1, 2, 3. The red arrows indicate possible migration pathways for gas from the carboniferous source rock in the area. The migration pathways indicated in the cross-section through lead 1 are similar for lead 2 and 3. For the location of the leads in the graben see figure 5.6. Color scale same as figure 5.2.

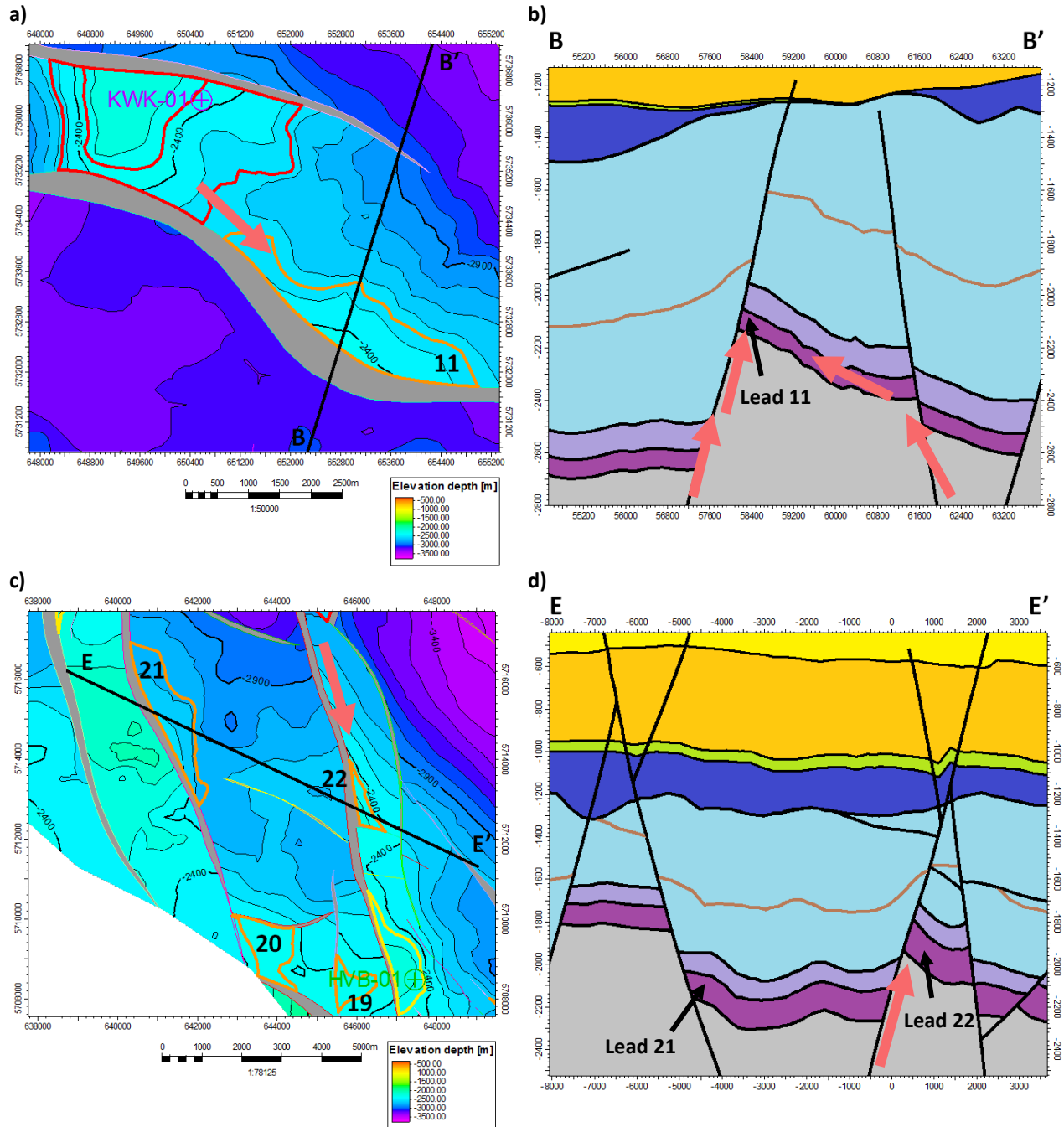


Figure 6.8: Possible gas migration into the structural closure of lead 11 and 22. The red arrows indicate possible migration pathways for gas from the carboniferous source rock in the area. For the location of the leads in the graben see figure 5.6. Color scale same as figure 5.2.

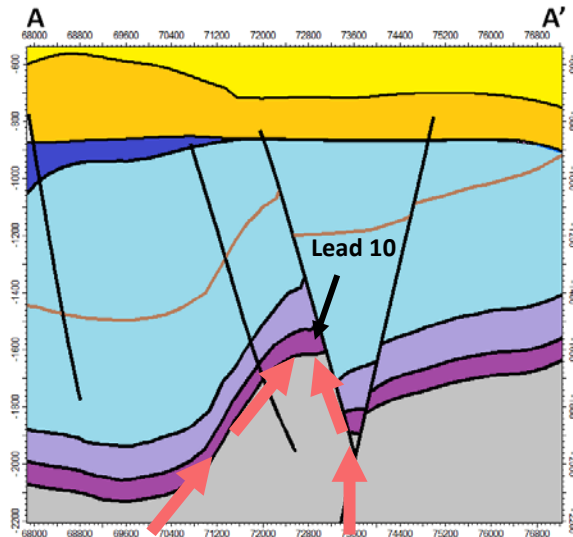


Figure 6.9: Possible gas migration into the structural closure of lead 10. The red arrows indicate possible migration pathways for gas from the carboniferous source rock in the area. The migration pathway is similar for lead 9. For the location of the leads in the graben see figure 5.6. Color scale same as figure 5.2

6.4 Risk qualification

Each identified lead has been qualified as a low, intermediate or a high risk (figure 6.10). This classification is based on the trap type, configuration and its location with respect to already drilled sites as well as the probability of maturity. This is not a probability of success classification (POS). It is a relative comparison of the leads compared to each other. All down-thrown fault-dip closures have been qualified as a high risk as these traps have a high chance at lateral fault seal failure and in most cases require sealing faults to be present at several sides of the trapped structure. Thus a higher chance that a local sandy interval in the lateral seals is present or that the fault is not sealing. If a lead is in the close proximity of a previously drilled structure that was proved dry, this structure is also classified as a high risk structure. Here there is a higher chance that a good seal is absent or seal breach has occurred. The remaining fault-dip closures have been identified as low risk, with several exceptions which are classified as intermediate risk. These will be discussed below.

Lead 5 (minimum), both an oil and gas lead, has been classified as an intermediate risk for the oil scenario and as a high risk for the gas scenario. It is classified as a high risk lead for gas due to the close proximity to two dry structures, Hilvarenbeek and Broekzijde. However, based on the juxtaposition configuration of the Posidonia Shale with respect to the Main Buntsandstein Subgroup, this trap may have the potential for oil accumulation (see figure 6.6). Also the previously drilled structures Hilvarenbeek and Broekzijde have oil shows. Hilvarenbeek encountered weak shows at the Röt Fringe Sandstone and Claystone Member, the Lower Muschelkalk Member, the Brabant Formation and the Posidonia Shale. Broekzijde showed weak to good oil shows in the Lower Werkendam Member, Sleen Formation, Röt Fringe Sandstone Member and several good oil shows in the Detfurth and Volpriehausen Formations (see section 4.4.3). Another scenario for this lead could be oil charge in the Röt Formations situated slightly above the Main Buntsandstein Subgroup (figure 6.6). Due to the occurrence of positive oil shows in the area, the lead has been classified as intermediate risk, instead of high risk due to its close proximity to dry structures. It should be noted however, that the maturity in the area is questionable and it involves only a small area of source rock in the local through. Thus actual accumulation of oil and the STOIIP calculated are deemed high risk.

Lead 1 to 3, also identified as both oil and gas leads, classify as intermediate risk for lead 1 and high risk for lead 2 and 3 in the oil scenario (figure 6.10). The three structures have a close approximation to a favorable

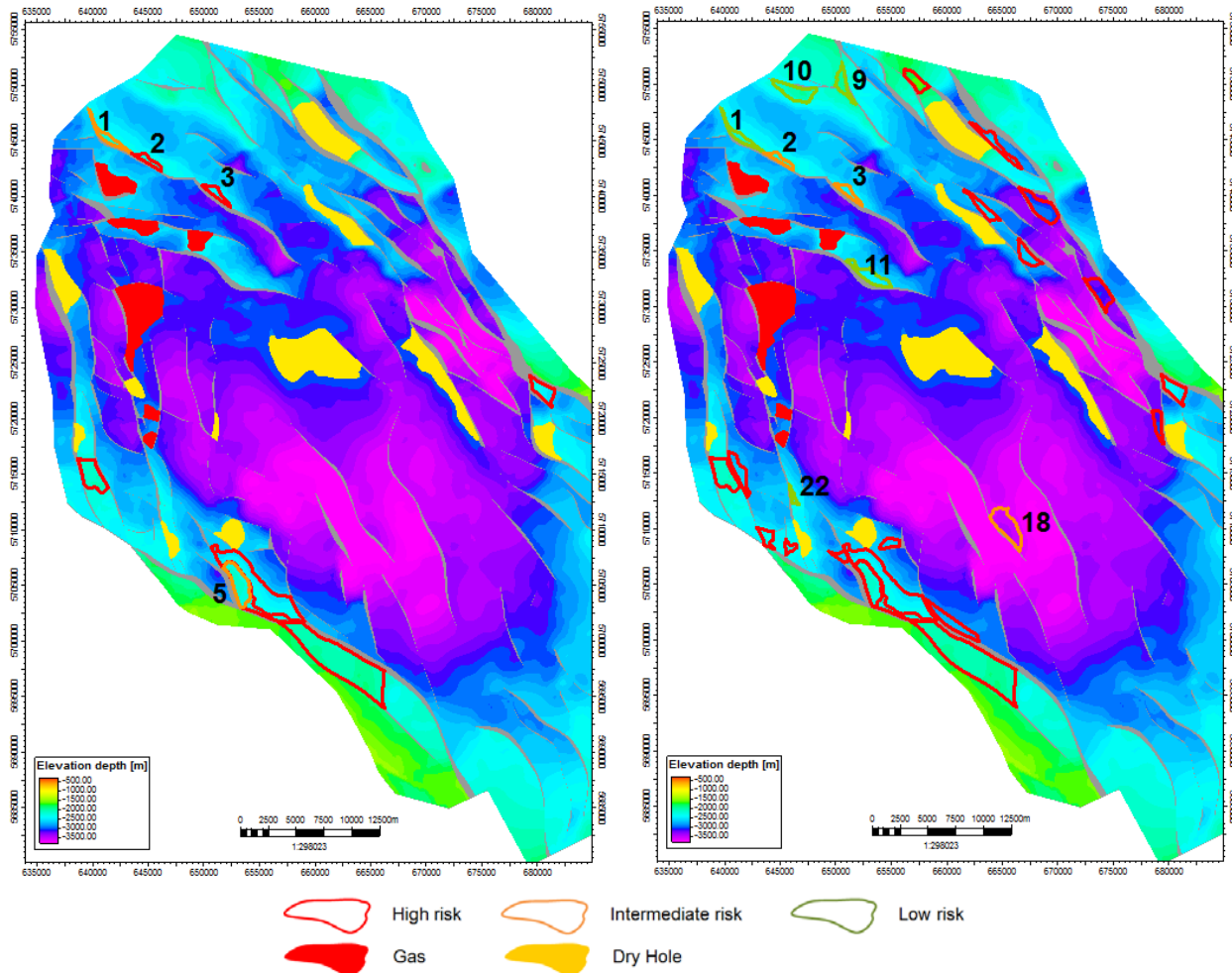


Figure 6.10: Risk qualification of the oil (left) and gas leads (right).

juxtaposition configuration with respect to the Posidonia shale and the Main Buntsandstein Subgroup, however it is questionable if the Posidonia has been mature enough for oil generation in this area (see figure 4.6 & 6.5) as has been previously discussed (see section 6.2). The structural closures of lead 2 and 3 are also questionable due to their location on the boundary of 2D and 3D seismic, giving these leads a higher risk than lead 1. Drilled wells in the proximity of these structures (BRAK-01, AND-06 and KWK-01) however did encounter good oil shows in the Detfurth and Upper Volpriehausen and Röt Fringe Formations (see section 4.4.1), making oil accumulation in these leads an option but still very unlikely due to its configuration with respect to the Posidonia Shale. For the gas scenario these leads have a low risk due to the proximity of the Brakel, Andel and Kerwijk structures which are all three gas fields. Lead 2 and 3 however are classified as intermediate risk due to the uncertainties in the mapped structure. It can be assumed that in the area enough charge has occurred for gas accumulation in the structures.

Gas lead 18 is identified as a fault-dip closure, but due to its location within the center of the graben it is very likely that porosity and permeability within this structure are low. This has been observed in well SMG-01. Here porosities were recorded of approximately 6%. Thus this structural closure has been classified as an intermediate risk.

The remaining leads 9, 10, 11 and 22 are all classified as low risk gas leads. These leads have no drilled dry wells in their proximity and are all fault-dip structural closures. Lead 11 and 22 also have proven gas reserves nearby, namely the undeveloped Kerkwijk field and the Waalwijk South field, respectively. Thus charge is proven in these areas. Spill from these fields might also have accumulated in the lead structures.

In table 4 an overview of the risk classification is given with corresponding STOIIP and GIIP calculations. It can be concluded that the most promising leads are gas leads of which lead 1, 11 and 22 have proven gas accumulations nearby (Brakel, Kerkwijk and Waalwijk South, respectively). The juxtaposition of the Possidonia Shale below the Main Buntsandstein Subgroup seems problematic throughout the area and only two probable leads with the closest approximation of this configuration have been identified, namely lead 1 and 5. Of these two, lead 5 seems to be most probable due to the oil shows in the surrounding drilled structures but still very unlikely. The structures probably has a higher chance of being filled with gas if off course the structure is correctly sealed by the shale formations of the Röt Formation and Altena Group. It should be noted that the presented STOIIP and GIIP are a rough estimates as several assumption were made regarding the porosity, net-to-gross, hydrocarbon saturation and the formation volume factors which can vary per structure.

Lead no.		STOIIP (m ³)	GIIP (BCM)
1		9.38E+06	1.79
2		2.83E+06	0.54
3		3.65E+06	0.75
4		1.78E+07	3.91
5	Min	2.08E+07	4.02
5	Int	3.08E+07	6.01
5	Max	2.66E+08	57.75
6		1.91E+08	34.77
7		1.96E+07	3.66
8			1.19
9			1.3
10			5.47
11			2.92
12			1.37

Lead no.	GIIP (BCM)
13	1.29
14	1.61
15	5.76
16	2.46
17	1.36
18	2.58
19	0.06
20	0.38
21	1.72
22	0.44
23	1.14
24	0.3
25	2.46

Table 4: STOIIP and GIIP calculations color coded according to risk. Red = high risk, Orange = medium risk and Green = low risk.

7. Conclusions

The aim of this study was to re-assess the conventional prospectivity of the Roer Valley Graben with a focus on oil charge from the Posidonia Shale Formation into Triassic reservoir of the Main Buntsandstein Subgroup. A second objective was to assess the value of digitizing old paper copies of 2D seismic lines. The following can be concluded:

- Seismic digitization greatly enhances the quality and usefulness of old 2D seismic data. After digitization the full spectrum of the seismic signal can be used in the interpretation on a workstation. This includes mis-tie correction as well as automated tracking utilities for seismic interpretation.
- The structural Framework Module of Petrel is a great tool for modeling in an area with limited data density and quality. The option to guide a horizon interpretation by another surface was particularly useful to shape the Main Buntsandstein subgroup interpretation by combining isochore data from wells and the interpretation of the base Altona, the last horizon which was fully mappable in the area.
- The well review of oil shows indicated that there lies some potential for oil in the Bunter reservoirs. However, based on the detailed mapping of the Posidonia Shale and Main Buntsandstein it can be concluded that juxtaposition of the Posidonia below the Main Buntsandstein Subgroup seems very unlikely. Only in several scenarios this was found where maturity is questionable or dry holes have been drilled. Based on shows there seems more potential in younger formations when it comes to charge.
- The lead which qualifies best for oil and juxtaposition of the Posidonia Shale against the Main Buntsandstein Subgroup is a fault-dip closure situated in the southern sector of the graben (lead 5). Although maturity and position of the Posidonia Shale is questionable. The surrounding wells HVB-01 and BKZ-01 do show signs of oil in the Triassic reservoir formations and there is also a possibility that the stratigraphically higher Röt Fringe Sandstone could have accumulated oil in this structure.
- From the risk qualification made, the leads with the lowest risk are gas leads situated in the northwestern sector of the graben and towards the south of the Waalwijk South field in several fault-dip closures (Lead 1, 9, 10, 11 and 22). This is based on the trap type, configuration and its location with respect to already drilled sites and the probability of maturity. Of these leads the most promising are lead 1, 11 and 22 as these have proven gas accumulations nearby (Brakel, Kerkwijk and Waalwijk South, respectively).

8. Recommendations

A next step in the prospectivity re-assessment of the Roer Valley Graben should be to identify potential structures at the level of the Early Jurassic Brabant Limestones (top Altena Group). Several wells in the area indicated oil shows at the level of this formation, namely Hilvarenbeek-1, Oisterwijk-1, Loon op Zand-1, Veldhoven-1 and the Andel wells. This indicates that this formation could have hydrocarbon potential. The detailed framework at the level of the Posidonia shale, base Altena Group and Main Buntsandstein Subgroup could be extended by re-evaluating the interpretation at the level of the Schieland Group and the above lying formations. This could be combined when evaluating the potential of the Brabant Limestones in the area. Another aspect that might prove useful is to look better into the basin shoulders (the Campine Block and the Peel Block), as hydrocarbon potential might have been missed here as the focus of this study was on the graben structures.

9. Acknowledgements

First of all, I would like to thank Maarten-Jan Brolsma and Michiel Harings for giving me the opportunity to apply for this internship project at EBN. This made it possible for me to be involved in a challenging working environment and be part of a great team of people. Especially, I would like to thank my direct supervisor Michiel Harings for his insightful and continued support both professionally and personally and the quick reviews of the work in progress. Hans de Bresser (UU) is thanked for his continued support and useful ideas throughout the research. Lastly, I would like to thank my colleagues at EBN for their support, advise and hospitality during my stay at EBN.

10. References

- Adrichem Boogaert, H. A. v. and W. F. P. Kouwe 1993-1997.** Stratigraphic Nomenclature of the Netherlands. RGD and NOGEPA, Geological Survey of the Netherlands.
- Bless, M. J. M., Bouckaert, J. and Paproth, E. 1983.** Recent exploration in pre-Permian rocks around the Brabant Massif in Belgium, the Netherlands and the Federal Republic of Germany. *Geologie en Mijnbouw*, 62, 51-63.
- BP, British Petroleum Exploratie Mij. Nederland B.V., Van Zutphen, A.C.A. (1987).** Geological Completion Report Waalwijk-1
- BP, British Petroleum Exploratie Mij. Nederland B.V., Chapman, J. and Pressage, S. (1989).** Broekzijde-1 Geological Completion Report.
- Bouw, S., & Lutgert, J. (2012).** *Shale Plays in The Netherlands*. In SPE/EAGE European Unconventional Resources Conference & Exhibition-From Potential to Production.
- Clyde Petroleum Exploratie B.V., Browne, L., 1992.** Keldonk-1 End of Well Report.
- Clyde Petroleum Exploratie B.V., Jaggie, F. and Robbermond, R.H.C. (1996).** Hilvarenbeek-1 Final Wellsite Geological Report.
- Clyde Petroleum, Taylor G.B., Jaggie, F. and Robbermond, R.H.C. (1999).** Final Wellsite Geological Report, Waalwijk N3, Waalwijk Prospect, Onshore, the Netherlands.
- De Jager, J. 2003.** Inverted basins in the Netherlands, similarities and differences. *Netherlands Journal of Geosciences, Geologie en Mijnbouw* 82 (4): 355-366.
- De Jager, J., 2007.** Geological development. In: Wong, Th.E., Batjes, D.A.J. & de Jager, J. *Geology of the Netherlands*. Royal Netherlands Academy of Arts and Sciences, 2007: 5-26.
- De Jager, J. & Geluk, M.C., 2007.** Petroleum geology. In: Wong, Th.E., Batjes, D.A.J. & de Jager, J. *Geology of the Netherlands*. Royal Netherlands Academy of Arts and Sciences, 2007: 241-264.
- De Lugt, I.R., Van Wees, J.D., Wong, Th.E., 2003.** The tectonic evolution of the southern Dutch North Sea during the Paleogene: basin inversion in distinct pulses. *Tectonophysics* 373 (1-4), 141-159.
- De Mulder, E.F.J., Geluk, M.C., Ritsema, I., Westerhoff, W.E., Wong, Th.E., 2003.** *De ondergrond van Nederland*. Nederlandse Organisatie voor toegepast-natuurwetenschappelijk onderzoek TNO, p. 379.
- EBN (2012).** Oil Play in the Eastern part of the West Netherlands Basin and Roer Valley Graben in Zuid Holland and Noord Brabant.
- Fina. American Petrofina Exploration Company. Hoppener, H., 1969.** Rapport géologique puits Sint Michielsgestel No. 1 Pays-Bas.
- Geluk, M.C., Duin, E.J. Th., Duser, M., Rijkers, R.H.B., van den Berk, M.W., van Rooijen, P., (1994).** Stratigraphy and tectonics of the Roer Valley Graben. *Geologie en mijnbouw* 73, 129-141.
- Geluk, M.C. & Rohling H.-G., 1997.** High-resolution sequence stratigraphy of the Lower Triassic 'Buntsandstein' in the Netherlands and northwestern Germany. *Geologie en Mijnbouw* 76: 227-246.

- Geluk, M.C. & Rohling, H.-G., 1999.** High-resolution sequence stratigraphy of the Lower Triassic Buntsandstein: a new tool for basin analysis. In: Bachmann, G.H. & Lerche, I. (eds): The Epicontinental Triassic. *Zentralblatt für Geologie und Paläontologie* 7-8: 545–570.
- Geluk, M.C. 1999b.** Palaeogeographic and structural development of the Triassic in the Netherlands- new insights. In: Bachmann, G.H. & Lerche, I. (eds). The Epicontinental Triassic. *Zentralblatt für Geologie und Paläontologie*, Heft 7-8, p.727-745.
- Hergreen, G.F.W., Kouwe, W.F.P. & Wong, Th.E., 2003.** The Jurassic of the Netherlands. In: Ineson, J.R. & Surlyk, F. (eds): The Jurassic of Denmark and Greenland. *Geological Survey of Denmark and Greenland Bulletin* 1: 217–229.
- Hergreen, G.F.W. & Wong, Th.E 2007.** Cretaceous. In: Wong, Th.E., Batjes, D.A.J. & De Jager, J. (eds): *Geology of the Netherlands*. Royal Netherlands Academy of Arts and Sciences (Amsterdam): 127–150.
- Kley, J. & Voigt, T., 2008.** Late Cretaceous intraplate thrusting in central Europe: Effect of Africa-Europe-Iberia convergence, not Alpine collision. *Geology* 36: 839-842.
- Lokhorst, A. (Ed.), 1998.** The Northwest European gasatlas. Netherlands Institute of Applied Geosciences TNO (Haarlem): ISBN 90-72869-60-5.
- Luijendijk, E., Ter Voorde, M., Van Balen, R., Verweij, H., Simmelink, H., 2010.** Thermal state of the Roer Valley Graben, part of the European Cenozoic Rift System. *Basin Research* doi: 10.1111/j.1365-2117.2010.00466.x.
- NITG, 2001.** Geological Atlas of the subsurface of the Netherlands, Explanation to Map Sheets XIII-XIV Breda-Valkenswaard and Oss-Roermond (1:250000). Netherlands Institute for Applied Geoscience TNO (Utrecht): 150 pp.
- Nelskamp, S., David, P., Littke, R., 2008.** A comparison of burial, maturity and temperature histories of selected wells from sedimentary basins in The Netherlands. *Int J of Earth Sci (Geol Rundsch)* (2008) 97:931-953.
- NITG, 2002.** Geological Atlas of the Subsurface of the Netherlands: Explanation to mapsheets VII and VIII: Noordwijk-Rotterdam and Amsterdam–Gorinchem. Utrecht, 135pp.
- NITG, 2004.** Geological atlas of the subsurface of the Netherlands–onshore. Netherlands Institute of Applied Geoscience TNO (Utrecht): 104 pp.
- NPN (2008) Northern Petroleum Nederland**, NPN Document nr: NPN-BRAK-OPS-0-2008-002. Hydraulic Fracturing and Clean out Guidelines.
- Pharaoh, T.C., Dusar, M., Geluk, M.C., Kockel, F., Krawczyk, C.M., Krzywiec, P., Scheck-Wenderoth, M., Thybo, H., Vejbaek, O.V. & Van Wees, J.D., 2010.** Tectonic evolution. In: Doornenbal, J.C. and Stevenson, A.G. (editors): *Petroleum Geological Atlas of the Southern Permian Basin Area*. EAGE Publications b.v. (Houten): 25-57.
- Standing, M.B. and Katz, D.L. 1942.** Density of Natural Gases. In *Transactions of the American Institute of Mining and Metallurgical Engineers*, No. 142, SPE-942140-G, 140–149. New York: American Institute of Mining and Metallurgical Engineers Inc.

- Van Balen, R.T., Van Bergen, F., de Leeuw, C., Pagnier, H., Simmelink, H., Van Wees, J.D., Verweij, J.M., 2000.** Modelling the hydrocarbon generation and migration in the West Netherlands Basin, the Netherlands. *Geologie en Mijnbouw/Netherlands Journal of Geosciences* 79 (1), 29–44.
- Van Dalfsen, Drs. W., van Gessel, Drs. S.F. and Doornenbal, Drs. J.C. 2007.** TNO report 2007-U-R1272C Veldmod-2 Joint Industry Project.
- Van Hulten (2009).** Brief History of Petroleum Exploration in the Netherlands.
- Van Leverink, D.J.; Bergen, F. van; 2008;** Influence of Early Jurassic tectonics on present day source rock distribution; TNO internal study
- Van Wijhe, D. H. (1987).** Structural evolution of inverted basins in the Dutch Offshore. *Tectonophysics*, **137**, 171-219.
- Vercoutere, C. & van den Haute, P. (1993)** Post-Palaeozoic cooling and uplift of the Brabant Massif as revealed by apatite fission track analysis. *Geol. Mag.*, 130, p. 639-646.
- Winstanley, A.M. (1993).** A review of the Triassic play in the Roer Valley Graven, SE onshore Netherlands, in *Petroleum Geology Conference Series*, vol 4, edited by J.R. Parker, pp 595-607, Geol. Soc., London.
- Worum, G., Michon, L., van Balen, R. T., van Wees, J.-D., Cloetingh, S., and Pagnier, H., 2005.** Pre-Neogene controls on present-day fault activity in the West Netherlands Basin and Roer Valley Rift System (southern Netherlands): role of variations in fault orientation in a uniform low-stress regime: *Quaternary Science Reviews*, 24(3-4), p. 473-488.
- Ziegler, P.A., 1990.** Geological Atlas of Western and Central Europe. Shell Internationale Petroleum Maatschappij, 2nd edition. Geological Society Publishing House (Bath): 239 pp.
- Zijerveld, L., Stephenson, R., Cloetingh, S., Duin, E., Van den Berg, M.W., 1992.** Subsidence analysis and modelling of the Roer Valley Graben (SE Netherlands). *Tectonophysics* 208, 159–171.
- De Jager, J., Doyle, M.A., Grantham, P.J. Mabillard, J.E., 1996.** Hydrocarbon habitat of the West Netherlands Basin. In: Rondeel et al. (eds), *Geology of gas and oil under the Netherlands*, 191-209, 1996.

Appendix A: Hydrocarbon shows

Well	OIL	GAS	HC Significance	MD HC Shows (m)	Show Description
AND-01	TRUE		Presence of light yellow fluorescing liptodetrinite (VR.E: around 0.60%; just mature for oil	1940	-999.25
AND-02	TRUE	FALSE	Fluorescentie intensiteit 30000 ppm	960	Fluorescentie ppm schnb olie
AND-02	TRUE	FALSE	Fluorescentie intensiteit 15000 ppm	968	Fluorescentie ppm schnb olie
AND-02	TRUE	FALSE	Fluorescentie intensiteit 3500 ppm	1002	Fluorescentie ppm schnb olie
AND-02	TRUE	FALSE	Fluorescentie intensiteit 1500 ppm	1033	Fluorescentie ppm schnb olie
AND-02	TRUE	FALSE	Fluorescentie intensiteit 1400 ppm	1062	Fluorescentie ppm schnb olie
AND-02	TRUE	FALSE	Fluorescentie intensiteit 1300 ppm	1160	Fluorescentie ppm schnb olie
AND-02	TRUE	FALSE	Fluorescentie intensiteit 2700 ppm	1220	Fluorescentie ppm schnb olie
AND-02	TRUE	FALSE	Fluorescentie intensiteit 2600 ppm	1230	Fluorescentie ppm schnb olie
AND-02	TRUE	FALSE	Fluorescentie intensiteit 1500 ppm	1375	Fluorescentie ppm schnb olie
AND-02	TRUE	FALSE	Fluorescentie intensiteit 2100 ppm	1460	Fluorescentie ppm schnb olie
AND-04	TRUE	FALSE	Fluorescentie intensiteit 1100 ppm	1540	-999.25
AND-05	TRUE	FALSE	Thin Oil bearing fine sand	892	-999.25
AND-05	TRUE	FALSE	Oil traces	980	-999.25
AND-05	TRUE	FALSE	Oil spots and odor	1543	-999.25
AND-06	FALSE	TRUE	Gas Detection While Drilling 5816 ppm	720	-999.25
AND-06	FALSE	TRUE	Gas Detection While Drilling 25932 ppm	1040	-999.25
AND-06	FALSE	TRUE	Gas Detection While Drilling 4576 ppm	1460	-999.25
AND-06	FALSE	TRUE	Gas Detection While Drilling 9500 ppm	1925	-999.25
AND-06	FALSE	TRUE	Gas Detection While Drilling 5050 ppm	2140	-999.25
AND-06	FALSE	TRUE	Gas Detection While Drilling 2315 ppm	2585	-999.25
AND-06	FALSE	TRUE	Gas Detection While Drilling 26000 ppm	2760	-999.25
AND-06	FALSE	TRUE	Gas Detection While Drilling 16700 ppm	2781	-999.25
AND-06	FALSE	TRUE	Gas Detection While Drilling 8000 ppm	3114	-999.25
BKZ-01	FALSE	TRUE	2513 ppm	2284	-999.25
BKZ-01	TRUE	FALSE	Trace	1720	v. dull brown fluorescence, v dull poor yellow crush cut
BKZ-01	TRUE	FALSE	Trace	2300	Dead oil stain (decreasing with depth), dull brown fluorescence, slow-strong yellow white cut fluor, dark brown residue.
BRAK-01	FALSE	TRUE	12000 ppm	1190	Gas detection while drilling
BRAK-01	FALSE	TRUE	9800 ppm	2103	Gas detection while drilling
BRAK-01	FALSE	TRUE	63800 ppm	2336	Gas detection while drilling
BRAK-01	FALSE	TRUE	9700 ppm	2484	Gas detection while drilling
BRAK-01	TRUE	FALSE	Good	1190	Asphalt: Heavy Tarry dead oil
BRAK-01	TRUE	FALSE	Weak	2375	?
BRAK-01	TRUE	FALSE	Weak	2450	?
BRAK-01	TRUE	FALSE	Fair	2480	Weak-fair white -yellow fluor
BRAK-01	TRUE	FALSE	Weak	2510	?
BUM-01	TRUE	FALSE	Trace to Fair?	2060	-999.25
GWD-01	TRUE	FALSE	-999.25	-999.25	-999.25
GWD-01-S1	TRUE	FALSE	Weak	1535	wk flor WH str solv
GWD-01-S1	TRUE	FALSE	Weak	1670	wk flor WH br str solv
GWD-01-S1	TRUE	FALSE	Weak	1850	Oil show in DM only
HBV-01	FALSE	TRUE	2552 ppm	1789	Werkendam Fm
HBV-01	FALSE	TRUE	4580 ppm	1834	Werkendam Fm
HBV-01	FALSE	TRUE	2170 ppm	1903	Sleen Fm
HBV-01	TRUE	FALSE	Weak	1575	Direct Fluor: mod. Weak, bright yellowish white, diffuse to patchy. Cut Fluor: Weak diffuse yellowish white. Residue: yellowish white. No stain
HBV-01	TRUE	FALSE	Weak	2030	Locally weak yellow direct fluor, traces of slow yellow cut fluor, no stain, no residue.
HBV-01	TRUE	FALSE	Weak	2070	Locally weak yellow direct fluor, traces of slow yellow cut fluor, no stain, no residue.

Well	OIL	GAS	HC Significance	MD HC Shows (m)	Show Description
HBV-01	TRUE	FALSE	Weak	2115	Trace to 50% spotty; weak light brown - bluish white direct fluor. Very slow dull yellowish green, blooming cut fluor, no stain, no residue.
HPT-01	TRUE	FALSE	Trace	1310	zeer geringe oliesporen, slechts op splijt vlakken, goede oliereuk.
HPT-01	TRUE	FALSE	Trace	1412	zeer geringe oliesporen op splijt vlakken
HPT-01	TRUE	FALSE	Weak	1752	white-yellow fluorescing liptinites (VR. E: around 0.50%)
HVB-01	FALSE	TRUE	0,68 - 0,99%	1732	-999.25
HVB-01	FALSE	TRUE	1.11%	1750	-999.25
HVB-01	FALSE	TRUE	0.69%	2030	-999.25
HVB-01	TRUE	FALSE	Weak	1320	Yellowish brown direct fluor, poor yellowish white crush cut fluor with a yellowish white fluor residue.
HVB-01	TRUE	FALSE	Weak	1335	Yellowish brown direct fluor, poor yellowish white crush cut fluor with a yellowish white fluor residue.
HVB-01	TRUE	FALSE	Weak	1360	Yellowish brown direct fluor, poor yellowish white crush cut fluor with a yellowish white fluor residue.
HVB-01	TRUE	FALSE	Weak	1380	Bright white to light yellow direct fluor, instant streaming yellowish white cut fluor, bright yellow fluor residue and occasionally light brown stain.
HVB-01	TRUE	FALSE	Weak	1760	Bright white direct fluor, poor slow straming yellowish white cut fluor and a bright yellowish white fluor residue.
HVB-01	TRUE	FALSE	Weak	1800	Bright yellow fluor, slow streaming yellowish white cut fluor.
HVB-01	TRUE	FALSE	Weak	2200	Yellow direct fluor, slow streaming white cut fluor and a yellow white fluor residue.
HVB-01	TRUE	FALSE	Weak	2230	Occasionally light brown stain, bright yellow to dull yellow direct fluor, instant slow streaming white cut fluor and a yellow fluor residue.
HVB-01	TRUE	FALSE	Weak	2245	Occasionally light brown stain, bright yellow to dull yellow direct fluor, instant slow streaming white cut fluor and a yellow fluor residue.
KDK-01	TRUE	FALSE	Trace	1435	-999.25
KDK-01	TRUE	FALSE	Fair	1485	-999.25
KDK-01	TRUE	FALSE	Good	1545	-999.25
KDK-01	TRUE	FALSE	Good	1582	-999.25
KDK-01	TRUE	FALSE	Weak	1535	Dull yel fluor
KDK-01	TRUE		Weak	1960	Dull-bri spty fluor, sl wk yel-fast bri yel blmg cut fluor
KWK-01	FALSE	TRUE	5000 ppm	1800	Gas detection while drilling
KWK-01	FALSE	TRUE	3500 ppm	2175	Gas detection while drilling
KWK-01	FALSE	TRUE	40000 ppm	2417	Gas detection while drilling
KWK-01	FALSE	TRUE	6700 ppm	3145	Gas detection while drilling
KWK-01	TRUE	FALSE	Fair	1520	wh yell fluor./w. wh cut flu/ult tea Chl.
KWK-01	TRUE	FALSE	Weak	2415	bright wh-yel fluo, v lt Chl cut, weak wh cut fluo
KWK-01	TRUE	FALSE	Weak	2455	dull-bright wh yel fluo, extra lt Chl cut, v weak wh cut flue, oil stain
KWK-01	TRUE	FALSE	Weak	2555	v pale wh yel fluo, v lt Chl cut, v weak wh cut fluo.
KWK-01	TRUE	FALSE	Weak	2605	pale-dull wh yel fluo, extr lt Chl cut, v weak wh cut fluo.

Well	OIL	GAS	HC Significance	MD HC Shows (m)	Show Description
SPC-01	FALSE	TRUE	3900 ppm	2350	ppm Total Gas
SPC-01	FALSE	TRUE	20000 ppm	2515	ppm Total Gas
SPC-01	TRUE		very weak	1627	no nat fluor, some min fluor
SPG-01	FALSE		7.3%	2156	anomalously high gas peak
SPG-01	TRUE		Fair	3050	yellowish white fluor and a slow streaming white cut.
SPG-01-S2	TRUE	FALSE	Fair	3010	yel wh fluor, slow streaming wh cut.
VRK-01	TRUE	FALSE	Weak	1486	?
WWK-01	FALSE	TRUE	4672 ppm	1347	Sandstone (Delfland Group)
WWK-01	FALSE	TRUE	3089 ppm	1681	Coal/Sandstone (Delfland Group)
WWK-01	FALSE	TRUE	5500 ppm	2685	Carbonaceous Mudstone (Posidonia Shale)
WWK-01	FALSE	TRUE	3489 ppm	3220	Limestone/Mudstone (Aalburg Shale)
WWK-01	FALSE	TRUE	12800 ppm	3487	Sandstone/Mudstone (Bunter Group)
WWK-01	TRUE	FALSE	Weak	1754	5-10% nat fluor, slow wh-yel crush-cut fluor.
WWK-01	TRUE	FALSE	Weak	1885	occ dull wh-bright yel nat fluor, slow cut, mod milky wh crush-cut fluor.
WWK-01	TRUE	FALSE	Weak	2000	occ dull yel nat fluor, slow wh crush-cut fluor.
WWK-01	TRUE	FALSE	Weak	2426	3-5% yel nat fluor slow streaming wh-yel cut, fast milky crush cut fluor.
WWK-01	TRUE	FALSE	Weak	3580	loc bituminous residual oil: dull wh-yel nat fluor, fast wh-dull yel blooming cut becoming slow with depth
WWN-01-S2	FALSE	TRUE	16%	3210	-999.25
WWN-01-S2	FALSE	TRUE	2.40%	3295	-999.25
WWN-02-S1	TRUE	FALSE	Fair	1705	traces-20% dull yell nat fluor, slow-mod str-blmg cut fluor.
WWN-02-S1	TRUE	FALSE	Fair	2610	tr-30% dull yel nat fluor, fast str-blmg cut fluor.
WWN-02-S3	TRUE	FALSE	Fair	2610	tr-10% dull yell fluor, mod-fast str/blm cut
WWN-02-S4	FALSE	TRUE	30600 ppm	2585	-999.25
WWN-02-S4	FALSE	TRUE	43400 ppm	2925	-999.25
WWN-02-S4	FALSE	TRUE	15800 ppm	3015	-999.25
WWN-02-S4	FALSE	TRUE	21300 ppm	3285	-999.25
WWN-02-S4	FALSE	TRUE	11000 ppm	3340	-999.25
WWN-02-S4	FALSE	TRUE	12000 ppm	3558	-999.25
WWN-02-S4	FALSE	TRUE	10000 ppm	3700	-999.25
WWN-02-S4	FALSE	TRUE	10000 ppm	3920	-999.25
WWN-02-S4	TRUE	FALSE	Fair	2600	nat fluo: gold-yell, spot, cut flue; bl-wh, slow, no rim, no stain.
WWN-02-S4	TRUE	FALSE	Fair	2655	nat fluo: gold-yell, spot, cut flue; bl-wh, slow, no rim, no stain.
WWN-03	FALSE	TRUE	50000 ppm	1434	-999.25
WWN-03	FALSE	TRUE	50000 ppm	1509	-999.25
WWN-03	FALSE	TRUE	20000 ppm	1624	-999.25
WWN-03	FALSE	TRUE	22000 ppm	2414	-999.25
WWN-03	FALSE	TRUE	50000 ppm	2469	-999.25
WWN-03	FALSE	TRUE	20000 ppm	3118	-999.25
WWN-03	FALSE	TRUE	23000 ppm	3410	-999.25
WWN-03	FALSE	TRUE	80000 ppm	3415	-999.25
WWN-03	FALSE	TRUE	65000 ppm	3427	-999.25
WWN-03	FALSE	TRUE	70000 ppm	3455	-999.25
WWN-03	FALSE	TRUE	25000 ppm	3505	-999.25
WWN-03	FALSE	TRUE	64000 ppm	3519	-999.25
WWN-03	TRUE	FALSE	Fair	1405	?
WWN-03	TRUE	FALSE	Weak	1450	?
WWN-03	TRUE	FALSE	Fair	1467	blu wh fluo, streaming with solvent cut, blu wh residu ring

Well	OIL	GAS	HC Significance	MD HC Shows (m)	Show Description
WWN-03	TRUE	FALSE	Fair	1520	blu wh fluo, streaming with solvent cut, blu wh residu ring
WWN-03	TRUE	FALSE	Good	1545	brn wh flue, streaming wh solvent cut, brn wh residu ring.
WWN-03	TRUE	FALSE	Good	1575	brn wh fluo streaming wh solvent cut, brn wh residue ring
WWN-03	TRUE	FALSE	Fair	1625	ple brn yel fluo, strm milky wh solvent cut, wh yel residu ring
WWN-03	TRUE	FALSE	Trace	1685	?
WWS-01-S1	TRUE	FALSE	Trace	1665	light brown oil stain, yellow natural fluor, white cut fluor in cuttings.
WWS-01-S1	TRUE	FALSE	Trace	1720	locally yel nat fluor, fast blooming wh cut fluor, brn oil stain.
WWS-01-S1	TRUE	FALSE	Trace	1770	traces of yel nat fluor
WWS-01-S1	TRUE	FALSE	Good	3120	tr pale yel wh nat fluor
WWS-01-S1	TRUE	FALSE	Good	3160	?
WWS-01-S1	TRUE	FALSE	Good	3190	?
WWS-01-S1	TRUE	FALSE	Good	3260	traces of pale yel wh nat fluor, slow streaming wh cut.
WWS-01-S1	TRUE	FALSE	Fair	3300	?

Appendix B: Cross-section Structural Framework Model

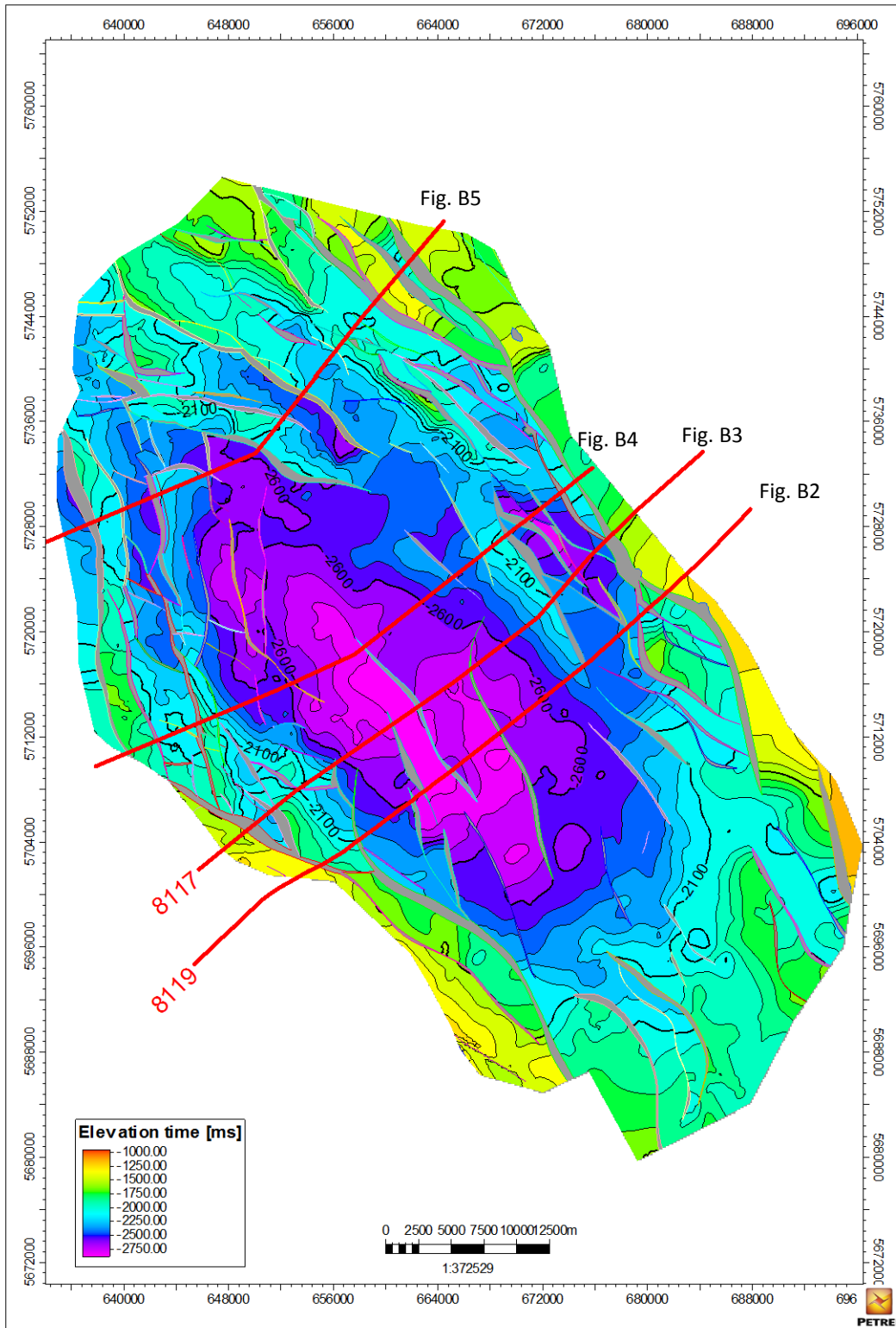


Figure B1: Time Elevation map of near top Main Buntsandstein Subgroup. The different cross-section are indicated.

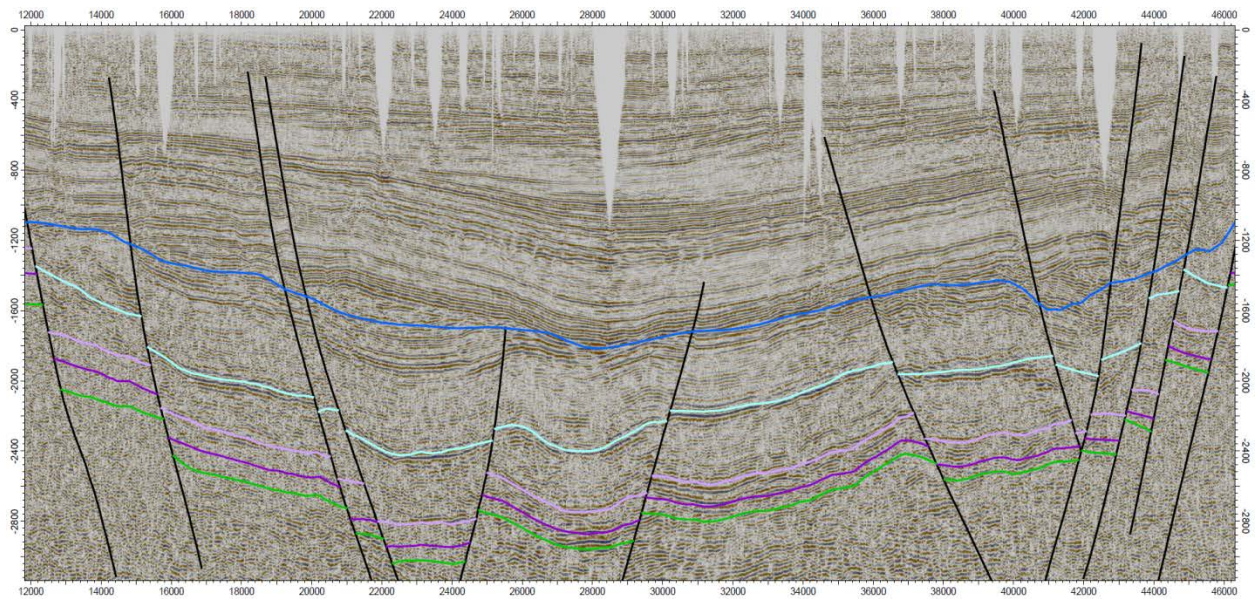


Figure B-2: Seismic cross-section of line 8119 survey L2BP1981A through the Structural Framework Model. green = near base Main Buntsandstein Subgroup, dark purple = near top Main Buntsandstein, light purple = near base Altena Group, cyan = near top Posidonia Shale and dark blue = base Schieland Group (TNO).

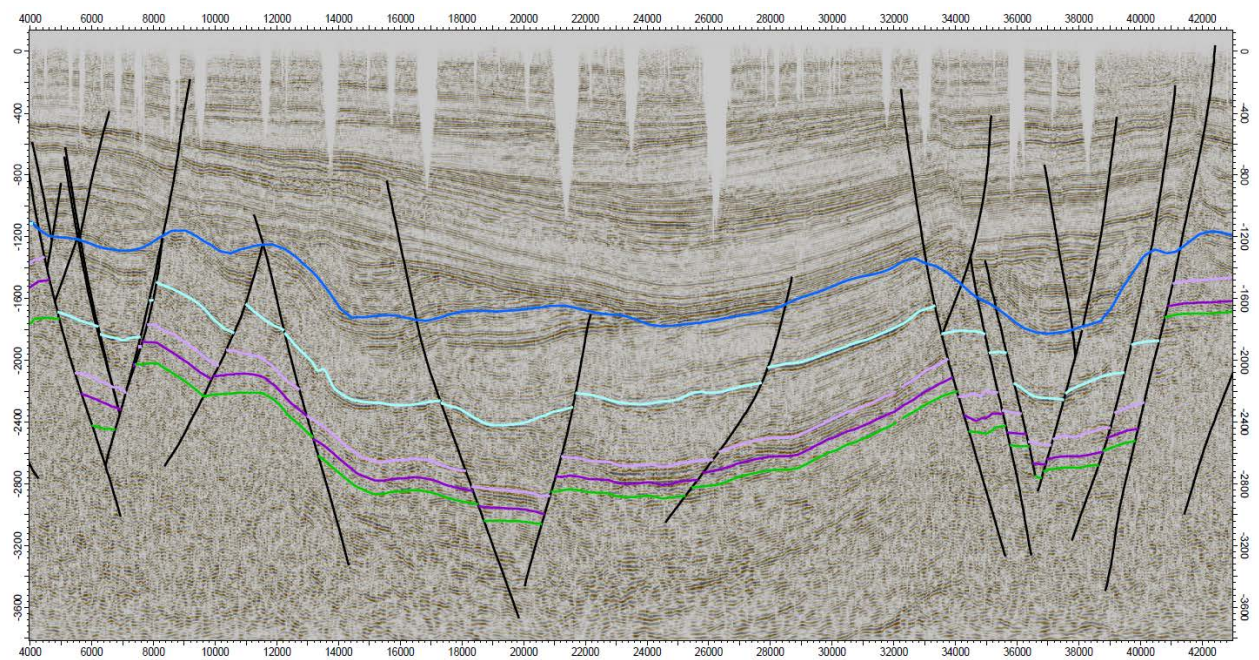


Figure B-3: Seismic cross-section of line 8117 survey L2BP1981A through the Structural Framework Model. green = near base Main Buntsandstein Subgroup, dark purple = near top Main Buntsandstein, light purple = near base Altena Group, cyan = near top Posidonia Shale and dark blue = base Schieland Group (TNO).

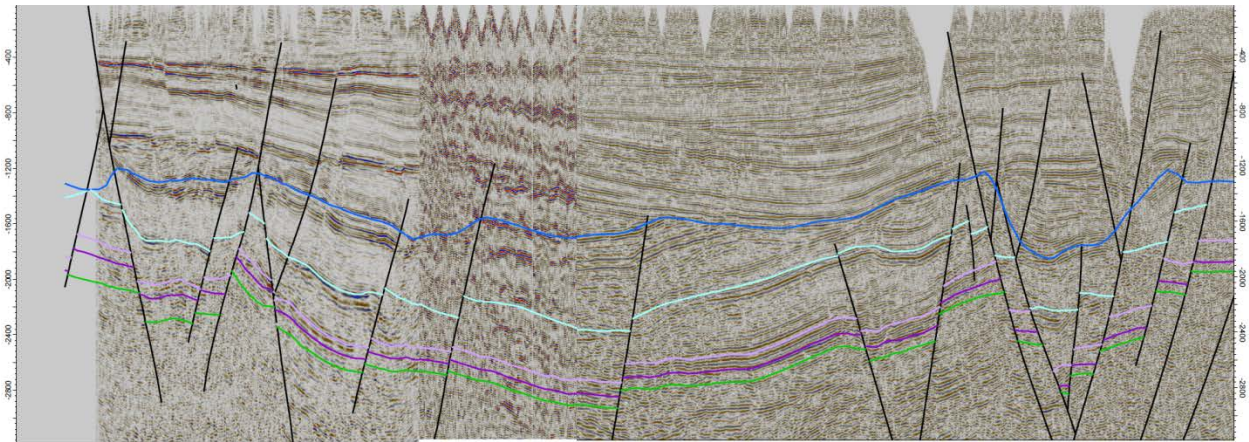


Figure B-4: Composite seismic cross-section of a random line of the L2CLY1992 3D cube, Line 1136 survey L2NAM1976C and Line 76208 survey L2NAM1976C through the Structural Framework Model. green = near base Main Buntsandstein Subgroup, dark purple = near top Main Buntsandstein, light purple = near base Altena Group, cyan = near top Posidonia Shale and dark blue = base Schieland Group (TNO).

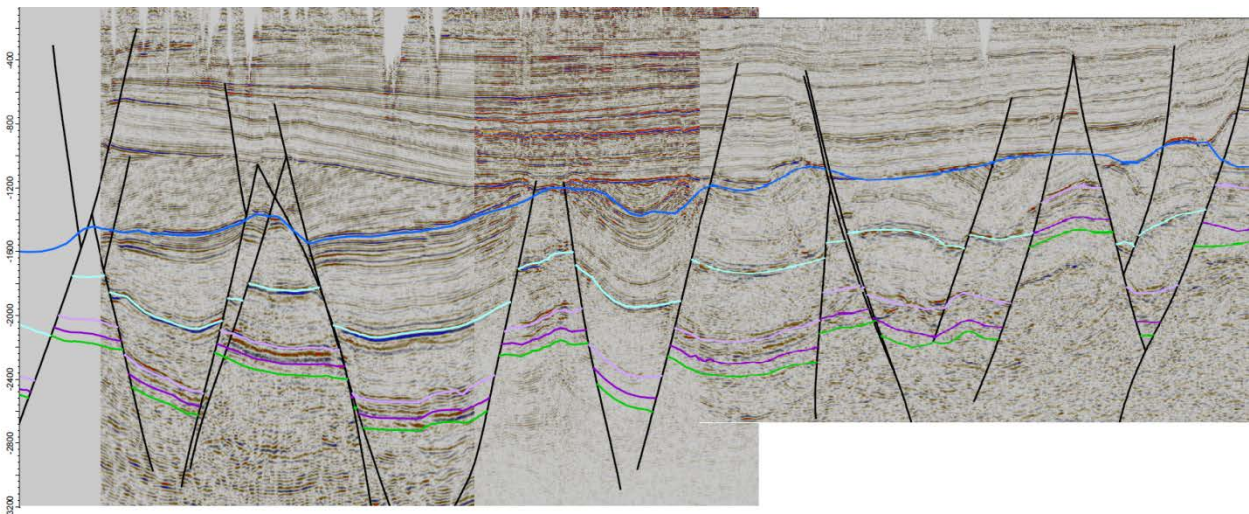


Figure B-5: Composite seismic cross-section of a random line of the L2CLY1992 3D cube, Line 871913 survey L2NAM1987J and Line 872103 survey L2NAM1987B through the Structural Framework Model. green = near base Main Buntsandstein Subgroup, dark purple = near top Main Buntsandstein, light purple = near base Altena Group, cyan = near top Posidonia Shale and dark blue = base Schieland Group (TNO).

Appendix C: Structural Framework Elevation Time Maps

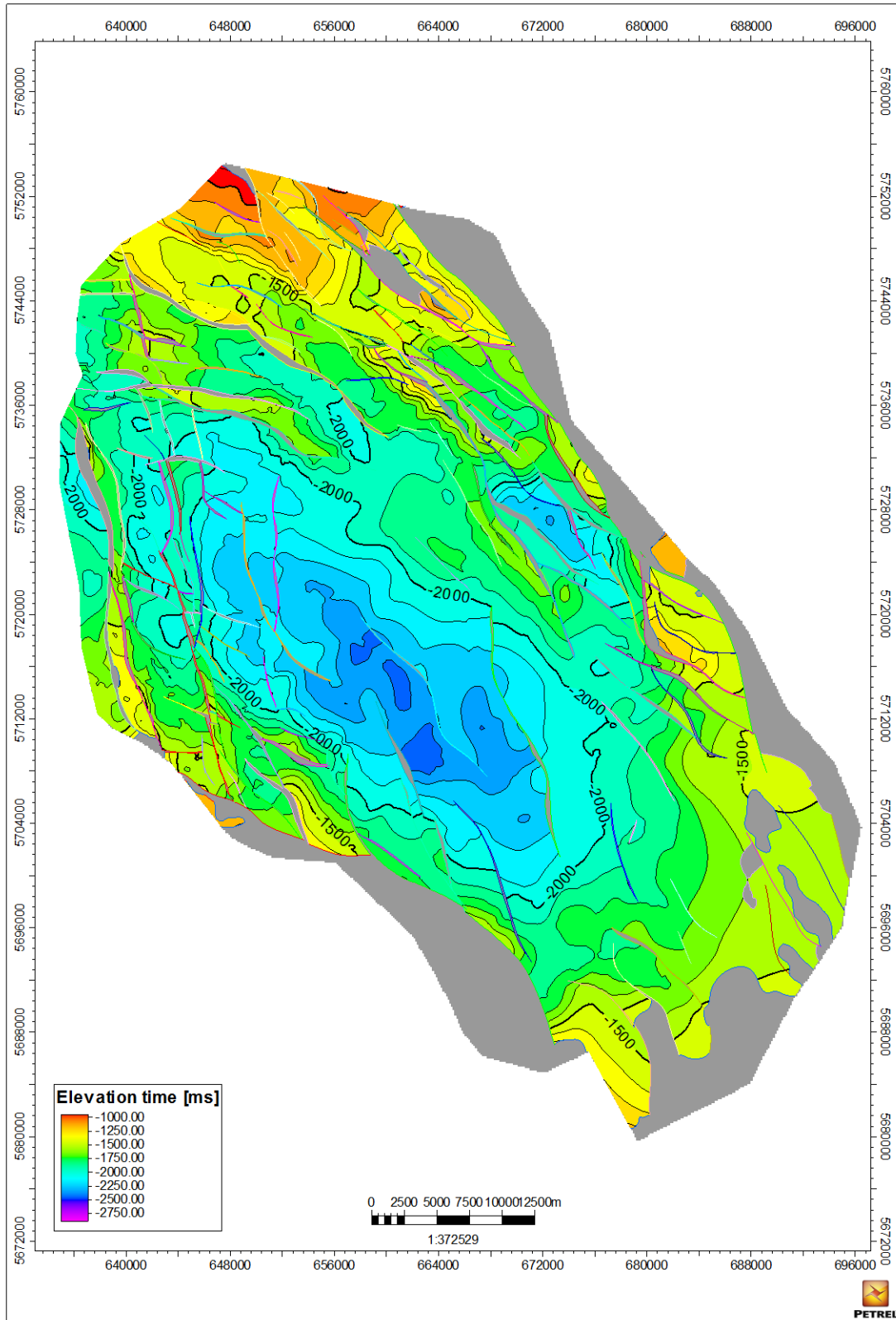
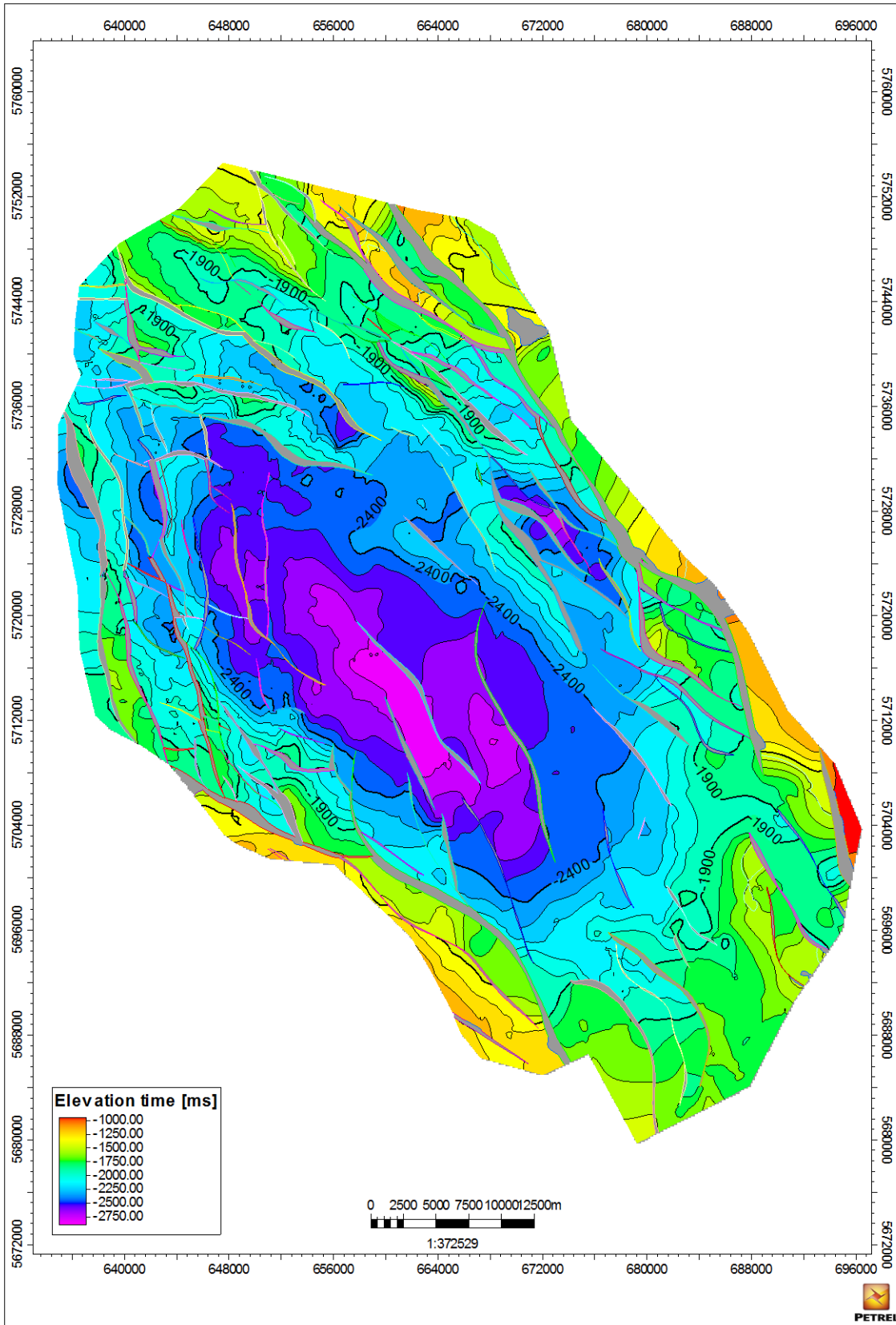


Figure C1: Elevation time map of the near top Posidonia Shale Formation. Contour interval = 100



FigureC2: Elevation time map of the near base Altaena Group. Contour interval = 100

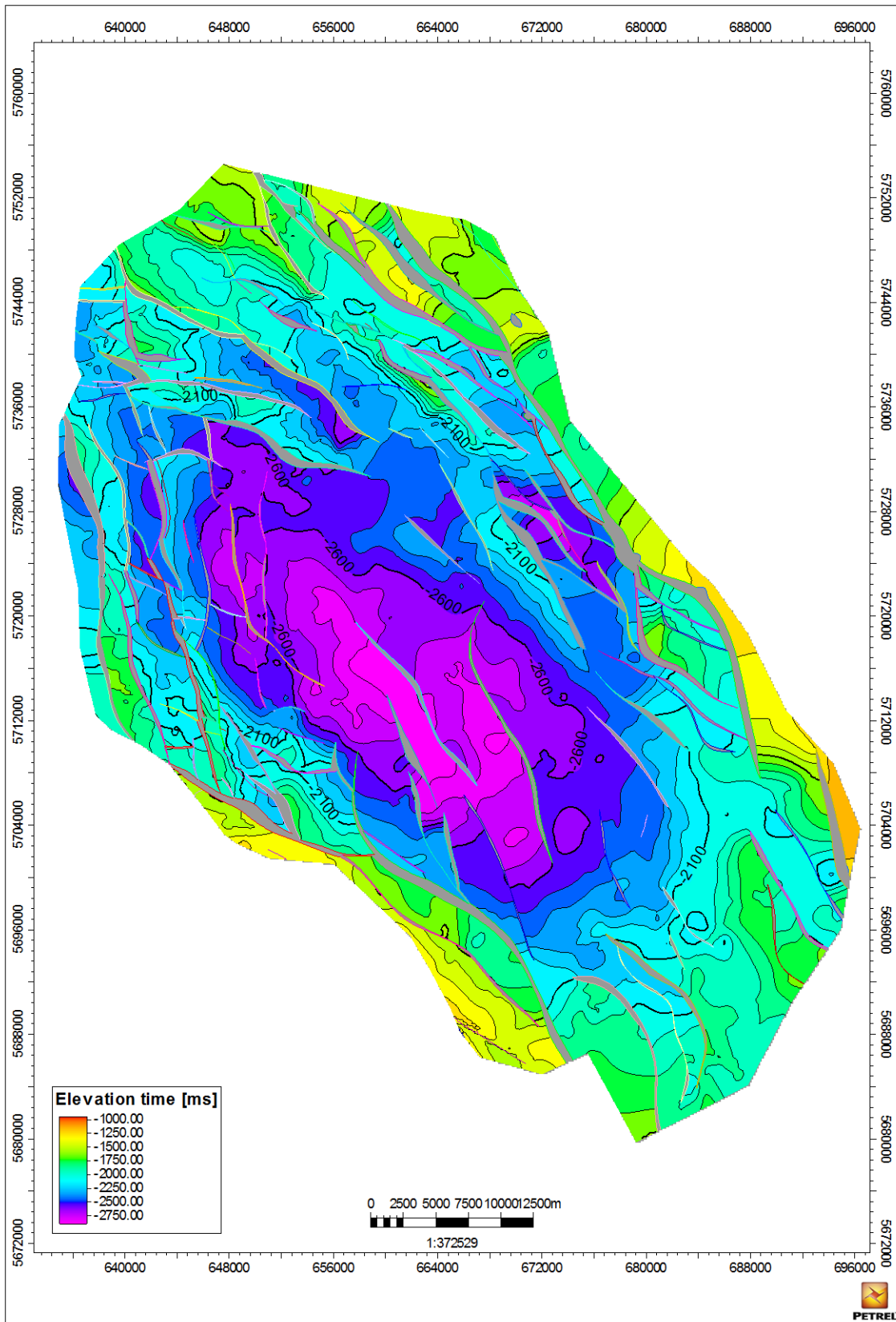


Figure C3: Elevation time map of the near top Main Buntsandstein Subgroup. Contour interval = 100

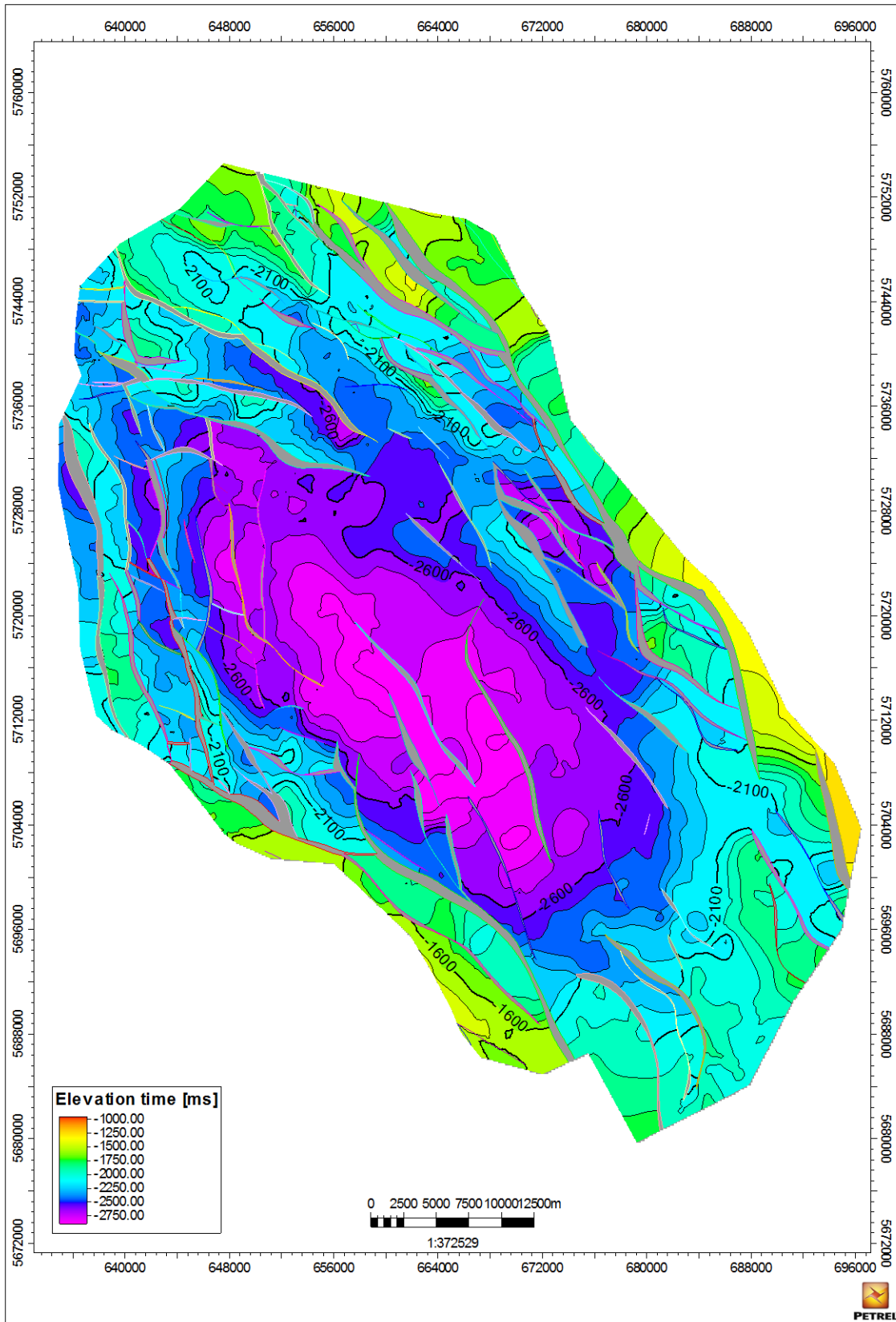


Figure C4: Elevation time map of the near base Buntsandstein Subgroup. Contour interval = 100

Appendix D: Structural Framework Elevation Depth Maps

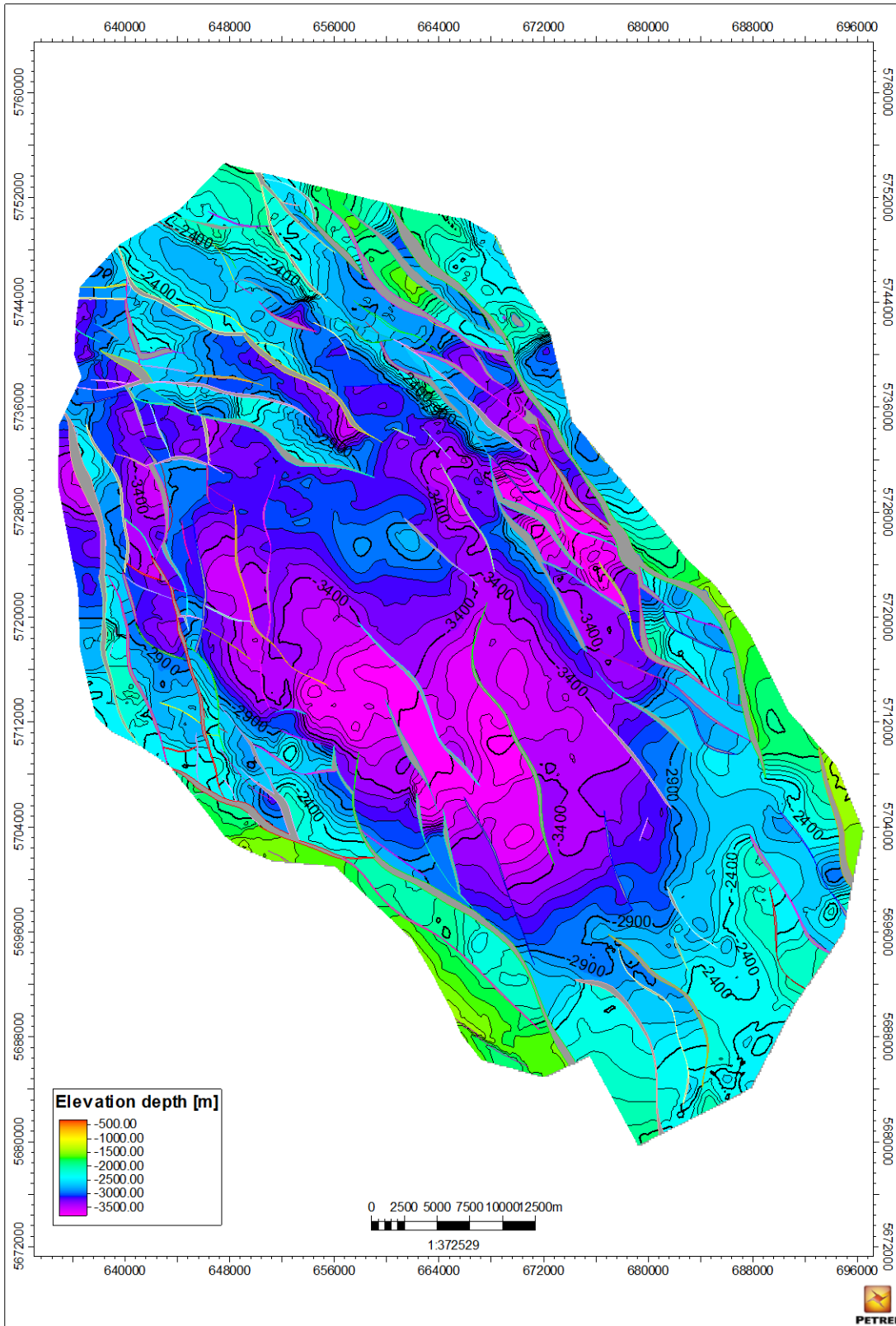


Figure D1: Elevation depth map of the near top Main Buntsandstein Subgroup. Contour interval = 100m

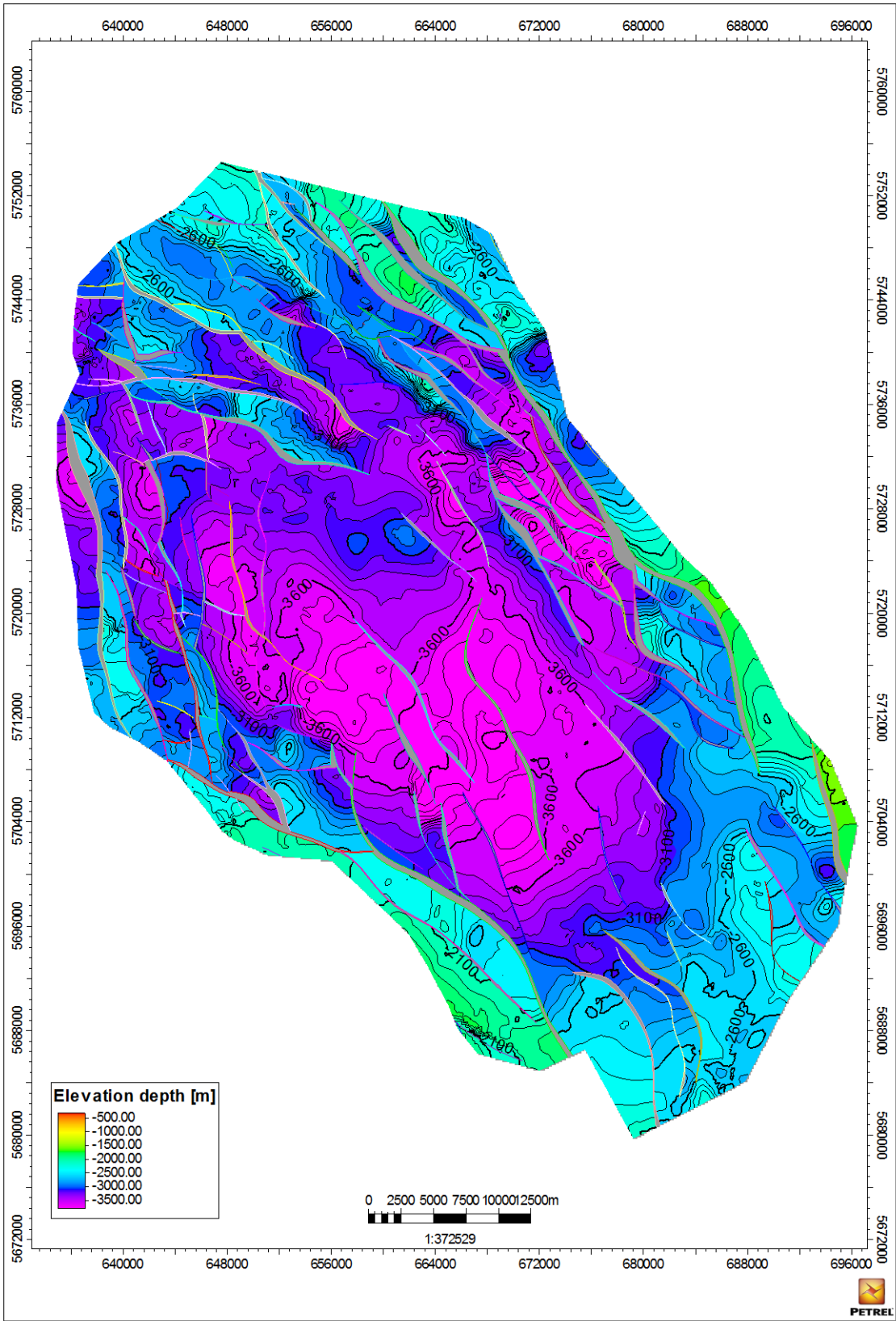


Figure D2: Elevation depth map of the near base Buntsandstein Subgroup. Contour interval = 100m

Appendix E: Derivation Expansion Factor

The formation volume factor of gas (expansion factor) is defined as the ratio of the volume of gas at the reservoir temperature and pressure to the volume at the standard conditions or surface temperature and pressure (p_{sc} and T_{sc}). The gas deviation factor is unity at standard conditions; hence, the equation for the gas formation volume factor can be calculated using the real gas equation (*SPE, petrowiki.org*):

$$B_g = \frac{V_R}{V_{SC}} = \frac{zn RT}{p} \frac{p_{SC} zT}{T_{SC} p} = \frac{p_{SC} zT}{T_{SC} p}$$

Here, n divides out because both volumes refer to the same quantity of mass. For standard conditions or surface temperature and pressure, p_{sc} is taken as 101.325 kPa and T_{sc} as 288.71 K. This allows the equation to be written in the following form:

$$0.350958 \frac{zT_{res}}{p_{res}}$$

In which z equals the compressibility factor, T_{res} the temperature at reservoir conditions (Kelvin) and p_{res} the pressure at reservoir conditions (kPa). An estimate of the compressibility factor (z) is determined with the use of the diagram presented in figure E1. For this an estimate of the pseudoreduced temperature and pressure is needed. These are expressed as:

$$p_r = \frac{p}{p_c} \quad T_r = \frac{T}{T_c}$$

where the subscript c stands for critical. The critical pressure and temperature can be obtained with the use of Key's Rule for natural gas mixtures expressed as followed:

$$p_c = \sum_i p_{ci} y_i \quad T_c = \sum_i T_{ci} y_i$$

The symbol y_i stands for mole fraction. The critical pressure and temperature for individual natural gas components are also available in handbooks and tables. For the purpose of this study, the critical pressure and temperature of methane are used, which are taken as 4.6 MPa and 190.56 K, respectively. The temperature at reservoir level has been roughly estimated with the temperature profile constructed by *Luijendijk et al., 2010* (figure E2) and the pressure with the hydrostatic gradient of water ($\rho \cdot g \cdot h$). In table 5 an overview is given of the values used and calculated for each lead.

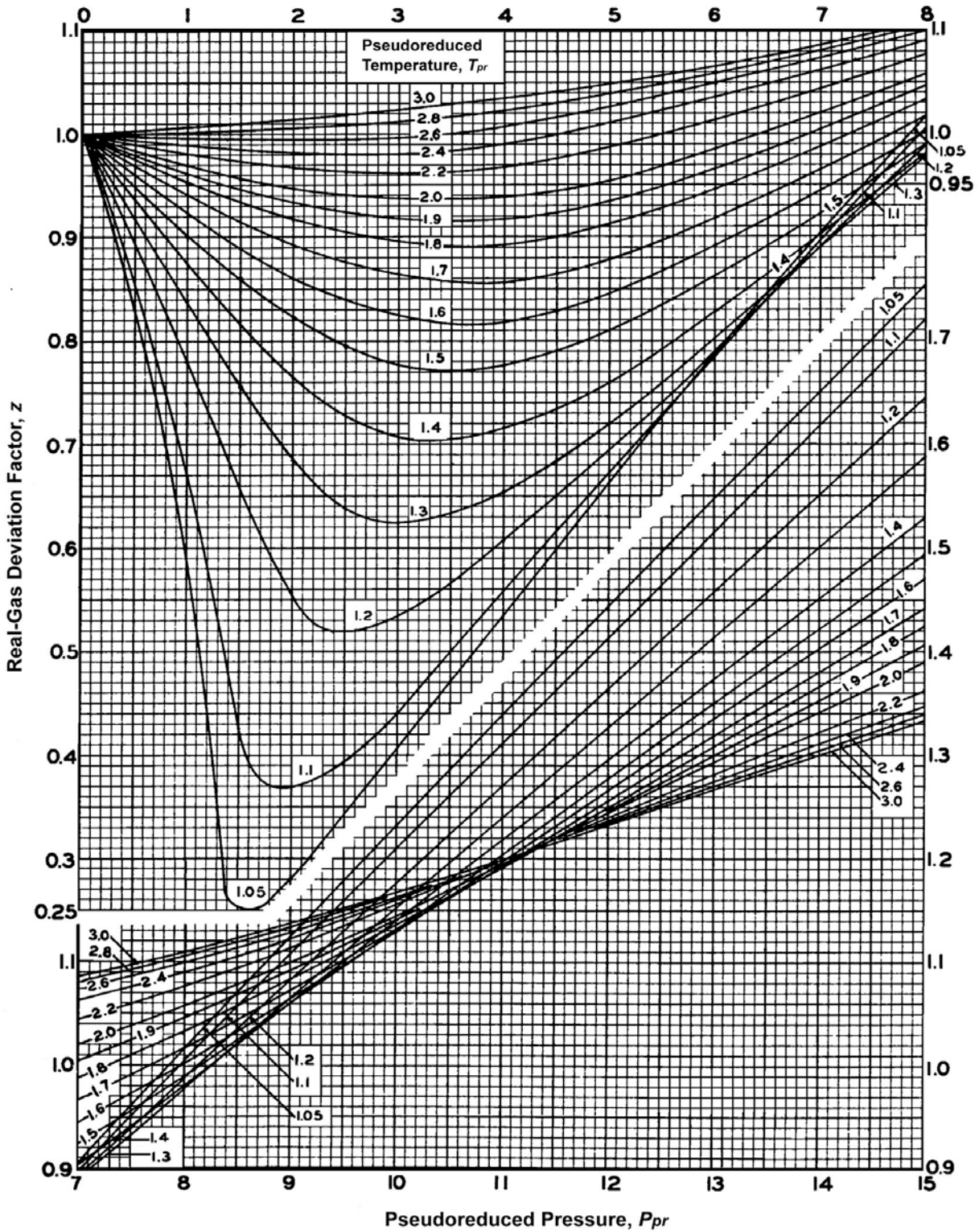


Figure E1: Gas deviation-factor chart for natural gases. Source *Standing and Katz* (1942).

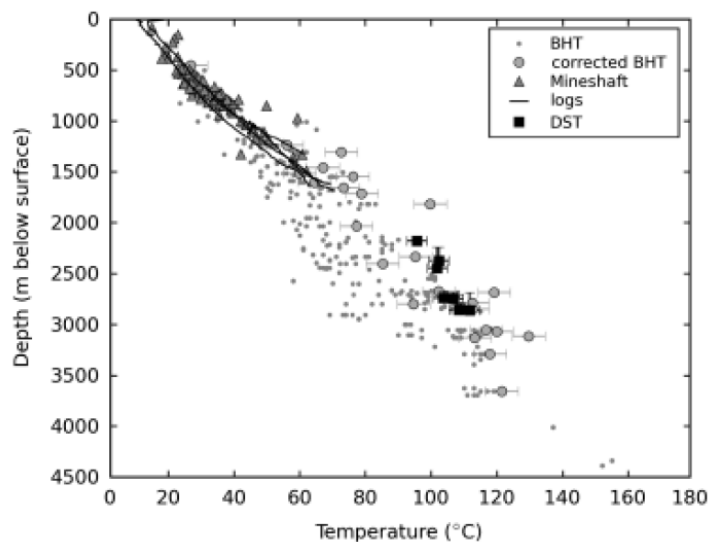


Figure E2: Temperature profile in the Roer Valley Graben. Source: Luijendijk et al., 2010.

Lead no.	Spill Point (m)	Temp at Spill Point (K)	Pressure (Pa)	Pseudoreduced Pressure (Pa)	Pseudoreduced Temperature (K)	z	1/Bg
1	2260	348.15	2.22E+07	4.8	1.8	0.91	199.40
2	2265	348.15	2.22E+07	4.8	1.8	0.91	199.84
3	2455	353.15	2.41E+07	5.2	1.9	0.94	206.72
4	2630	353.15	2.58E+07	5.6	1.9	0.95	219.12
5	Min 2290	348.15	2.25E+07	4.9	1.8	0.91	202.04
5	Int 2310	348.15	2.27E+07	4.9	1.8	0.91	203.81
5	Max 2600	353.15	2.55E+07	5.5	1.9	0.95	216.62
6	2150	348.15	2.11E+07	4.6	1.8	0.9	191.80
7	2210	348.15	2.17E+07	4.7	1.8	0.905	196.06
8	1765	338.15	1.73E+07	3.8	1.8	0.89	163.93
9	2020	343.15	1.98E+07	4.3	1.8	0.905	181.82
10	2240	348.15	2.20E+07	4.8	1.8	0.91	197.63
11	2555	353.15	2.51E+07	5.4	1.9	0.945	214.00
12	2765	358.15	2.71E+07	5.9	1.9	0.96	224.79
13	2655	353.15	2.60E+07	5.7	1.9	0.955	220.05
14	2765	358.15	2.71E+07	5.9	1.9	0.96	224.79
15	3185	383.15	3.12E+07	6.8	2.0	1.015	228.92
16	3265	383.15	3.20E+07	7.0	2.0	1.02	233.52
17	3210	383.15	3.15E+07	6.8	2.0	1.015	230.72
18	3620	393.15	3.55E+07	7.7	2.1	1.05	245.12
19	2355	348.15	2.31E+07	5.0	1.8	0.91	207.78
20	2370	348.15	2.32E+07	5.1	1.8	0.915	207.96
21	2735	358.15	2.68E+07	5.8	1.9	0.96	222.35
22	2380	348.15	2.33E+07	5.1	1.8	0.915	208.84
23	2680	353.15	2.63E+07	5.7	1.9	0.955	222.12
24	2665	353.15	2.61E+07	5.7	1.9	0.955	220.88
25	2875	363.15	2.82E+07	6.1	1.9	0.97	228.14

Table 5: Overview of the values used in the calculation of the formation volume factor for gas.